1986

Determination of equilibrium and rate constants for concanavalin A and various sugars using high-performance affinity chromatography

David J. Anderson
Iowa State University

Anderson, David J.

DETERMINATION OF EQUILIBRIUM AND RATE CONSTANTS FOR CONCANAVALIN A AND VARIOUS SUGARS USING HIGH-PERFORMANCE AFFINITY CHROMATOGRAPHY

Iowa State University PH.D. 1986

Determination of equilibrium and rate constants for concanavalin A and various sugars using high-performance affinity chromatography

by

David J. Anderson

A Dissertation Submitted to the
Graduate Faculty in Partial Fulfillment of the
Requirements for the Degree of
DOCTOR OF PHILOSOPHY

Department: Chemistry
Major: Analytical Chemistry

Approved:

Signature was redacted for privacy.

In Charge of Major Work

Signature was redacted for privacy.

For the Major Department

Signature was redacted for privacy.

For the Graduate College

Iowa State University
Ames, Iowa

1986

TABLE OF CONTENTS

GENERAL INTRODUCTION

Background

Quantitative affinity chromatography refers to the use of affinity chromatography for the determination of equilibrium and rate constants, for a system of specifically interacting molecules. Andrews et al. (1) published the first report describing the quantitative use of affinity chromatography, in which the equilibrium constant for the interaction of D-glucose (as well as N-acetyl-D-glucosamine) with the enzyme A protein of human lactose synthetase was determined chromatographically. The enzyme was injected onto a column containing α-lactalbumin immobilized on a Sepharose matrix, with a mobile phase containing the sugar. Equations were derived relating the retention volume for the enzyme with the concentration of sugar in the mobile phase. Dunn and Chaiken (2) extended the model to include the equilibrium constant for the immobilized ligand-analyte interaction, from which the equilibrium constants were determined for the binding of staphylococcal nuclease to thymidine-5'-phosphate-3'-aminophenylphosphate-Sepharose, and to thymidine-3',5'-bisphosphate, which was present in the mobile phase.

Quantitative affinity chromatography has been used to determine equilibrium constants for other biochemical systems,

as reviewed by Chaiken (3) and Dunn (4). While many studies have been done to determine equilibrium constants, only a few studies have been done to determine rate constants (3,5-7).

Determination of Equilibrium Constants

In general, retention in affinity chromatography can be described by the equilibrium constants of the various species present within the chromatographic system. Thus, for an affinity chromatographic system in which a ligand L is immobilized and a solute E is isocratically eluted using a competing inhibitor I, the reactions of interest are:

$$E + L \underset{}{\overset{K_3}{\rightleftharpoons}} EL \tag{1}$$

$$E + I \underset{}{\overset{K_2}{\rightleftharpoons}} EI \tag{2}$$

where K_2 and K_3 are the association equilibrium constants. An equation relating the equilibrium constants to retention can be derived, as shown in Section II, and is written below:

$$k' = \frac{K_3\{L\}A}{V_m(1 + K_2[I])} \tag{3}$$

where {L} is the surface concentration of immobilized ligand,

[I] is the solution concentration of inhibitor, V_m is the column mobile phase volume, and A is the column surface area. The capacity factor (k') is a measure of retention, as given by (8):

$$k' = (t_r - t_o)/t_o \tag{4}$$

where t_r is the retention time and t_o is the void time. Equation 3 also applies for the "reversed-role" case, in which the inhibitor affects retention by interaction with the immobilized species.

For a divalently interacting solute, the following equation can be derived (see Section II):

$$k' = \frac{K_3\{L\}A}{V_m} \cdot \frac{2(1 + K_2[I]) + K_4\{L\}}{(1 + K_2[I])^2} \tag{5}$$

where K_4 is the equilibrium association constant for the binding of the second site. Limiting cases of Equation 5 can also be written, which assume either complete independence or high-cooperativity in the binding of the two sites on the solute molecule to the affinity matrix. All three models are discussed in detail in Section IV.

Frontal analysis, in which the solute is continually pumped through the column and the time (or volume) of solute

break-through is measured, has also been used to determine equilibrium constants. The quantitative use of frontal analysis in affinity chromatography has been reviewed by Dunn (4). From Equation 3, the following equation is readily derived, from which K_3 can be obtained from frontal data:

$$m_{EL} = K_3[E]m_L/(1 + K_3[E]) \qquad (6)$$

where m_{EL} is the number of moles of solute bound, m_L is the total number of moles of ligand sites (both free and bound), and $[E]$ is the concentration of solute applied.

Determination of Rate Constants

While equilibrium constants can be calculated from the peak retention time (more exactly, the first moment of the peak), rate constants can be obtained from the quantitation of peak broadness, as determined by the variance or second moment of the peak. There are, however, several factors, in addition to the kinetics of the solute molecule binding to the immobilized ligand, which contribute to the broadening of the peak. These additional sources of peak-broadening (band-broadening) have to be minimized, or the effects quantified and subtracted from the total band-broadening, before rate constants of the interaction can be determined.

The most well-known work pertaining to chromatographic band-broadening is the text entitled "Dynamics of Chromatography" (9) by J. C. Giddings. This work has not only proven to be a foundation for chromatographic theory, but also remains at the forefront. Other important works include references 8, 10-17. Hethcote and DeLisi (18,19) have extended the theory to encompass chromatographic conditions often present in affinity chromatography, such as the presence of a competitive inhibitor in the mobile phase.

Various processes within the chromatographic system are contributory to the overall broadening of the band. For the most part, each of these processes is considered to be independent of one another and, thus, the variances for each can be added to obtain the total variance (20). Equation 7 shows plate heights (H) are proportional to variance and, thus, are also additive (20).

$$\sigma_L^2 = HL \tag{7}$$

In Equation 7, σ_L^2 is the peak variance measured in column lengths, L.

For an adsorption chromatographic method using packed columns (e.g., affinity chromatography), the total plate height can be written as a summation of the following H terms (17):

$$H_t = H_{ec} + H_l + H_m + H_{sm} + H_k \quad (8)$$

where H with the subscripts t, ec, l, m, sm, and k refer to the total, extra-column, longitudinal diffusion, mobile phase, stagnant mobile phase, and adsorption-desorption kinetic plate heights, respectively. Theoretical expressions are given below for the more important terms.

The assessment of plate height with respect to the mobile phase velocity, particle size, and retention is of particular importance for the present work. The understanding of the dependence of each H term in Equation 8 on retention is important because retention is varied in this work. In addition, description of the plate height in terms of another variable, the mobile phase velocity, is helpful (if not necessary) in separating H_t into the various components given in Equation 8. The description of the plate height in terms of the particle diameter is qualitatively useful in understanding the experimental design.

Extra-column band-broadening has been extensively studied (21,22). The theoretical understanding of band-broadening resulting from extra-column effects is not essential, however, because contributions are usually small relative to column effects. In addition, extra-column band-broadening can be readily estimated from experiments performed without the column in place.

Longitudinal diffusion refers to the diffusion of the solute in the axial direction (parallel to the flow). Broadening of the band by longitudinal diffusion is negligible relative to other column processes in the normal practice of liquid chromatography and, thus, H_l is insignificant (17).

The H_m term presents the greatest challenge to theoretical treatment. This term describes band-broadening resulting from non-homogeneous flow velocities within the column (eddy diffusion) and from resistance to mass transfer (or resistance to diffusion) within the mobile phase (20). Presently, these effects cannot be described rigorously, because of the complexity of the flow profile within a packed bed. A further complication is the variability in the packing structure for any given column. Empirical parameters accounting for flow inequalities and different packing structures have, therefore, been employed in theoretical treatments. Although this approach simplifies the mathematics, these parameters are difficult to determine experimentally.

Five different expressions for H_m have been derived in the literature: van Deemter et al. (10), Giddings (23), Huber (24), Horvath and Lin (12), and Kennedy and Knox (11). van Deemter et al. (10) consider only the eddy diffusion contribution to H_m and do not include an expression for the resistance to mass transfer within the mobile phase. The

expression for H_m used by them is part of the well-known van Deemter relationship, and is (10):

$$H_m \cong H_{ed} = 2\lambda d_p \tag{9}$$

where H_{ed} is the plate height due to the eddy diffusion, d_p is the particle diameter, and the empirical parameter λ accounts for the flow inequality within the column.

The treatments by Giddings (23), Huber (24), and Horvath and Lin (12) describe H_m in terms of both H_{ed} and a diffusional resistance plate height, H_d. In contrast to the additivity of most H terms, H_{ed} and H_d are considered to be coupled (9). Giddings, Huber, and Horvath and Lin express H_m in terms of a coupled H_d and H_{ed}, by the following equation:

$$H_m = 1/(1/H_{ed} + 1/H_d) \tag{10}$$

While each of the three formulations utilize Equation 9 for H_{ed} in Equation 10, different expressions for H_d are used. These are given below:

Giddings (23):

$$H_d = F_1 \cdot (ud_p^2)/D_m \tag{11}$$

Huber (24):

$$H_d = F_2 \cdot (ud_p^3/D_m)^{1/2} \qquad (12)$$

Horvath and Lin (12):

$$H_d = F_3 \cdot (ud_p^4/D_m)^{1/3} \qquad (13)$$

In Equations 11, 12, and 13; F_1, F_2, and F_3 are structural parameters, u is the mobile phase velocity, d_p is the particle diameter, and D_m is the diffusion coefficient of the solute in the mobile phase.

Finally, Kennedy and Knox (11) assume H_m to be described by the function Au^x, where A is constant for a particular column packing structure and x is constant for all chromatographic systems. By fitting experimental data, Kennedy and Knox determined H_m to be (11):

$$H_m = Au^{1/3} \qquad (14)$$

Equation 14 is the first term in the so-called Knox equation.

The controversy surrounding the u dependence of the H_m term is made apparent by examination of Equations 9-14. The van Deemter equation predicts H_m to be independent of flowrate, while the other theories predict H_m to be a function

of u to different exponential factors. The discrepancy between the van Deemter equation and the other expressions might be resolved by consideration of the $1/H_{ed}$ and $1/H_d$ terms in Equation 10. At high mobile phase velocities, the $1/H_{ed}$ term might dominate the $1/H_d$ term, because Equations 11, 12, or 13 predict an increase in H_d with an increase in u, while H_{ed} does not change with u (Equation 9). Thus, H_m might be independent of flowrate at high u. At low u, the reverse might be true, with the $1/H_d$ term dominating.

Experiments showing the dominance of either H_{ed} or H_d have been published. GC experiments by Done et al. (25) at reduced velocities show a $u^{1/3}$ dependence of H_m, in accordance with Equations 13 and 14. At higher u (experiments show the range of u to be at least 500-6000 μm/sec), the van Deemter relationship has been substantiated (15,20). The discrepancies in the u dependence, however, have not yet been totally resolved, as pointed out by the study of Stout et al. (16). In this study, plate height data were found to be equally well fit by both the van Deemter and Knox equations.

Uncertainty in the retention dependence of the H_m term also exists. All the H_m equations (Equations 9-13) are derived for a non-retained solute (9). Although no theoretical equations have been proposed for the dependence of H_m on retention, most investigators assume retention to have little or no effect (16). This, however, needs more

consideration. Knox points out that, in some cases, H_m might be a weak function of capacity factor (26). In addition, the plate height equation for open tubular columns shows an increase for H_m with increase of k' in the range $0 < k' < 10$ (20). If one considers the interstitial space of a packed column to be many interweaving channels, each of which is characterized by a laminar flow profile (the flow profile for open tubular columns), then a k' dependence of H_m is a reasonable hypothesis.

The fourth term in Equation 8, H_{sm}, is the plate height due to mass transfer in the stagnant mobile phase. The theoretical expressions for H_{sm} for porous spherical particles, as derived by Horvath and Lin (13) and written in a slightly different form, is:

$$H_{sm} = \frac{\theta k_o d_p^2 u(1 + k' + k'/k_o)^2}{30 D_m (1 + k_o)(1 + k')^2} \qquad (15)$$

where θ is the tortuosity factor for the pore structure of the particles and k_o is the ratio of the intraparticulate void volume (volume of mobile phase within the pores, V_p) to the interstitial void volume (volume of mobile phase outside the pores, V_e) in the column.

Equation 15 is consistent with H_{sm} expressions derived by others (18,27). Another expression, convenient for this work,

can be derived from the H_{sm} expression of Hethcote and DeLisi (18,19), and is given below:

$$H_{sm} = \frac{2uV_p(1 + V_m k'/V_p)^2}{k_{-1}V_m(1 + k')^2} \qquad (16)$$

where k_{-1} is the first order rate constant for the diffusion of the solute out of the pores into the interstitial void volume (18).

With respect to this work, the most important term in Equation 8 is H_k, from which the dissociation rate constants of biochemical pairs can be determined by affinity chromatography. H_k is the plate height due to the kinetics of the adsorption-desorption of the solute molecule on the stationary phase. Identical expressions for H_k have been derived by Giddings (28), Denizot and Delaage (29), Horvath and Lin (13), and Hethcote and DeLisi (18,19), as given below:

$$H_k = \frac{2uk'}{k_{-3}(1 + k')^2} \qquad (17)$$

where k_{-3} is the dissociation rate constant.

Having discussed each plate height term in Equation 8, the plate height expressions are combined to give the equation pertinent to this work:

$$H_t - H_{ec} = 2\lambda d_p + \frac{\theta k_o d_p^2 u(1 + k' + k'/k_o)^2}{30D_m(1 + k_o)(1 + k')^2} + \frac{2uk'}{k_{-3}(1 + k')^2} \quad (18)$$

It is assumed in this equation that the mobile phase velocity is sufficiently large, such that the van Deemter equation holds and the longitudinal diffusion is negligible.

Equation 18 reveals the important parameters which will guide the experimental design and strategy. It is seen that the H_k term (third term) is not a function of particle diameter (d_p) while H_m and H_{sm} (the first and second terms, respectively) are proportional to d_p and d_p^2, respectively. Thus, small particle diameters reduce H_m and H_{sm} with respect to H_k. However, even at small particle diameters, there might still be significant contribution of H_m and H_{sm} to the total plate height. If this is the case, one needs to determine the contribution of each term in Equation 18.

The first and second terms in Equation 18 can be determined from H versus u studies on a non-retained solute (i.e., $k' = 0$). Examination of Equation 18 reveals that when $k' = 0$, the equation simplifies to:

$$H_t - H_{ec} = 2\lambda d_p + \frac{\theta k_o d_p^2}{30D_m(1 + k_o)} \cdot u \quad (19)$$

Thus, an H versus u plot for a non-retained solute is predicted to be linear, with the intercept yielding a value for H_m and the slope giving a value for the factor $\theta k_o d_p^2/[30D_m(1 + k_o)]$. By knowing k_o (which can be determined experimentally), H_m and H_{sm} can be calculated at any k', using the slope and intercept of the above analysis and Equations 9 and 15. These values can be used in Equation 18 to calculate H_k, from which a rate constant can be determined. Note that this analysis is valid only if the non-retained solute has a similar value for D_m as the solute of interest.

Substituting Equation 16 for the H_{sm} term in Equation 18, yields the equation used in this work for calculating rate constants:

$$H_t - H_{ec} = H_m + \frac{2uV_p(1 + V_m k'/V_p)^2}{k_{-1}V_m(1 + k')^2} + \frac{2uk'}{k_{-3}(1+k')^2} \qquad (20)$$

Extension of Quantitative Studies to HPAC

The main import of this dissertation work was to improve the methodology of quantitative affinity chromatography, through the use of high-performance affinity chromatography (HPAC). A few studies using HPAC for the determination of

equilibrium and rate constants have been published (3,5-7). However, these studies were deficient with regard to the experimental design, or the data analysis, casting doubt on the accuracy of the results. This was especially true for the determination of rate constants.

The majority of the work for the determination of equilibrium constants has been done on conventional matrices (the so-called "soft gels", such as agarose). These matrices, however, are disadvantageous to use because of their slow mass transport properties (3), which result in peak-broadening. In quantitative and preparative uses this decreases sensitivity and increases separation time. Furthermore, the increased magnitude of the H_m and H_{sm} band-broadening terms prevent the measurement of k_{-3}, since H_k can become negligible. The more efficient matrices used in HPAC greatly help in this regard.

Further investigation is warranted with respect to equilibrium constant determination by HPAC, as several problems have been noted in the few studies that have been done. Nilsson and Larsson (6) noted a deviation of approximately 50 percent in the experimentally determined equilibrium constant for a particular solute, immobilized ligand pair when different inhibitors were used in the mobile phase. In another study, non-linear isotherm conditions were used (7). Non-linear isotherm conditions result when the

concentration of the solute injected is too high. Under such conditions, saturation of the stationary phase sites at the microscopic level occurs, resulting in a non-ideal distribution of the solute between the mobile and stationary phases. The retention models (Equations 3 and 5) are not valid at these conditions.

Much work needs to be done in affinity chromatography in the area of rate constant determination. One fact is clear; the use of high-performance matrices is imperative. As mentioned previously, very few quantitative HPAC studies have been performed. Dissociation rate constants obtained from these studies have been factors of 10 to 100 times lower than the solution values (6,7). The accuracy of these results is questionable, however. In several of these studies (5,6), no attempt was made to correct H_t for H_m and H_{sm}, leading to serious doubts about the rate constants determined. The most thorough kinetic study by HPAC was done by Muller and Carr (7). In this study, corrections for the "non-kinetic" plate heights (H_m and H_{sm}) were made. The utility of this study, however, was greatly impaired because of the non-linear isotherm conditions used. The presently used band-broadening model (Equation 20) was derived assuming linear isotherm conditions.

Improvements in the experimental design were made in the present work to circumvent the problems encountered in these

previous studies. Chromatography was done at the lowest concentrations of solute feasible, so that linear (or near-linear) isotherm conditions were obtained. Further efforts were made to reduce band-broadening from sources other than the adsorption-desorption kinetics. All the previous studies were done using 10 μm silica. A four-fold reduction in H_{sm} and a two-fold reduction in H_m could theoretically be obtained by using 5 μm silica (see Equations 9 and 15). In addition, H_m and H_{sm} were estimated, as described previously, and subtracted off from the total plate height.

Another aspect of the present work was an assessment of the band-broadening models used. Recent work on silica gel has shown that none of the theoretical relationships accurately described H_t as a function of k' (14,15). Although determination of kinetic constants by HPAC requires the use of band-broadening theory, no attempt has been made in the HPAC studies done so far to verify this theory. The validity of presently used band-broadening theory was tested in the present work by fitting the total plate height data, as a function of retention, to the model (Equation 20).

Properties of the Concanavalin A, Sugar System

The biochemical system chosen for this study was the Concanavalin A (Con A), sugar system. Much work has been done

in the determination of equilibrium and rate constants for Con A and various sugars in solution (30), making it a suitable system for study.

Con A belongs to a class of proteins known as lectins. A lectin is classified as any protein which specifically binds sugars, with the exception of immunoglobulins (31). The source of Con A is the seeds of the jack bean plant (Canavalia ensiformis).

Several references have been published which extensively discuss the properties of Con A (32-34). Con A is a multimeric protein consisting of either two or four identical subunits, depending on the solution conditions (34-38). The dimensions of the dimer are 30 x 45 x 80 Å (39). Each monomer has a molecular weight of 27000 daltons (40). There is one sugar binding site on each monomer (34). In addition, each monomer has a separate hydrophobic, calcium, and manganese binding site; one of each type (34). The distance separating the two sugar binding sites on the Con A dimer is approximately 80 Å (41).

Whether Con A exists as a dimer or a tetramer depends upon the pH and temperature (34-38). The dimer form exists exclusively in solutions below a pH of 5.5, in a temperature range of at least 4 °C to 31 °C (34,35). At higher pH values, however, association of the dimer units into tetramer units occurs. The position of this dimer-tetramer equilibrium

depends upon the pH and the temperature (35). In general, the extent of tetramer formation is greater at higher pH and higher temperature. The tetramer form predominates in solutions at or above a pH of 7.2, at 25 °C (35).

Molecules containing the α-D-mannopyranosyl unit have the greatest binding strength to the Con A sugar binding site. Most critical to the interaction of the sugar and the Con A binding site are the hydroxyl groups at the C-3, C-4, and C-6 positions of the mannopyranosyl unit (33). Glucopyranosyl molecules also have this configuration and, thus, specifically bind to Con A. The affinity of the glucopyranosyl moiety, however, is several-fold smaller in comparison to the affinity of the mannopyranosyl moiety (30).

Other factors affecting binding strength are given below. The α-mannopyranosyl and α-glucopyranosyl sugars are found to have higher binding constants than their β counterparts (42). Substituents attached to the sugar also affect the strength of the interaction. For example, the binding constant for 4-methylumbelliferyl α-D-mannopyranoside is ten times greater than that for methyl α-D-mannopyranoside (30). Finally, the binding activity of Con A requires the presence of Mn^{2+} (or similar transition metal ion) and Ca^{2+} (43).

Outline of the Experimental Sections

Equilibrium and rate constants were determined for Con A and various sugars using the HPAC technique. "Reversed-role" experiments were performed, in which the macromolecule (Con A dimer) was immobilized and the ligands (sugars) chromatographed, as described in Section III. Zonal studies were performed, in which 4-methylumbelliferyl α-D-mannopyranoside (MUM) and p-nitrophenyl α-D-mannopyranoside (PNPM) solutes were injected into mobile phases containing various concentrations of methyl α-D-mannopyranoside (MDM). Since the solutes and inhibitor interacted with only one immobilized binding site at a time, association constants could be determined through the use of Equation 3.

Dissociation rate constants for the Con A, MUM and Con A, PNPM interactions were also determined from the zonal studies. The theoretical expression for the band-broadening for monovalent solutes in reversed-role affinity chromatography is the same as Equation 20 (19). It was expected that the role of the inhibitor in the reversed-role mode is to reduce k', by filling up some of the Con A sites, while exerting no effect on the solute-occupied sites. In this case, the inhibitor would not affect the rate of dissociation of the solute from the immobilized site and, thus, Equation 20 would be

applicable.

Frontal studies are also described in Section III. Association constants for MDM and PNPM were determined from separate studies, in which solutions of the solute were continually pumped through the Con A columns and the break-through volumes determined. Equation 6, modified for non-specific adsorption (derived in Section III), was used to calculate the association constants.

In Section IV, "normal" mode experiments are described. In this case, the sugar (glucosamine or p-aminophenyl α-D-mannopyranoside) was immobilized and the Con A was chromatographed, in the presence of various concentrations of the inhibitor MDM. The pH of the mobile phase was chosen such that the Con A existed as a dimer (pH = 5.0). Since the two sugar binding sites of the dimer are on the same side of the molecule, divalent adsorption of the Con A onto the column is possible (provided that the ligand density on the matrix is great enough). Equilibrium constants for the divalent Con A were determined from Equation 5, the independent, equivalent-site equation (Section IV), and the high-cooperativity equation (Section IV).

The accuracy of the equilibrium and rate constant results was dependent upon the accuracy with which the peak's first and second moments could be determined. The present HPAC studies required small solute concentrations to ensure linear

elution conditions. Thus, baseline noise and drift were important problems. For this reason, a computer study was done to determine the effect of errors in estimating the baseline position on the values calculated for the moments. Several methods for moment calculation were assessed. The method giving the least errors in the moments would, thus, be the method of choice for peaks having an uncertain baseline. The results of these computer studies are described in Section I.

Finally, Section II examines a retention model used for determining the number of sites of interaction between the solute and the matrix.

SECTION I.

EFFECT OF BASELINE ERRORS ON THE CALCULATION OF STATISTICAL MOMENTS OF TAILED CHROMATOGRAPHIC PEAKS

SUMMARY

A frequent problem in the measurement of the statistical moments and number of plates of a tailed chromatographic peak is uncertainty in locating the beginning and end of the peak. This study examines several methods for the calculation of moments using simulated exponentially-modified Gaussian peaks that were further altered to model common baseline errors. It is found that methods based on the B/A ratio of a peak are substantially less affected by these errors than are methods based on the commonly used summation methods.

INTRODUCTION

The statistical moments of a chromatographic peak in units of time are defined by the following equations (1):

$$\text{zero-th moment:} \quad M_0 = \int_0^\infty h(t)dt \tag{1}$$

$$\text{first moment:} \quad M_1 = \frac{\int_0^\infty t \cdot h(t)dt}{M_0} \tag{2}$$

$$\text{higher moments:} \quad M_n = \frac{\int_0^\infty (t-M_1)^n h(t)dt}{M_0} \tag{3}$$

where h(t) is the peak height at time t. M_0, M_1, and M_2 are the peak area, retention time, and variance, respectively. M_1 and M_2 are especially useful because they are related to the thermodynamic and kinetic properties of the chromatographic system and to the number of theoretical plates (N):

$$N = \frac{M_1^2}{M_2} \tag{4}$$

Because chromatographic peaks often exhibit tailing, approximate calculations of the moments based on the assumption of Gaussian peak shape (e.g., the width-at-half-height method) can lead to considerable error (2,3). Computer methods based on Equations 1-3, although more accurate in principle, can be adversely affected by noise (1,4,5),

baseline drift (1), premature termination of data collection (2,5,6), and too few data points (5). The higher moments are especially sensitive to peak tailing (1).

In this paper, baseline-associated problems are examined. When peaks elute very slowly, the baseline may drift or the tailing may be such that one cannot be certain that the detector has returned to baseline. It is also common for trace impurities to elute in the tail of the peak. Thus, it is worthwhile to examine several methods for calculating peak moments to see if some methods are less sensitive than others to baseline errors. Simulated data based on exponentially-modified Gaussian (EMG) peaks are used. EMG peaks are reported to be good models for real chromatographic peaks (3,7-9). The EMG peak model is recently reviewed (10).

THEORY AND EXPERIMENTAL

Apparatus

A Model IIe 64K computer (Apple) with a 64K RAM card (Legend Industries) was used for all calculations. Programs were written in Applesoft BASIC.

EMG Peak Generation

An EMG peak is a Gaussian peak of first moment t_G and variance σ_G^2 that has been distorted by an exponential function of time constant τ. The moments of the EMG peak are given by (11):

$$M_1 = t_G + \tau \tag{5}$$

$$M_2 = \sigma_G^2 + \tau^2 \tag{6}$$

The peak height, h, as a function of time, t, can be written as:

$$h(t) = \frac{A}{\tau} \cdot \exp\left[\left(\frac{\sigma_G}{\tau}\right)^2 \frac{1}{2} - \frac{(t-t_G)}{\tau}\right] \cdot \int_{-\infty}^{Z} \frac{\exp(-x^2/2)dx}{\sqrt{2\pi}} \tag{7}$$

where A is the area. Z is given by:

$$Z = [(t-t_G)/\sigma_G - \sigma_G/\tau] \quad (8)$$

Chromatograms were simulated using Equations 7 and 8 according to the method of Foley and Dorsey (12), in which the integral was calculated using an accurate polynomial approximation (13). A Gaussian peak was also generated using a standard equation (14). The values used are given in Table I.

Baseline Modification

To simulate the effect of drift or errors in locating the baseline, the EMG peaks were altered by subtraction. Because such errors are more likely to occur at the end of the peak than at the beginning, the EMG peaks were altered by drawing a line from a point near the beginning of the peak closest to 0.1 % of the maximum peak height to a point on the tailing portion of the peak closest to 0.1, 1.0, 2.5, 5.0, or 10.0 % of the maximum peak height (Figure 1). The baseline-corrected data set consisted of the difference between the original EMG peak and the baseline. Data points before and after the intersection of the baseline with the peak were set to 0. A corrected peak is shown in Figure 2. The errors caused by this type of baseline correction will be called "sloping baseline errors".

A second baseline-corrected data set was also generated,

Table I. Parameters used to generate EMG peaks[a]

τ (sec)	Time interval between points(sec)	Measured $B/A_{0.1}$
0	0.05	1.00
0.5	0.05	1.09
1.8	0.05	1.91
3.0	0.05	2.77
4.2	0.1	3.60
5.3	0.1	4.35
6.6	0.1	5.21

[a]For all peaks, t_G=25 sec, σ_G=1 sec.

Figure 1. A simulated EMG peak with τ/σ_G = 6.6. Sloping baselines were drawn from 0.1 % of maximum peak height on the leading side of the peak to 0.1, 1, 2.5, 5, or 10 % of the maximum peak height on the trailing edge of the peak

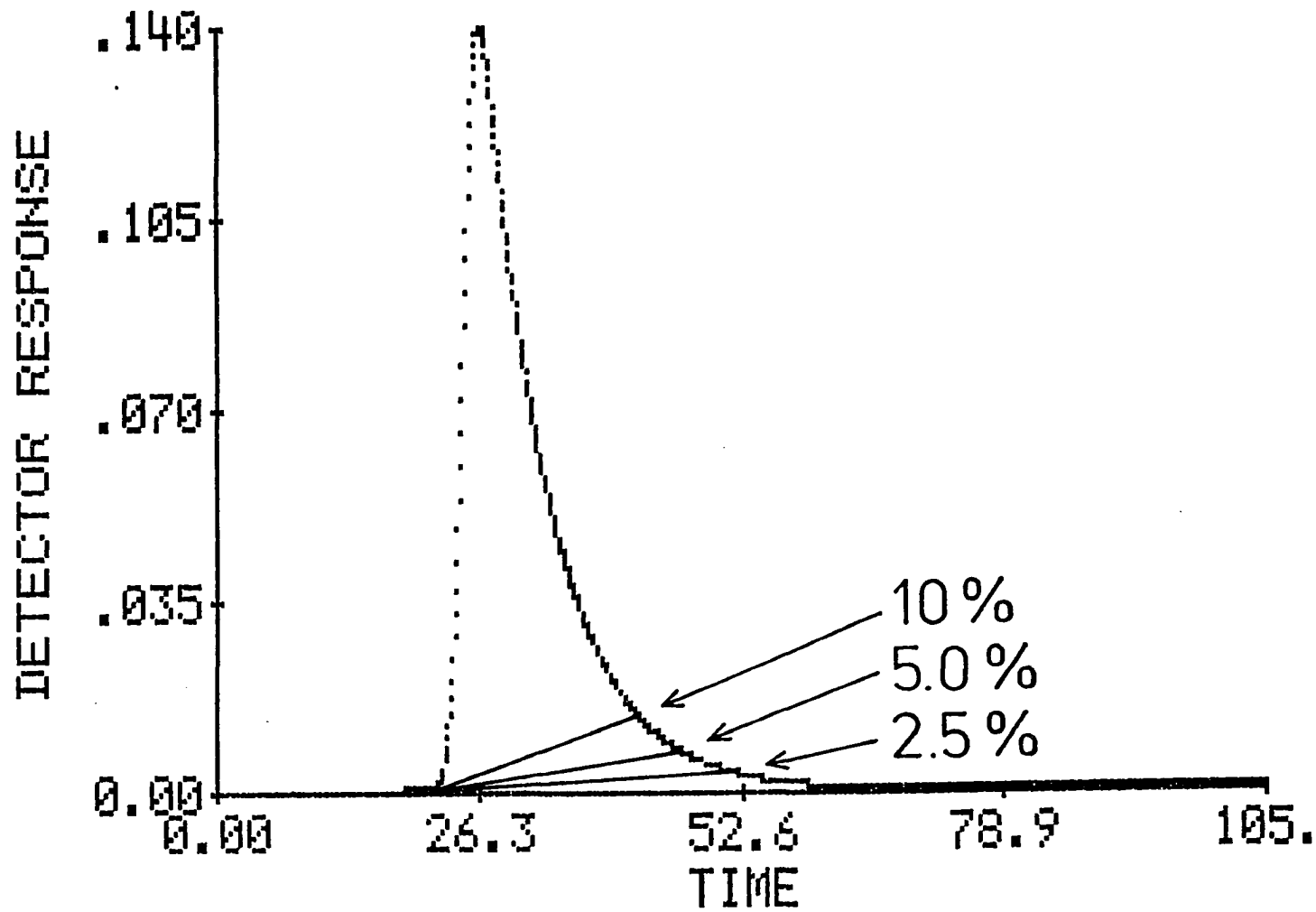
.140
.105
.070
.035
0.00
DETECTOR RESPONSE
0.00
26.3
52.6
78.9
105.
TIME
10 %
5.0 %
2.5 %

Figure 2. Output of the fitting routine indicating the points used to calculate t_p, $W_{0.5}$, $B/A_{0.5}$, $W_{0.1}$, and $B/A_{0.1}$. This is the "baseline-corrected" peak with 5 % baseline error derived from the parent EMG peak of Figure 1

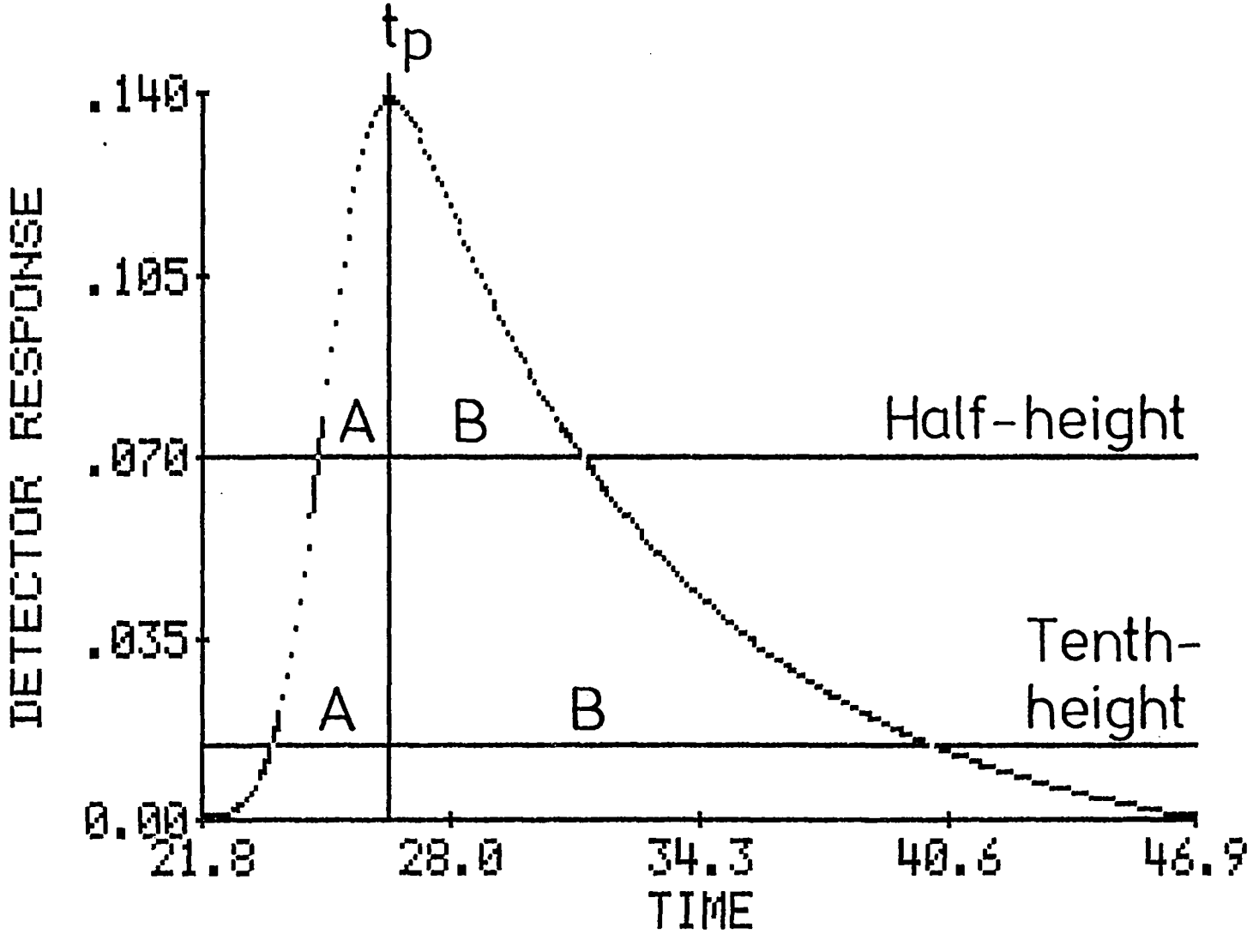
t_p
.140
.105
.070
.035
0.00
DETECTOR RESPONSE
A
B
Half-height
A
B
Tenth-height
21.8
28.0
34.3
40.6
46.9
TIME

in which the baseline points were set at the same percentage of maximum peak height on both sides of the peak. The errors caused by this correction will be called "horizontal baseline errors".

Moments Calculation

Five methods were used to calculate the peak moments: summation method, Yau method (15), Gaussian approximation, and two methods based on the work of Foley and Dorsey (12).

Summation method

This is the standard method used for peak moment calculations. No assumptions about peak shape are made. Point-by-point summations of the terms within the integrals of Equations 1-3 were performed from the beginning to the end of the peak.

Yau method (15)

This method is based on a property of the EMG peak model. The retention time of the Gaussian component of the peak, t_G, always corresponds to a point of height, $h(t_G)$, on the rising portion of the EMG peak. When this point is located, τ can be calculated using M_{0-}, the area of the peak up to t_G, and M_0:

$$\tau = (M_0/2 - M_{0-})/h(t_G) \tag{9}$$

To locate t_G, M_0 and M_1 were first calculated by the summation method above. Then, a second search through the data was made, using each time point in turn temporarily as t_G and calculating by summation M_{0-} and M_{1-}, the zero-th and first moments up to t_G, respectively. After each new M_{0-} and M_{1-} was obtained, the values of τ calculated according to Equations 5 and 9 were compared. The search was continued until τ from Equation 5 was larger than τ from Equation 9.

To exactly locate the value of t_G between the previous two time points, a procedure different from that of Yau was used. The four h(t) points surrounding t_G were fit to a straight line, then t_G was calculated by solving a quadratic equation which involved the equation of the fitted line, Equations 5 and 9, and M_{0-} calculated up to two time points before t_G. The exact values of M_{0-} and M_{1-} were then calculated.

After locating t_G, the Yau method was used to calculate τ from Equation 5 and σ_G, with σ_G given by the following equation:

$$\sigma_G = M_{0-}\sqrt{2\pi}(M_1 - M_{1-})/M_0 \tag{10}$$

The second moment was then calculated according to

Equation 6.

Gaussian approximation

By assuming the peak to be Gaussian, the variance can be calculated from the width-at-half-height, $W_{0.5}$(16):

$$M_2 = W_{0.5}^2/(8 \cdot \ln 2) \qquad (11)$$

To determine $W_{0.5}$, the upper five points of the peak were fit to a quadratic equation, from which the time, t_p, and height, $h(t_p)$, of the maximum were calculated (Figure 2). The data points between $0.45h(t_p)$ and $0.55h(t_p)$ on each side of the peak were fitted to a straight line. From this, $W_{0.5}$ was calculated. M_1 was assumed to be equal to t_p.

Foley and Dorsey methods (12)

These methods are based on the B/A ratio of a peak, calculated as the width of the trailing half of the peak beginning at t_p divided by the width of the leading half of the peak (Figure 2). B/A is generally calculated at $0.1h(t_p)$, but can be calculated at any level of the peak. $B/A_{0.1}$ and $B/A_{0.5}$ are considered here.

Based on the EMG peak model, Foley and Dorsey developed equations for calculating M_2, σ_G, τ, and M_1 based on t_p, $W_{0.1}$ or $W_{0.5}$, and $B/A_{0.1}$ or $B/A_{0.5}$. At $0.1h(t_p)$, the equations

are:

$$M_2 = \frac{W_{0.1}^2}{1.764(B/A_{0.1})^2 - 11.15(B/A_{0.1}) + 28} \quad (12)$$

$$\sigma_G = \frac{W_{0.1}}{3.27(B/A_{0.1}) + 1.2} \quad (13)$$

$$t_G = t_p - \sigma_G(-0.193(B/A_{0.1})^2 + 1.162(B/A_{0.1}) - 0.545) \quad (14)$$

M_1 and τ are calculated from Equations 5 and 6, respectively. Over the $B/A_{0.1}$ range of 1.09 to 2.76, the errors in M_1 and M_2 are less than ±1.5 % (12). This method will be referred to as the $B/A_{0.1}$ method.

Similar equations were developed by Foley and Dorsey for the same $B/A_{0.1}$ range but based on $B/A_{0.5}$:

$$M_2 = \frac{W_{0.5}^2}{-8.28(B/A_{0.5})^3+41.8(B/A_{0.5})^2-72.3(B/A_{0.5})+44.6} \quad (15)$$

$$\sigma_G = \frac{W_{0.5}}{2.5(B/A_{0.5})} \quad (16)$$

$$t_G = t_p - \sigma_G(-1.46(B/A_{0.5})^2 + 5(B/A_{0.5}) - 3.14) \quad (17)$$

The errors in M_2 are reported to be less than ±2 % (12). This method will be referred to as the $B/A_{0.5}$ method.

In this program, moments based on $B/A_{0.5}$ were calculated using additional data from the Gaussian approximation method.

Moments based on $B/A_{0.1}$ were obtained by first fitting the data between $0.05h(t_p)$ and $0.15h(t_p)$ on each side of the peak to a quadratic equation (Figure 2). The fitted curves were used to calculate $B/A_{0.1}$.

Calculation of Percent Error

The errors in the measured values of M_0 and M_2 for the baseline corrected peaks were calculated relative to respective values for the parent, i.e., uncorrected EMG peak. M_1 presented a problem in that t_G was arbitrarily chosen and, thus, the errors in M_1 could take on any value by changing t_G. Foley and Dorsey (12) chose $t_G/\sigma_G = 20$ and calculated their error ranges accordingly. However, it seemed that the error in M_1 relative to a measure of peak width, e.g., $\sqrt{M_2}$, would be more useful, so the error was calculated according to the following equation:

$$\% \text{ error in } M_1 = \frac{100 \cdot (M_{1,\text{measured}} - M_{1,\text{parent peak}})}{\sqrt{M_{2,\text{parent peak}}}} \qquad (18)$$

This method of calculating % error in M_1 is closely related to equations for resolution and number of theoretical plates. It does, however, tend to exaggerate the error in M_1 when τ/σ_G is small.

RESULTS AND DISCUSSION

Sloping Baseline Errors

The simulated data were obtained by drawing the corrected baseline from a point near the true baseline at the front of the peak to a point on the tail of the peak. As shown in Figure 2, even a large error in the baseline resulted in a peak which appeared reasonably shaped. Thus, errors such as these would be difficult to detect experimentally. The errors would be most likely to occur for slowly eluting, badly tailed peaks, because the slow return to the true baseline could easily be mistaken for detector drift. Such problems have been encountered in affinity chromatographic measurement of kinetically slow biomolecular interactions. Peaks with $B/A_{0.1}$ ~5 eluted over a several hour time period and the final baseline could not be determined with any certainty.

Summation methods

Figure 3 shows the errors in M_0, M_1, and M_2 from the summation method. When the baseline error was small (0.1 %), the errors in M_0 and M_1 were quite small, but the error in M_2 was as large as -9 % for the most tailed peak. This problem is discussed in more detail in a later section. The errors for all three moments increased as the baseline error and τ/σ_G

Figure 3. Plots of percent error in the various moments for the summation (a-c) and Yau (d) methods. Sloping baseline errors of 0.1 % (□), 1 % (■), 2.5 % (X), 5 % (◇), and 10 % (◆), were used. The dotted lines indicate 0 % error in the moments

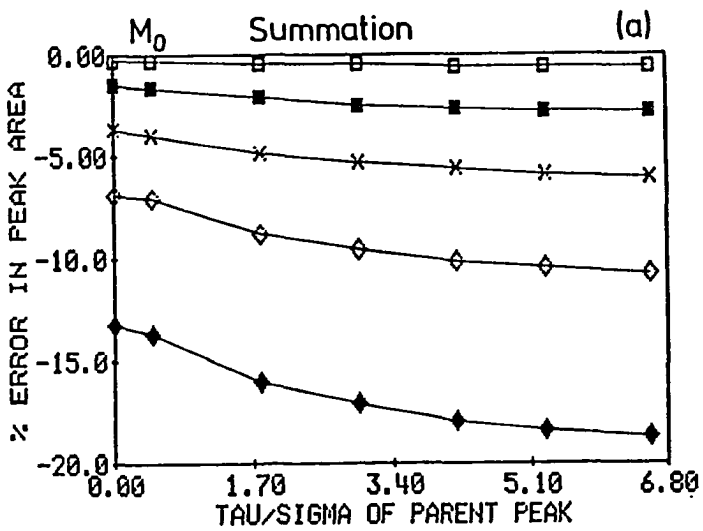
M0 Summation
(a)
0.00
-5.00
-10.0
-15.0
-20.0
% ERROR IN PEAK AREA
0.00
1.70
3.40
5.10
6.80
TAU/SIGMA OF PARENT PEAK

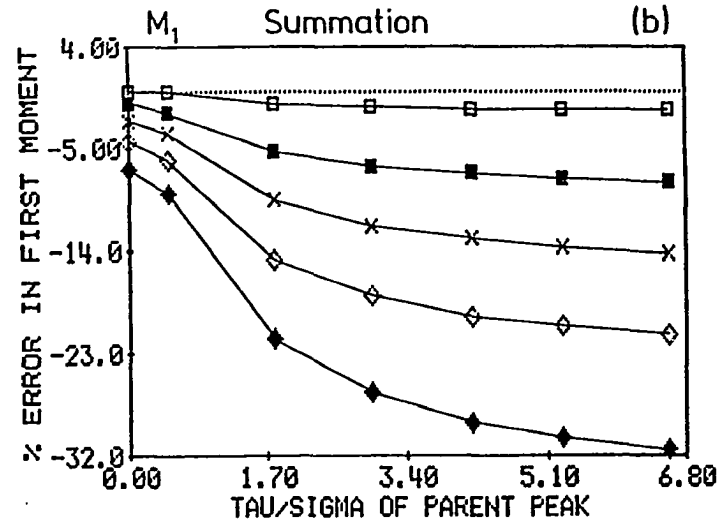
M1 Summation
(b)
4.00
-5.00
-14.0
-23.0
-32.0
% ERROR IN FIRST MOMENT
0.00
1.70
3.40
5.10
6.80
TAU/SIGMA OF PARENT PEAK

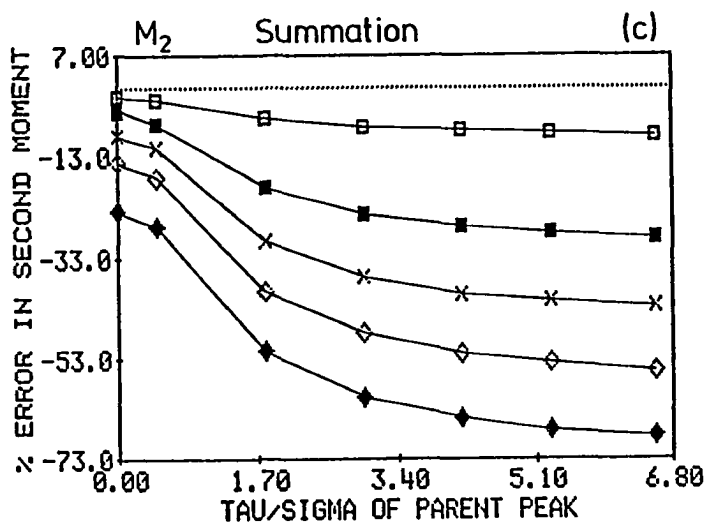
M2 Summation
(c)
7.00
-13.0
-33.0
-53.0
-73.0
% ERROR IN SECOND MOMENT
0.00
1.70
3.40
5.10
6.80
TAU/SIGMA OF PARENT PEAK

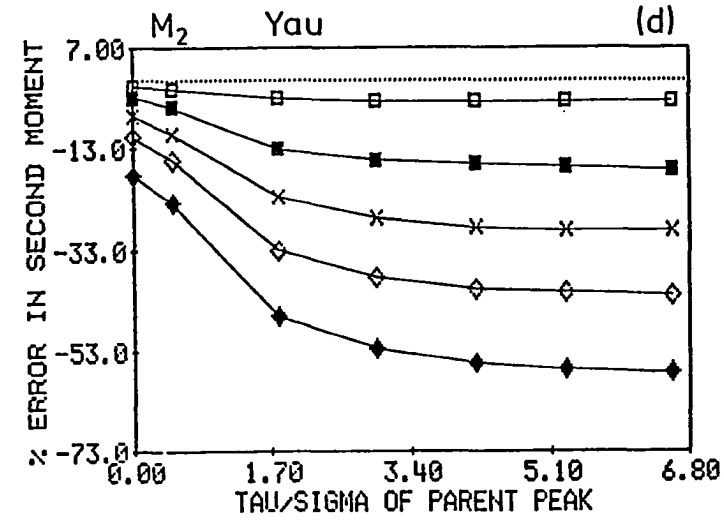
M2 Yau
(d)
7.00
-13.0
-33.0
-53.0
-73.0
% ERROR IN SECOND MOMENT
0.00
1.70
3.40
5.10
6.80
TAU/SIGMA OF PARENT PEAK

increased. The error in the peak area was moderate, being as great as -19 %. It is well-known that the higher moments are increasingly sensitive to the area in the tail of the peak (1), thus the errors in M_1 and M_2 were as great as -32 and -69 %, respectively. A -69 % error means that the measured M_2 was only one-third of its true value. These percentages should be kept in mind when comparing the alternative methods below. Note also that, for easy comparison, all of the figures showing errors in M_1 are drawn to the same scale, as are all of the figures for M_2.

Yau method

This method for the calculation of M_2 was designed to be less sensitive to the area in the tail of the peak because only zero-th and first moments were calculated (15). Two of these moments, M_{0-} and M_{1-}, were calculated for the beginning portion of the peak, in which the baseline errors were small. Thus, significantly less error in M_2 was expected from this method compared to the summation method. When the baseline error was small (0.1 %), the maximum error decreased to -4 % (Figure 3d). However, for the largest baseline errors, the error was as great as -58 %, i.e., not much better than the summation methods. The reason for this was found to be errors in M_1. When the true value of M_1 was used instead of the measured value, M_2 was only in error by +13 % or less.

Gaussian approximation

This method led to very large errors in M_1 and M_2 for badly tailed peaks, in agreement with the work of others (2,3). The errors in M_1 and M_2 were as great as -75 and -83 %, respectively. Neither moment, however, was significantly affected by baseline error. For example, for $\tau/\sigma_G=0$, the errors in M_1 and M_2 ranged from 0 to -2 % and 0 to -9 %, respectively, and for $\tau/\sigma_G=6.6$, the error was -75 % for all M_1 values and ranged from -81 to -83 % for M_2. This resulted from the fact that t_p and $W_{0.5}$ were not affected very much by the baseline errors.

Foley and Dorsey methods

These methods, although designed for manual calculation of moments (12), were easily adapted for computer calculations by fitting certain portions of the peak to quadratic or linear equations. The great advantage of these methods is that, if the detector baseline is assumed to be constant, the peak can be truncated as soon as the response has decreased to less than 10 % (or 50 %) of the maximum peak height. Some caution should be used in applying these methods to real data, particularly with regard to fitting the top portion of the peak. Noise, peak asymmetry, and the number of points fitted can affect the accuracy and precision of the methods (3,10).

The methods are, however, simpler and more reliable than total peak-fitting methods (8,9).

Figure 4 shows the errors in M_1 and M_2 for both the $B/A_{0.1}$ and $B/A_{0.5}$ methods. Foley and Dorsey fitted the equations for τ/σ_G up to 3.0. Above this value, the errors in the moments rapidly increased, even for small baseline errors, due to the quadratic or cubic nature of the equations for M_2.

For $\tau/\sigma_G \leq 3$ and for small baseline errors, excellent values for M_2 were obtained and somewhat poorer values for M_1, particularly for the peak with $\tau/\sigma_G=0$. Foley and Dorsey (12) reported that the error in M_1 should be less than ± 1 % when calculated from the $B/A_{0.1}$ method. When calculated as the error in M_1 relative to the true value of M_1, this was indeed the case, but when calculated according to Equation 18 the error was much larger.

To compare with the summation method, consider the maximum errors in M_1 and M_2 for $\tau/\sigma_G=3$. The errors were -27 and -61 %, respectively, for the summation method. For the $B/A_{0.1}$ method, the errors declined to -22 and -41 %, respectively. For the $B/A_{0.5}$ method, the errors decreased to -7 and -18 %. Thus, the $B/A_{0.1}$ method was somewhat better than the summation method, and the $B/A_{0.5}$ method was far superior to all of the others. The better accuracy of the $B/A_{0.5}$ method was related to the earlier observations that t_p and $W_{0.5}$ were almost unaffected by the baseline errors.

Figure 4. Plots of percent error in the moments for the $B/A_{0.1}$ (a,b) and $B/A_{0.5}$ (c,d) methods. The symbols are the same as in Figure 3. The vertical line at $\tau/\sigma_G = 3$ represents the upper limit specified by Foley and Dorsey (12) for the equations used in the calculations

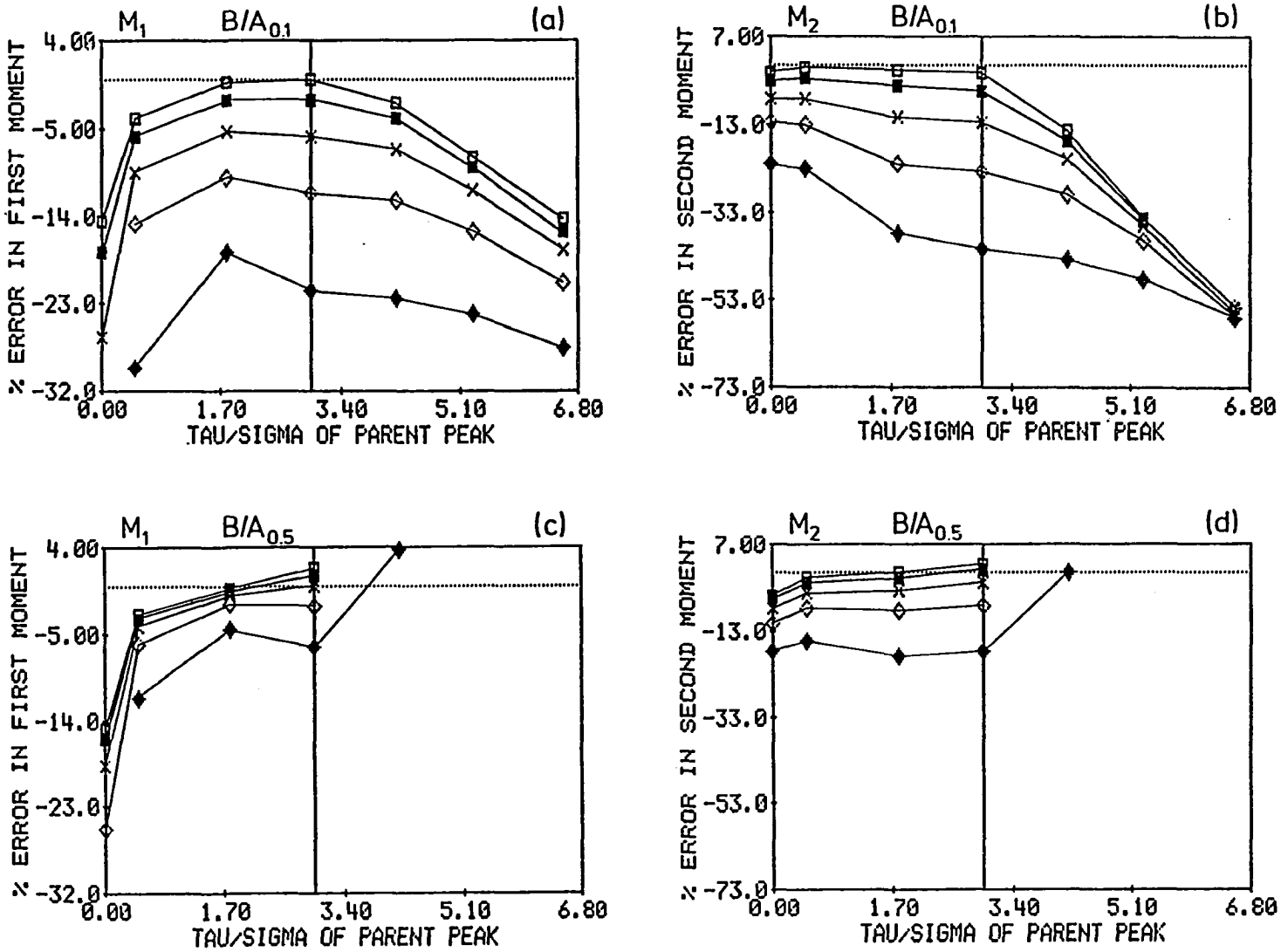
M1 B/A0.1 (a)
4.00
-5.00
-14.0
-23.0
-32.0
% ERROR IN FIRST MOMENT
0.00
1.70
3.40
5.10
6.80
TAU/SIGMA OF PARENT PEAK
M2 B/A0.1 (b)
7.00
-13.0
-33.0
-53.0
-73.0
% ERROR IN SECOND MOMENT
0.00
1.70
3.40
5.10
6.80
TAU/SIGMA OF PARENT PEAK
M1 B/A0.5 (c)
4.00
-5.00
-14.0
-23.0
-32.0
% ERROR IN FIRST MOMENT
0.00
1.70
3.40
5.10
6.80
TAU/SIGMA OF PARENT PEAK
M2 B/A0.5 (d)
7.00
-13.0
-33.0
-53.0
-73.0
% ERROR IN SECOND MOMENT
0.00
1.70
3.40
5.10
6.80
TAU/SIGMA OF PARENT PEAK

Unfortunately, this method worked properly only over a relatively narrow range of τ/σ_G.

Modifications of the $B/A_{0.1}$ and $B/A_{0.5}$ Methods

The Foley and Dorsey equations (12) were very useful, but the τ/σ_G upper limit of 3 limited the general utility of the equations. A second problem was that M_1 was calculated indirectly via equations for M_2, σ_G, and t_G. In some cases when τ/σ_G was greater than 3, σ_G was greater than $\sqrt{M_2}$, so τ and M_1 could not be calculated. Thus, it would be desirable to calculate both M_1 and M_2 directly from experiment data and to have the eqations work over a wider range of τ/σ_G.

To obtain a set of empirical equations, the parent EMG peaks were generated using a time interval of 0.0001 seconds between the points so that the peak parameters could be calculated very precisely. Then, the following plots were made: (A) $W_{0.1}{}^2/M_2$, $(M_1-t_p)/W_{0.1}$, and $\sigma_G/W_{0.1}$ versus $B/A_{0.1}$; (B) $W_{0.5}{}^2/M_2$, $(M_1-t_p)/W_{0.5}$, and $\sigma_G/W_{0.5}$ versus $B/A_{0.5}$. These were all monotonically increasing or decreasing functions which flattened out at large values of B/A, so an attempt was made to fit the equations to exponential and inverse functions. The best fits are given in Tables IIa and IIb, along with the maximum error range for the points tested. All the peak parameters could be calculated with good accuracy.

Table IIa. Modified equations for the $B/A_{0.1}$ method[a]

Equations	Maximum error range[b] (%)	Maximum error range[c] (%)
$M_1 = t_p + W_{0.1}(0.306-0.490\exp(-0.475 \cdot B/A_{0.1}))$	-0.2,+0.1[d]	-0.03,+0.04[e]
$M_2 = W_{0.1}^2/(7.35+22.6\exp(-0.708 \cdot B/A_{0.1}))$	-0.7,+1.0	-0.9, +1.1
$\sigma_G = W_{0.1}/(3.38 \cdot B/A_{0.1} + 0.969)$	-1.3,+1.6	-0.7, +2.3
$\tau = \sqrt{M_2 - \sigma_G^2}$	-4.0,+0.4[f]	-6.6, +0.7
$t_G = M_1 - \tau$	-0.6,+0.1	-0.03,+0.08[e]

[a]Fits were performed using a program called NLLSQ (17).

[b]Calculated for the points in Table I relative to the true values.

[c]Calculated relative to the Foley and Dorsey equations (12) over the range $B/A_{0.1}$ = 1.10 - 2.76 at intervals of 0.02.

[d]Calculated from Equation 18.

[e]For t_p = 20 and $W_{0.1}$ or $W_{0.5}$ = 1.

[f]Excluding τ = 0.

Table IIb. Modified equations for the $B/A_{0.5}$ method[a]

Equations	Maximum error range [b] (%)	Maximum error range [c] (%)
$M_1 = t_p + W_{0.5}(0.925-2.17\exp(-0.848 \cdot B/A_{0.5}))$	-0.1, +0.1[d]	-0.12, +0.05[e]
$M_2 = W_{0.5}^2/(1.06+54.0\exp(-2.49 \cdot B/A_{0.5}))$	-4.1, +4.0	-4.7, +3.8
$\sigma_G = W_{0.5}/(2.58 \cdot B/A_{0.5} - 0.151)$	-3.1, +3.2	+0.3, +2.7
$\tau = \sqrt{M_2 - \sigma_G^2}$	-3.7, +4.6[f]	-3.4, -1.0
$t_G = M_1 - \tau$	-1.0, +0.4	-0.09, +0.07[e]

[a] Fits were performed using a program called NLLSQ (17).

[b] Calculated for the points in Table I relative to the true values.

[c] Calculated relative to the Foley and Dorsey equations (12) over the range $B/A_{0.1}$ = 1.10 - 2.76 at intervals of 0.02.

[d] Calculated from Equation 18.

[e] For t_p = 20 and $W_{0.1}$ or $W_{0.5}$ = 1.

[f] Excluding τ = 0.

M_1 was fitted particularly well by the equations. Both the equations for σ_G were similar to those of the Foley and Dorsey equations (12). The maximum percent errors were similar to those of the Foley and Dorsey equations (12), but the modified equations covered a much wider range of τ/σ_G. This is further shown by Figure 5, where the modified $B/A_{0.1}$ equation for M_2 is plotted in comparison with that of Foley and Dorsey. The advantage of a monotonic fitting equation is apparent. It is likely that the modified equations are fairly accurate beyond the maximum values tested.

Foley and Dorsey used 51 points to fit the region of $B/A_{0.1}$=1.09 to 2.76 (12). The authors of the present work had only 3 points in this region. To ensure that fits were sufficiently accurate over this region, the various peak parameters were calculated according to both the authors' equations of the present work and the Foley and Dorsey equations at B/A intervals of 0.02 over this range. The last columns in Tables IIa and IIb show that the maximum errors were not significantly affected, i.e., the points fitted were sufficient to define the curves.

Using the equations in Table IIa and IIb, the simulated data with the sloping baseline errors were again examined. Figure 6 shows that when the baseline error was small, both M_1 and M_2 were calculated with excellent accuracy by both B/A methods. For large baseline errors, the $B/A_{0.1}$ method gave

Figure 5. Plot of $W_{0.1}{}^2/M_2$ versus $B/A_{0.1}$ calculated from the Foley and Dorsey $B/A_{0.1}$ equation (upper curve) and the modified $B/A_{0.1}$ equation of Table IIa (lower curve). The vertical line marks the upper limit specified for the Foley and Dorsey equation. The points used in the fitting procedure for the modified equation are also shown (■)

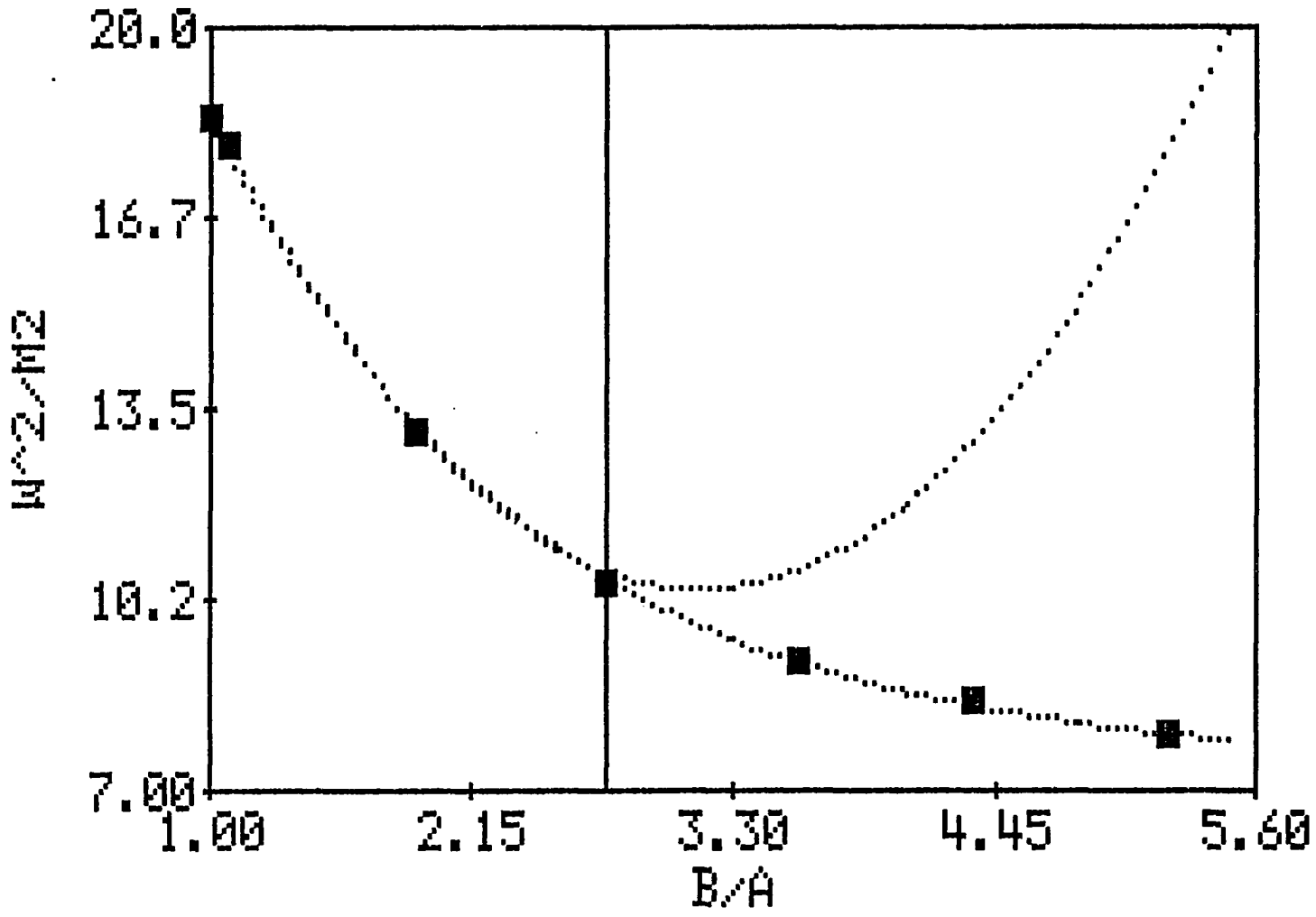
20.0
16.7
13.5
10.2
7.00
w^2/M2
1.00
2.15
3.30
4.45
5.60
B/A

Figure 6. Plots of percent error in the moments for the modified $B/A_{0.1}$ (a,b) and modified $B/A_{0.5}$ (c,d) methods. The symbols are the same as in Figure 3

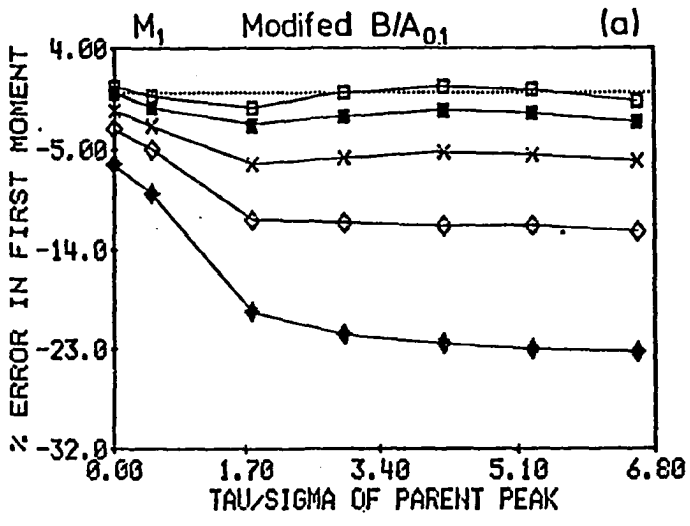
M1 Modifed B/A01
(a)
4.00
-5.00
-14.0
-23.0
-32.0
% ERROR IN FIRST MOMENT
0.00
1.70
3.40
5.10
6.80
TAU/SIGMA OF PARENT PEAK

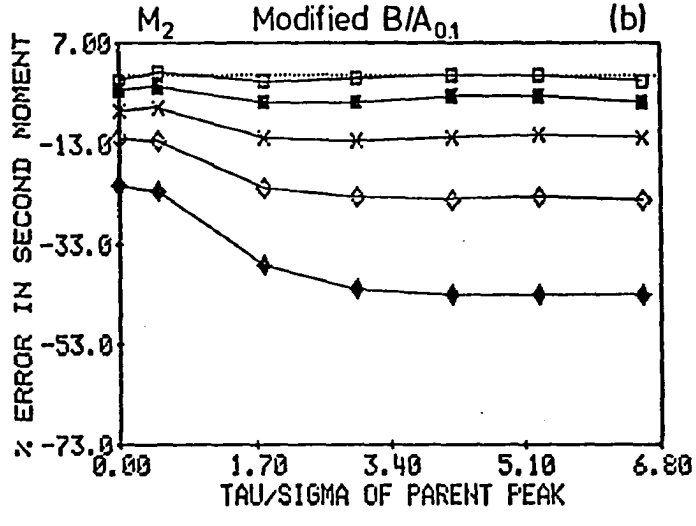
M2 Modified B/A01
(b)
7.00
-13.0
-33.0
-53.0
-73.0
% ERROR IN SECOND MOMENT
0.00
1.70
3.40
5.10
6.80
TAU/SIGMA OF PARENT PEAK

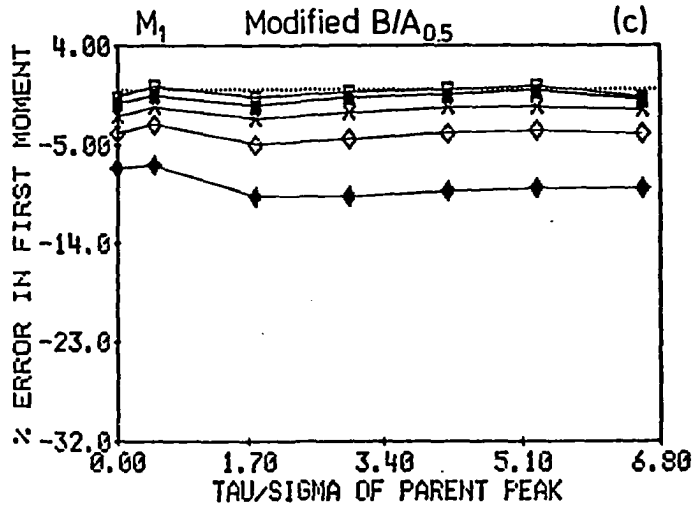
M1 Modified B/A05
(c)
4.00
-5.00
-14.0
-23.0
-32.0
% ERROR IN FIRST MOMENT
0.00
1.70
3.40
5.10
6.80
TAU/SIGMA OF PARENT PEAK

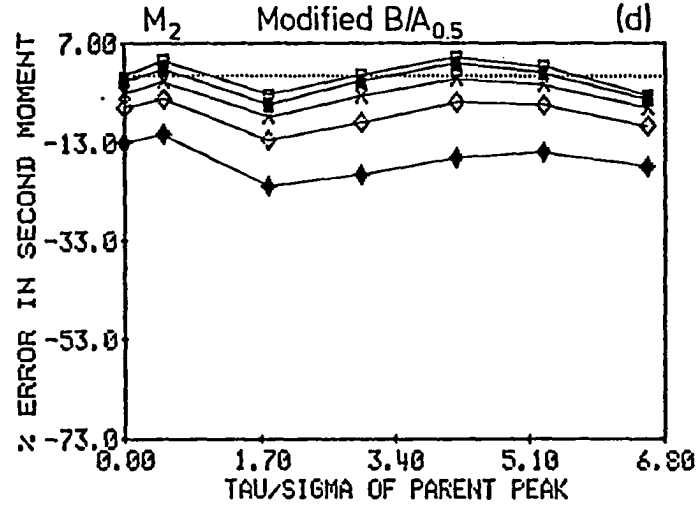
M2 Modified B/A05
(d)
7.00
-13.0
-33.0
-53.0
-73.0
% ERROR IN SECOND MOMENT
0.00
1.70
3.40
5.10
6.80
TAU/SIGMA OF PARENT PEAK

errors in M_1 and M_2 as great as -23 and -43 %, respectively. These errors were less than for the summation method, but still quite large. The $B/A_{0.5}$ method gave errors in M_1 and M_2 as great as -10 and -22 %, respectively. This was clearly a major improvement over the other methods.

Foley and Dorsey recommended using their $B/A_{0.1}$ method rather than their $B/A_{0.5}$ method for several reasons (12). One important reason was that the precision of the measurements at $B/A_{0.5}$ may be poorer (12). In particular, a small error in locating t_p could cause much greater errors in the $B/A_{0.5}$ ratio and in the calculated moments. Nevertheless, the present study indicated that if baseline errors occur, the $B/A_{0.5}$ method may give more accurate, though possibly less precise, results than the $B/A_{0.1}$ method. The $B/A_{0.5}$ method would also be less affected by impurities eluting in the tail of the peak.

Because all of these methods can be easily programmed into a small computer, the use of two or three different methods to examine experimental data is recommended. Comparison of the results could indicate whether any baseline or peak shape problems are occurring.

Errors in N

The error in the number of plates calculated according to Equation 4 depended upon the arbitrary value of t_G chosen.

When M_1 and t_G were much greater than the width of the peak, almost all of the error in N was due to M_2. Thus, the negative errors in M_2 observed in most cases would cause corresponding positive errors in N.

Horizontal Baseline Errors

Some errors in the calculated second moment were observed for the summation method, even when the corrected baseline was set at 0.1 % of the maximum peak height (Figure 3c). The error increased as τ/σ_G increased. Two problems were actually occurring. Firstly, some of the data in the leading and trailing edges of the peaks were lost because of the choice of the beginning and ending points. This problem has been examined by others (2,5,6). Secondly, the establishment of the corrected baseline slightly above the true baseline caused an additional error in the remaining data. This duplicated the experimental situation in which one would generally assign to the start and stop points a detector response of 0. This problem was examined further for a peak with $\tau/\sigma_G=3$ by setting baselines at 0.001, 0.01, and 1.0 % of the maximum peak height on both sides of the peak, i.e., horizontal baseline errors. As Table III shows, M_2 calculated by the summation method was particularly sensitive to such errors, with the error in M_2 being as great as -26 % for a 1 % baseline error. Use of the

Table III. Effect of horizontal baseline errors for a peak with $\tau/\sigma_G = 3$

Baseline error[a] (%)	Method			
	Summation	Yau	Modified $B/A_{0.1}$	Modified $B/A_{0.5}$
	Error in M_1[b] (%)			
0.001	0.0	-	+0.2	-0.4
0.01	-0.3	-	+0.2	-0.4
0.1	-1.4	-	0.0	-0.4
1.0	-6.9	-	-2.5	-1.3
	Error in M_2 (%)			
0.001	-0.3	-0.1	+0.1	+0.6
0.01	-1.6	-0.7	+0.1	+0.5
0.1	-7.4	-3.6	-0.6	+0.3
1.0	-26.1	-17.0	-6.8	-2.1

[a]Baseline set at the given percentage of maximum peak height on both sides of peak.

[b]Calculated according to Equation 18.

B/A methods decreased the errors by a factor of three or more.

From an experimental standpoint, this is a very important problem. Noise and detector drift frequently lead to uncertainties in the baseline of 0.1 to 1 % or even more. Also, the computer data acquisition system may limit the precision of the data. Many such systems record the data with a precision of 12 bits, i.e., one part in 4096. Thus, the data acquisition system can cause baseline errors of more than 0.02 %, even in the most favorable case where the peak covers the full range of the analog-to-digital converter. If the peak does not cover this full range, the error in the baseline can easily be 10- to 100-fold larger.

In summary, it has been shown that empirical equations based on B/A ratios can significantly improve the accuracy of peak moment calculations for tailed peaks when errors in locating the baseline occur. By curve fitting of portions of the peaks, these calculations can be conveniently performed on a small computer.

ACKNOWLEDGEMENT

The authors gratefully acknowledge the support of the National Science Foundation under Grant CHE-8305057.

REFERENCES CITED

1. Grushka, E.; Myers, M. N.; Schettler, P. D.; Giddings, J. C. Anal. Chem. 1969, 41, 889.

2. Kirkland, J. J.; Yau, W. W.; Stoklosa, H. J.; Dilks, C. H. J. Chromatogr. Sci. 1977, 15, 303.

3. Pauls, R. E.; Rogers, L. B. Sep. Sci. 1977, 12, 395.

4. Petitclerc, T.; Guiochon, G. J. Chromatogr. Sci. 1976, 14, 531.

5. Chesler, S. N.; Cram, S. P. Anal. Chem. 1971, 43, 1922.

6. Rony, P. R.; Funk, J. E. J. Chromatogr. Sci. 1971, 9, 215.

7. Gladney, H. M.; Dowden, B. F.; Swalen, J. D. Anal. Chem. 1969, 41, 883.

8. Anderson, A. H.; Gibb, T. C.; Littlewood, A. B. J. Chromatogr. Sci. 1970, 8, 640.

9. Chesler, S. N.; Cram, S. P. Anal. Chem. 1973, 45, 1354.

10. Foley, J. P.; Dorsey, J. G. J. Chromatogr. Sci. 1984, 22, 40.

11. Grushka, E. Anal. Chem. 1972, 44, 1733.

12. Foley, J. P.; Dorsey, J. G. Anal. Chem. 1983, 55, 730.

13. Abromowitz, M.; Stegun, I. A., Eds. "Handbook of Mathematical Functions with Formulas, Graphs and Mathematical Tables"; U. S. Govt. Print. Off.: Washington, D. C., 1964; p. 932.

14. Zehna, P. W. "Probability Distributions and Statistics"; Allyn and Bacon: Boston, 1970; p. 156.

15. Yau, W. W. Anal. Chem. 1977, 49, 395.

16. Karger, B. L.; Snyder, L. R.; Horvath, C. "An Introduction to Separation Science"; John Wiley and Sons: New York, 1973; p. 137.

17. Christian, S. D.; Tucker, E. E. Am. Lab. 1982, 14(9), 31.

SECTION II.

AFFINITY CHROMATOGRAPHIC EXAMINATION OF A RETENTION MODEL FOR MACROMOLECULES

SUMMARY

Plots of log k' versus log (1/[mobile phase modifier]) were made for a monovalent and a divalent solute using affinity chromatography. Some of the plots were curved and all exhibited slopes (Z values) of less than the theoretical integer values. It was shown that this was an expected result when lower forms of the solute were present, e.g., a divalent solute adsorbed monovalently.

INTRODUCTION

The retention of macromolecules on various chromatographic stationary phases is a subject of considerable fundamental and practical interest. Knowledge of the mechanism of retention aids in the design of stationary phases with improved selectivity and in the choice of appropriate elution conditions. Several authors have described models for the retention of macromolecules in ion-exchange (1-4), reversed-phase (5-8), and hydrophobic interaction (9-11) chromatography. A parameter in many of these models is the number of sites on the surface of the macromolecule which adsorb to the stationary phase. Unfortunately, this number is seldom known from independent measurements, so, the models are difficult to verify.

Affinity chromatography provides a means to examine some aspects of these retention models, since the stoichiometry and the binding constants between stationary phase ligand, analyte, and mobile phase modifier are sometimes known when competitive elution is used (12-15).

The model of interest here has been widely utilized for small solutes and, more recently, by Regnier and co-workers for ion-exchange (3,4) and reversed-phase (8) chromatography of proteins. In analogy with Regnier's work, we write the

adsorption process as:

$$EI_z + Z \cdot L \rightleftharpoons EL_z + Z \cdot I \qquad (1)$$

where E is the macromolecule, I is the mobile phase modifier (inhibitor), and L is the immobilized ligand. One can then derive an equation for the capacity factor, k':

$$\log k' = \log c + Z\log(1/[I]) \qquad (2)$$

where c is a constant involving the equilibrium constant for Reaction 1, the concentration of immobilized ligand, and the phase ratio. A plot of log k' versus log $(1/[I])$ should have a slope equal to Z, the number of sites of adsorption (3). This will be referred to as a log k' plot in this paper.

In affinity chromatography, E usually contains 1-4 binding sites. Steric considerations generally limit Z to no more than 2. In this study, the validity of Equation 2 was examined using concanavalin A (Con A) and various sugars.

EXPERIMENTAL

Reagents

Con A (type IV), bovine serum albumin (BSA), D(+)-glucosamine hydrochloride, p-aminophenyl α-D-mannopyranoside (PAPM), p-nitrophenyl α-D-mannopyranoside (PNPM), 4-methylumbelliferyl α-D-mannopyranoside (MUM), methyl α-D-mannopyranoside (MDM, grade III), and 1-ethyl-3-(3-dimethylaminopropyl) carbodiimide hydrochloride (EDC) were obtained from Sigma (St. Louis, MO). Orcinol monohydrate, succinic anhydride, and 1,1'-carbonyldiimidazole (CDI) were obtained from Aldrich (Milwaukee, WI). The 10-μm LiChrospher SI 500 was obtained from Rainin (Woburn, MA). All other chemicals were reagent grade. Dioxane and acetonitrile were stored over molecular sieves.

Con A was further purified according to the procedure of Cunningham et al. (16), with two exceptions: dialysis of the Con A supernatant was against the mobile phase sodium acetate buffer instead of water and no lyophilization was done. Orcinol was purified according to the following procedure: 50 g of orcinol was dissolved in 100 ml of boiling water. The solution was cooled to room temperature and the white crystals were filtered and then washed with ice-cold water on a medium porosity glass filter. The filtrate was concentrated to

one-third volume and then the recrystallization procedure repeated. The crystals were vacuum-dried at room temperature.

Apparatus

A Model 344 gradient liquid chromatograph (Beckman, Berkeley, CA) and a V^4 variable-wavelength absorbance detector (ISCO, Lincoln, NE) were used. Data were collected and processed on an Apple IIe computer via an ADALAB interface board (Interactive Microware, State College, PA). A magnetic switch (Radio Shack) was attached to the injector to automatically initiate data collection. Columns were of a published design (17), with the outer connector modified as a water jacket. Column temperature was controlled by a Lauda K-2/RD refrigerated circulator (Brinkmann, Westbury, NY).

A 100-W ultrasonic cleaner (Fisher, St. Louis, MO) and a wrist-action shaker (Burrell, Pittsburgh, PA) were used for the stationary phase preparation. A Haskel air-driven pump (Alltech, Deerfield, IL) and a Model 705 stirred-slurry column packer (Micromeritics, Norcross, GA) were used for column packing.

Stationary Phase Preparation

A CDI activation method (18) was used for the immobilization of PAPM. Diol-bonded LiChrospher SI 500 was prepared as described earlier (19). An amount of 2.0 g of diol-bonded silica was activated by addition of 0.96 g CDI in 16 ml anhydrous acetonitrile, sonicated under vacuum for 10 minutes, and shaken for an additional 30 minutes at room temperature. The activated silica was washed with anhydrous acetonitrile and suction-dried over a medium porosity glass filter. To each of two test tubes was added 1 g activated silica, 4 ml of 0.1 M sodium phosphate buffer, pH 7, and 81 mg or 10 mg of PAPM. This reaction mixture was sonicated under vacuum for 10 minutes, flushed with nitrogen, stoppered, and shaken at room temperature for 48 hours. The silica was washed with 2 M sodium chloride and water.

A CDI activation procedure was also used for the immobilization of Con A with the following changes in the above procedure: to 2.0 g LiChrospher SI 500 diol was added 0.64 g CDI and 25 ml acetonitrile. Sonication time for the activation step was 20 minutes. For immobilization of Con A, 10 ml of 3.4 mg/ml purified Con A in sodium acetate buffer (buffer composition was the same as the mobile phase described below, with no MDM) was added to 2 g of activated silica. Sonication was performed for 15 minutes under conditions in

which a vacuum was repeatedly applied and released, so that the solution did not foam excessively. Flushing the sample with nitrogen was not necessary. The solution was shaken for five days at 4 °C.

An ester-amide (EA) activation procedure (20) was used for the immobilization of glucosamine. To 1.5 g of LiChrospher SI 500 diol was added 0.38 g of succinic anhydride in 75 ml of anhydrous dioxane. The reaction was allowed to proceed for 24 hours at room temperature with shaking. The carboxylated silica was then collected on a medium porosity glass filter and washed with several warm and room temperature portions of anhydrous dioxane, and dried under vacuum. An 8 ml volume of 0.1 M glucosamine in 0.1 M sodium phosphate (pH 7) solution and 0.154 g EDC were added to 0.61 g of carboxylated silica. This reaction mixture was sonicated under vacuum for five minutes, flushed with nitrogen, stoppered, and shaken for 24 hours. The glucosamine silica was then filtered, washed with 0.1 M sodium phosphate buffer (pH 7), water, and methanol.

Assay of Immobilized Ligands

All silica samples used in the assays were vacuum-dried at room temperature. PAPM silica samples were assayed by an orcinol method (21), which was adapted to silica samples, as

described below. The orcinol reagent consisted of 0.5 g of recrystallized orcinol dissolved in 1 L of 70 % v/v sulfuric acid and was stored in a brown bottle. Orcinol reagent (5.0 ml), aliquots of standard PAPM solutions or silica samples, and additional water to bring total volume to 5.5 ml were added to test tubes. Sample and standards were sonicated for 10 minutes and allowed to sit for an additional five minutes. The test tubes were heated in boiling water for 10 minutes, cooled, and the absorbance of the solution measured at 420 nm. Silica-containing samples were centrifuged and decanted prior to absorbance measurements. Analyses of the glucosamine silica and Con A-silica were by the alkaline ferricyanide (22) and Lowry et al. (23) methods, respectively. The results of the analyses are summarized in Table I.

Chromatography

Pertinent chromatographic conditions for each column are summarized in Table I. All columns were packed at 3000 p.s.i. using the acetate buffer described below and stored at 4 °C when not in use.

Chromatography was performed with the column thermostated at 25.0 °C. The mobile phase consisted of a 0.5 M sodium acetate buffer, pH 5.0, containing 1.00 mM calcium chloride and manganese chloride, and MDM of various concentrations.

Table I. Chromatographic conditions

Column Number	Immobilized Ligand	Conc. Immobilized Ligand Sites[a] (μmoles/m^2)	Column Parameters I.D. (mm)	Column Parameters Length (mm)	Analyte	Analyte Conc.	Amount Injected (μL)
1	PAPM	0.98	4.6	45.0	Con A	4 mg/ml	10
2	PAPM	0.28	4.6	50.0	Con A	4 mg/ml	10
3	Glucosamine	0.73	4.1	50.3	Con A	.06 mg/ml	10
4	Con A	0.012	4.1	100.0	MUM	6 μM	20
					PNPM	5 μM	20

[a]Based on ligand assays and manufacturer's (E. Merck, Darmstadt, G. F. R.) estimates of surface area.

The pH was adjusted with hydrochloric acid. The flowrate was 1.0 ml/min. Samples were pre-equilibrated with the mobile phase. The detector wavelength was 280 nm for Con A, uracil, sodium nitrate, and BSA; 316 nm for MUM; and 305 nm for PNPM.

Statistical moments of the peaks were determined by the modified $B/A_{0.1}$ and $B/A_{0.5}$ methods (24). Samples of either 4.6 mg/ml sodium nitrate, 16 µg/ml uracil, or 90 µg/ml BSA were injected and the first moment was taken to be the void time. The capacity factor (k') was calculated from the first moments of the peaks.

RESULTS AND DISCUSSION

The conditions of pH and ionic strength were chosen such that Con A would be present primarily in the form of a dimer (25), with two identical binding sites (26). With Con A as analyte, one would expect Z values of 1-2, depending on the surface density of sugar ligands and other steric effects. With monovalent sugars used as analytes and immobilized Con A, one would expect Z = 1.

The Z values were determined for the five systems given in Table I. Plots of log k' versus log $(1/[I])$ are shown in Figure 1. The plots for the immobilized PAPM columns were linear. The Z value for the high-coverage PAPM column was 1.8, indicating primarily divalent binding. The Z value decreased to 1.5 on the low-coverage column, indicating that divalent binding occurred less frequently as the surface concentration of ligand decreased.

The remaining three studies yielded non-linear plots. Not shown in Figure 1 are three points measured at $[I] = 0$, which clearly indicated that all three curves flattened out at large log $(1/[I])$. The high-coverage glucosamine column had a slope of only 0.7 in the linear portion of the curve, even though the surface concentration of ligand was comparable to the PAPM columns. The Z values for two analyte sugars on the Con A column were also significantly less than the expected

Figure 1. Affinity chromatographic retention data. The slope of the fitted line is given in parentheses after the column number (see Table I): 1 (1.8, ■); 2 (1.5, ◆); 3 (0.7, ▲); 4-MUM (0.6, +); and 4-PNPM (0.6, ●)

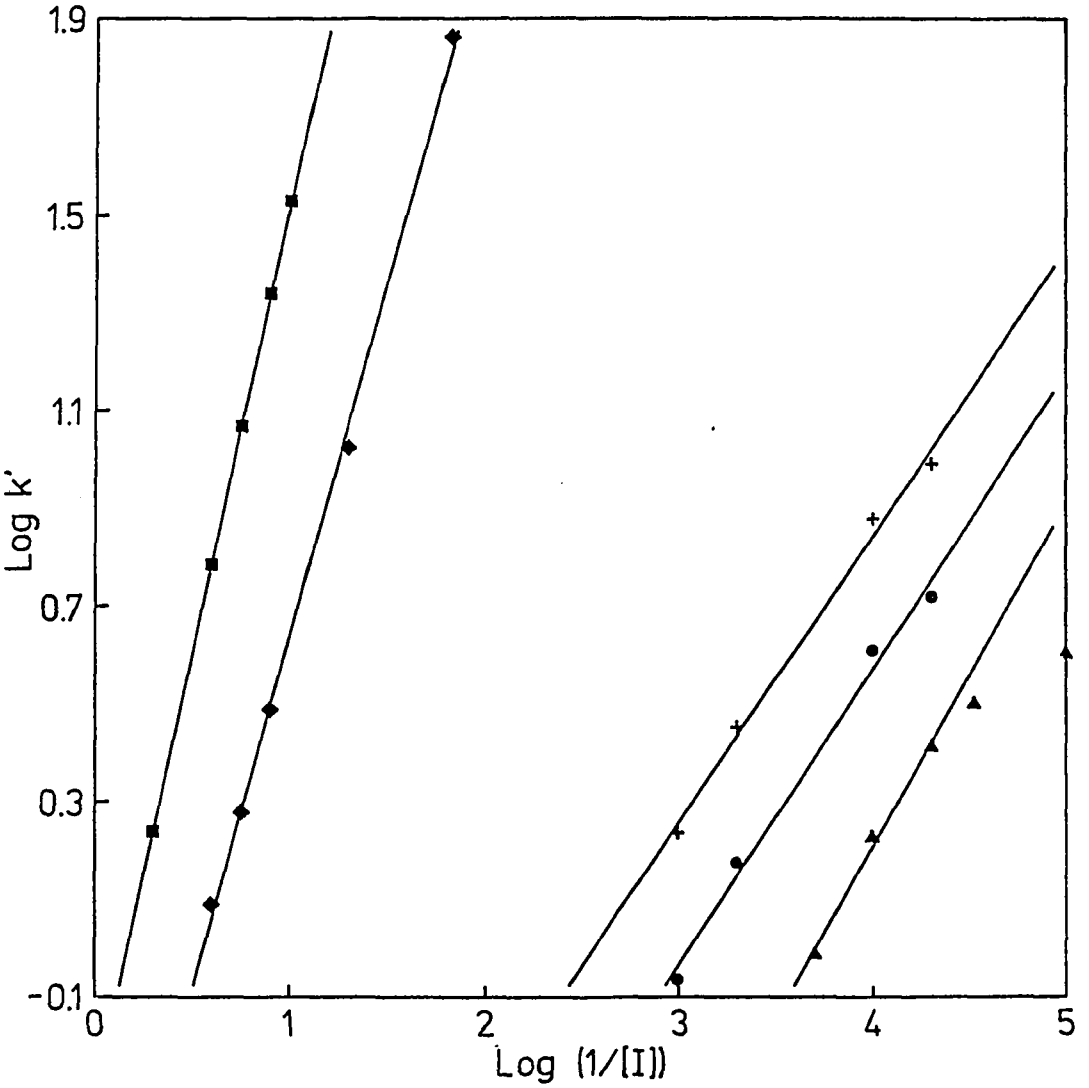
1.9
1.5
1.1
0.7
0.3
-0.1
Log k'
0
1
2
3
4
5
Log (1/[I])

value of one. These discrepancies and the curvature of the plots were, as will be shown below, due to limitations of the model used to derive Equation 2.

The data were also plotted according to the empirical relationship used by Stadalius et al. (7) for reversed-phase chromatography (log k' versus [I]). All of these plots exhibited considerable curvature. Thus, such plots appear to have little practical or fundamental use in affinity chromatography.

Modification of the Model

Examination of Reaction 1 indicates that a limitation of the model is likely to be the presence of other forms of the analyte, such as E, EI, and LEI. For the biochemical system used here, it is possible to experimentally determine how these lower forms affect the log k' plots.

Figure 2 shows the many different equilibria that can occur in a divalent system. Listed below are the equilibrium constants that govern the equilibria:

$$K_2 = \frac{[EI]}{[E][I]} = \frac{[EI_2]}{[EI][I]} = \frac{\{LEI\}}{\{EL\}[I]} \qquad (3)$$

$$K_3 = \frac{\{EL\}}{[E]\{L\}} = \frac{\{LEI\}}{[EI]\{L\}} \qquad (4)$$

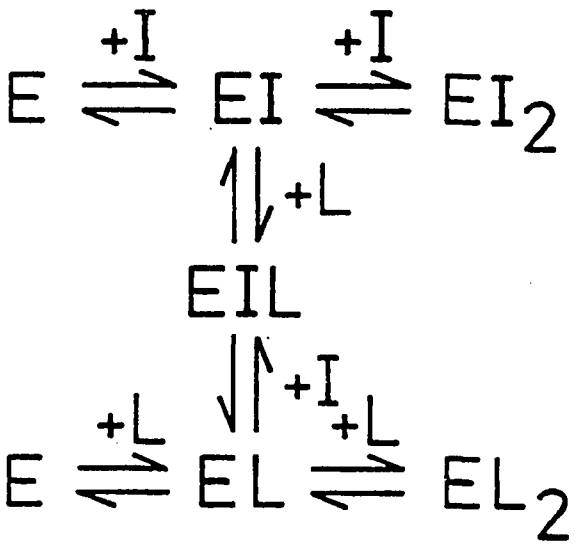

Figure 2. Equilibria in a competitive-binding affinity chromatograpic system, in which the solute (E) is divalent and the ligand (L) and mobile phase modifier (I) are monovalent

$$K_4 = \frac{\{EL_2\}}{\{EL\}\{L\}} \tag{5}$$

The {} represents a surface concentration (mol/dm^2). An assumption made in Equation 3 is that the two binding sites are identical, even when E is adsorbed, and, hence, K_2 is the same for the binding of I to either E, EI, or EL. Note that K_2 and K_3 have units of L/mol, while K_4 has units of dm^2/mol. K_4 is expected to be highly sensitive to steric effects. Also, since the immobilized ligand sites are not likely to be perfectly uniformly distributed, K_4 is an "average" divalent binding constant.

From the definition of k' one can write:

$$k' = \frac{A}{V_m} \frac{2\{EL\} + 2\{LEI\} + \{EL_2\}}{[E] + 2[EI] + [EI_2]} \tag{6}$$

where A is the column surface area (dm^2) and V_m is the void volume (L). The coefficients of 2 are due to the multiple microscopic forms of some of the species, e.g., LEI and IEL.

Substitution of Equations 3-5 into Equation 6 yields:

$$k' = \frac{K_3\{L\}A}{V_m} \frac{2(1 + K_2[I]) + K_4\{L\}}{(1 + K_2[I])^2} \tag{7}$$

The logarithmic form of this equation is:

$$\log k' = \log(K_3\{L\}A/V_m) + \log(2 + 2K_2[I] + K_4\{L\}) + 2\log(1/(1 + K_2[I])) \quad (8)$$

In general, a plot of log k' versus log $(1/[I])$ will not be linear. A Z value of two will be observed only under a limited range of conditions.

For the monovalent case, a similar derivation yields:

$$k' = \frac{K_3\{L\}A}{V_m(1 + K_2[I])} \quad (9)$$

$$\log k' = \log\left(\frac{K_3\{L\}A}{V_m}\right) + \log\left(\frac{1}{1 + K_2[I]}\right) \quad (10)$$

where {L} is the surface concentration of immobilized ligand sites. The Z value will be one only if $K_2[I] >> 1$. Expressions similar to Equations 7 and 9 can be obtained from the work of Dunn and Chaiken (12), Eilat and Chaiken (13), and Hethcote and DeLisi (15).

Experimental values for K_2, K_3, and K_4 were determined for the immobilized sugar columns using Equation 7 and a non-linear least squares program. Experimental values for K_2 and K_3 were determined for the immobilized Con A column, using Equation 9 and a linear least squares program. In every case, the fits to the data were excellent and indicated mixed divalent-monovalent interactions on the immobilized sugar

columns and only monovalent interactions on the immobilized Con A columns. These results will be discussed in more detail elsewhere. An important conclusion from the data was that divalent adsorption was a highly cooperative (27) process. A comparison of the dimensionless quantities $K_3 m_L/V_p$ and $K_4\{L\}$ (m_L = moles of ligand in column, V_p = pore volume) indicated that divalent binding was approximately ten times stronger than monovalent binding on the high-coverage PAPM column. This occurred in spite of the fact that the binding sites of Con A were identical. Cooperative binding of alkyl-agaroses to proteins has been extensively studied by Jennissen (9-11).

The fitted parameters were then used to prepare log k' versus log $(1/[I])$ plots according to Equations 8 and 10. Figure 3 shows that these plots contained straight regions and curved regions. For example, the glucosamine column data clearly lay on a curved region.

The divalent (upper curves) and monovalent (lower curve) plots of Equations 8 and 10, respectively, are expanded in Figure 4 to clearly show all of the regions. At large $[I]$, the slope is 1. At intermediate $[I]$, the slope is 2. At small $[I]$, the slope is 0. We will call these regions 1, 2, and 0, respectively. The monovalent plot has no region 2. At the transition between each region, there is a curved region. Experimentally, only a small part of the plot ($1 < k' < 10$) is accessible. It is apparent that a plot of experimental data

Figure 3. Expanded plots of the data of Figure 1 fitted with Equations 7 and 9. The fitted parameters are given in parentheses after the column number (see Table I): 1 (■, K_2 = 7000, $K_3\{L\}A/V_m$ = 880, $K_4\{L\}$ = 17400); 2 (◆, K_2 = 7000, $K_3\{L\}A/V_m$ = 920, $K_4\{L\}$ = 680); 3 (▲, K_2 = 8600, $K_3\{L\}A/V_m$ = 0.69, $K_4\{L\}$ = 4.6); 4-MUM (+, K_2 = 6700, $K_3\{L\}A/V_m$ = 13.1); 4-PNPM (●, K_2=7400, $K_3\{L\}A/V_m$ = 7.2)

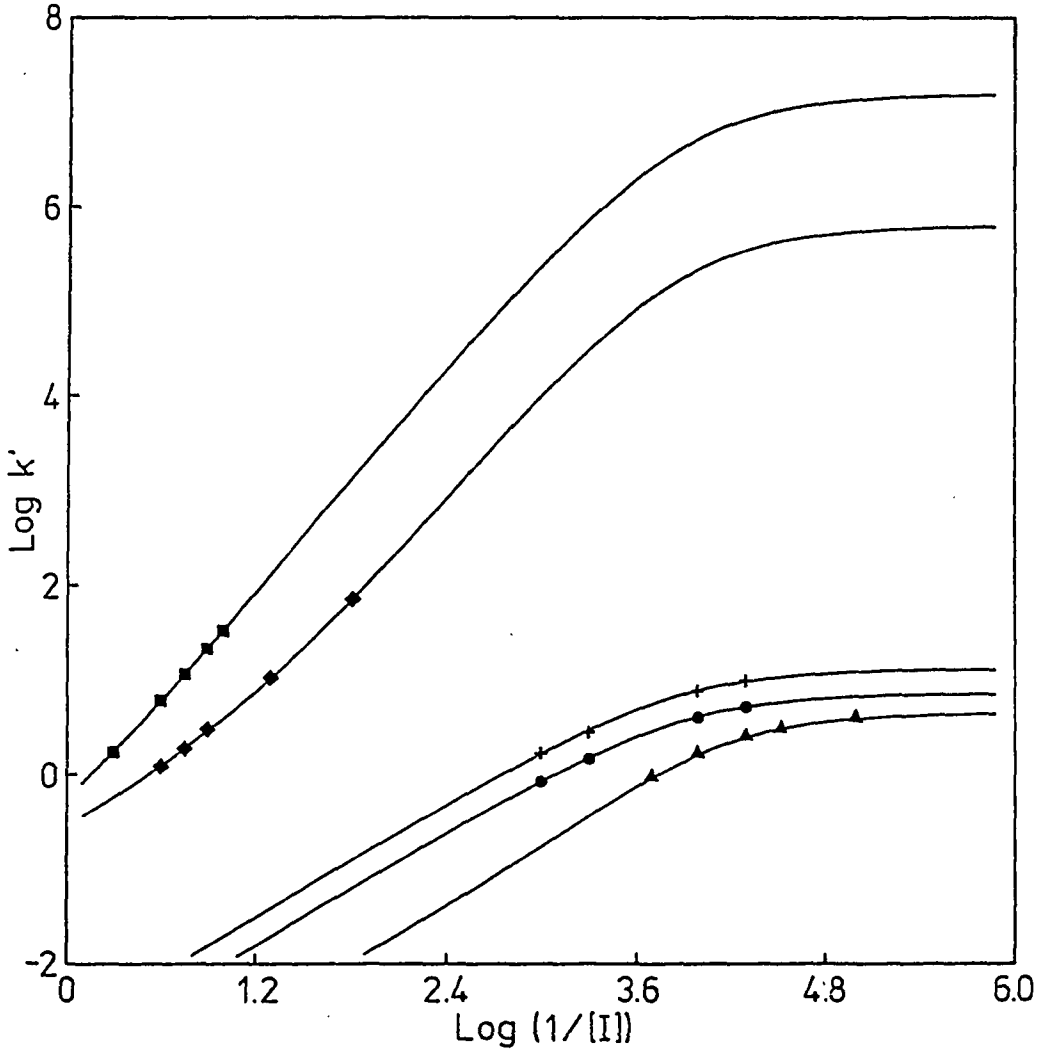
8
6
4
2
0
-2
Log k'
0
1.2
2.4
3.6
4.8
6.0
Log (1/[I])

may be either linear or curved, and that the slope may be less than the maximum number of binding sites. The boundary between regions 1 and 2 occurs at $[I] \sim K_4\{L\}/K_2$, while the boundary between regions 2 and 0 (or 1 and 0 in the case of monovalent binding) occurs at $[I] \sim 1/K_2$. Computer calculations show that in the mobile phase the dominant form of E in region 0 is free E, while in regions 1 and 2 the dominant form is EI_2. EI dominates at the transition between regions 0 and 2. On the surface, EL_2 dominates in regions 0 and 2 and LEI dominates in region 1. EL is not present in significant amounts at any inhibitor concentration.

There are three factors which determine the position and size of the various regions. These are: (1) the strength of monovalent binding of the analyte to the ligand (determined by K_3, $\{L\}$, and A/V_m); (2) the strength of the mobile phase modifier (K_2); and (3) the strength of divalent interaction (K_4). The effect of each factor was determined separately by generating plots of Equation 8 on a computer using arbitrarily chosen values of the parameters.

The amount of divalent interaction is reflected in the $K_4\{L\}$ term of Equation 8 relative to the terms $2K_2[I]$ and 2 (which represent the amounts of LEI and EL, respectively). Figure 4a shows that when K_4 is 0, there is no region 2 and the plot is the same as for a monovalent interaction. As K_4 increases, the width of the region with a slope of two

Figure 4. General plots of Equation 7 for a divalent system. $K_2 = K_3\{L\}A/V_m = K_4\{L\} = 1000$, except as follows: (a) from top to bottom, $K_4\{L\} = 10000$, 100, 0; (b) from top to bottom, $K_3\{L\}A/V_m = 10000$, 1000, 100; (c) from left to right, $K_2 = 100$, 1000, 10000

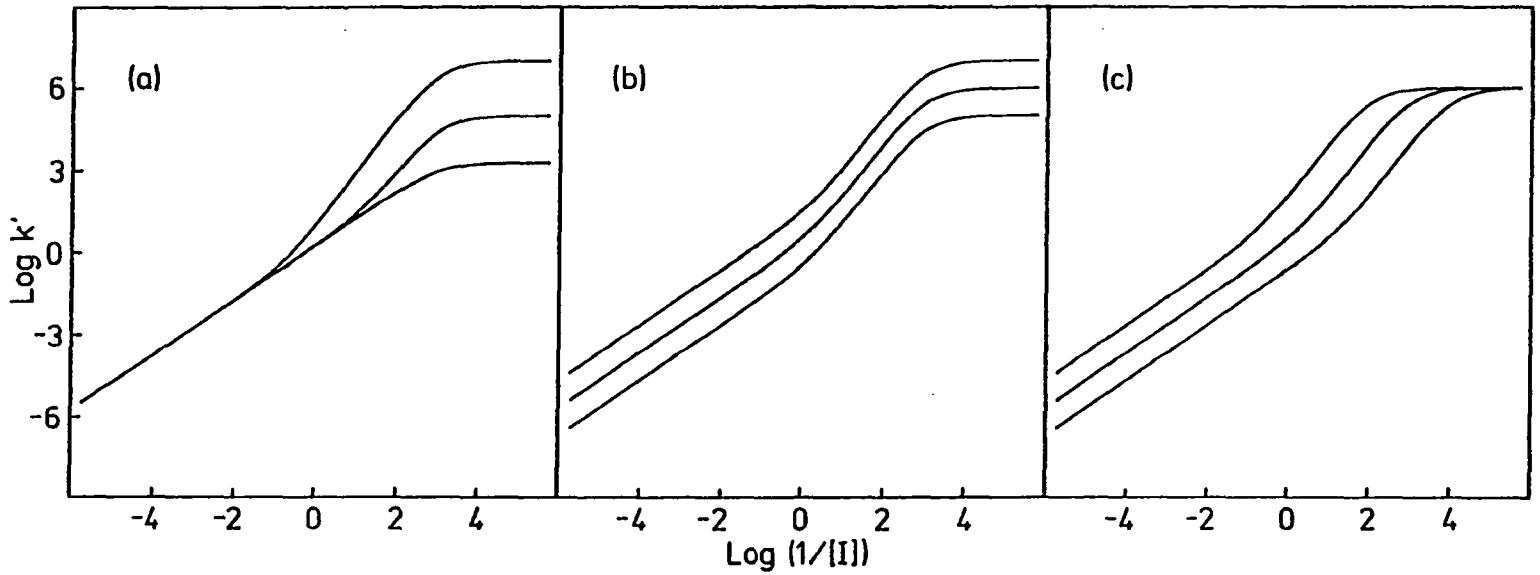
(a)
(b)
(c)
Log k'
6
3
0
-3
-6
-4
-2
0
2
4
Log (1/[I])

increases, and the height of region 0 increases. The latter region is the region where I does not significantly affect k' and, so, the plot plateaus. As K_4 increases, this plateau k' value also increases. These effects can be observed in comparing the immobilized sugar columns (Figure 3). The high-coverage PAPM column had a wide region 2, while the low-coverage PAPM column had a narrower region 2. The glucosamine column K_4 was so small that region 2 was nearly absent (slope just slightly greater than one).

Figure 4b shows the effect of changing the monovalent binding strength, $K_3\{L\}A/V_m$. The shape of the plot is unaffected, but increasing binding strength shifts the curve vertically to higher k'. This effect can be observed in comparing the high-coverage immobilized PAPM and glucosamine columns (Figure 3), which differed primarily in that K_3 was larger for the PAPM column (solution K_3 values for PNPM and N-acetyl-D-glucosamine are 71,400 and 140 M^{-1}, respectively, at 5 °C) (28). The larger K_3 caused the observed data to shift from the curved transition area between regions 0 and 2 to region 2.

Figure 4c shows that the value of K_2 influences the horizontal position of the plot, but not the shape. No new information is obtained by making measurements with different inhibitors. The same curve is obtained, but at different concentrations of I.

It is clear that the log k' plotting method generally yields a Z value which is less than the true valency of the analyte. In general, there is no way to determine the true value of Z, although in affinity chromatography it will usually be the next highest integer. The exception is for monovalent interactions, where a plot of log k' versus log $(1/(1 + K_2[I]))$ should have a slope of exactly one. Of course, this requires a preliminary determination of K_2, for which Z needs to be known in advance.

The log k' plotting method does have value in affinity chromatography for the semi-quantitative estimation of the degree of monovalent or divalent binding. A Z value of one or less indicates primarily monovalent interactions, while values approaching two indicate increasing strength of divalent interactions. A curved plot indicates a transition between two regions.

Another potential use of the log k' plotting method in affinity chromatography may be in the more common chromatographic cases, where elution of analyte is caused by pH, ionic strength, or other mobile phase modifiers rather than by competitive elution with inhibitors. For example, a plot of log k' versus log $(1/[H^+])$ might help to indicate the mechanism of elution during pH changes. The slope of the plot might indicate how many critical sites in the protein are being protonated or deprotonated during elution.

Extension to Other Chromatographic Methods

The more general affinity chromatographic model can be extended to other types of chromatography by making reasonable assumptions about the forms of solute present in each phase. Equilibrium constants can then be calculated for individual adsorption sites using retention data. The model can be used to explain the frequently-observed curvature in log k' plots of solutes with Z > 1, and to explain why the measured slopes may not be integer values.

A particularly interesting conclusion one can draw from such studies is that the individual site equilibrium constants must decrease as Z increases. This is particularly apparent from the reversed-phase studies of Geng and Regnier (8), which yielded Z values of 2-24 for a series of proteins. The straight log k' plots and large slopes indicated a high degree of cooperativity ($K_z > K_{z-1} > K_{z-2}$, etc.). One would have expected that the mobile phase modifier concentration needed to elute the protein with Z = 24 to have been many orders of magnitude greater than the proteins with smaller Z values (e.g., note the large range of [I] in Figure 1 where Z only changed by 1). However, only a fifteen-fold difference was observed. This indicates that the individual equilibrium constants must have decreased as Z increased. The use of the

general model, thus, provides some additional insight into the mechanism of retention.

ACKNOWLEDGEMENTS

The authors thank Mary Landgrebe for synthesizing the glucosamine packing. This work was supported by the National Science Foundation under Grant CHE-8305057.

REFERENCES CITED

1. Boardman, N. K.; Partridge, S. M. Biochem. J. 1955, 59, 543.

2. Jandera, P.; Janderova, M.; Churacek, J.; J. Chromatogr. 1978, 148, 79.

3. Kopaciewicz, W.; Rounds, M. A.; Fausnaugh, J.; Regnier, F. E. J. Chromatogr. 1983, 266, 3.

4. Rounds, M. A.; Regnier, F. E. J. Chromatogr. 1984, 283, 37.

5. Barford, R. A.; Sliwinski, B. J.; Breyer, A. C.; Rothbart, H. L. J. Chromatogr. 1982, 235, 281.

6. Hearn, M. T. W.; Grego, B. J. Chromatogr. 1983, 255, 125.

7. Stadalius, M. A.; Gold, H. S.; Snyder, L. R. J. Chromatogr. 1984, 296, 31.

8. Geng, X.; Regnier, F. E. J. Chromatogr. 1984, 296, 15.

9. Jennissen, H. P. J. Chromatogr. 1981, 215, 73.

10. Jennissen, H. P.; Heilmeyer, L. M. G. Biochemistry 1975, 14, 754.

11. Jennissen, H. P. Biochemistry 1976, 15, 5683.

12. Dunn, B. M.; Chaiken, I. M. Proc. Nat. Acad. Sci. USA 1974, 71, 2382.

13. Eilat, D.; Chaiken, I. M. Biochemistry 1979, 18, 790.

14. Winzor, D. J.; Ward, L. D.; Nichol, L. W. J. Theor. Biol. 1982, 98, 171.

15. Hethcote, H. W.; DeLisi, C. J. Chromatogr. 1982, 248, 183.

16. Cunningham, B. A.; Wang, J. L.; Pflumm, M. N.; Edelman, G. M. Biochemistry 1972, 11, 3233.

17. Walters, R. R. Anal. Chem. 1983, 55, 591.

18. Bethell, G. S.; Ayers, J. S.; Hearn, M. T. W.; Hancock, W. S. J. Chromatogr. 1981, 219, 353.

19. Walters, R. R. J. Chromatogr. 1982, 249, 19.

20. Landgrebe, M. E.; Walters, R. R., Dept. of Chemistry, Iowa State University, Ames, IA; unpublished results.

21. Kesler, R. B. Anal. Chem. 1967, 39, 1416.

22. Robyt, J. F.; Ackerman, R. J.; Keng, J. G. Anal. Biochem. 1972, 45, 517.

23. Lowry, O. H.; Rosebrough, N. J.; Farr, A. L.; Randall, R. J. J. Biol. Chem. 1951, 193, 165.

24. Anderson, D. J.; Walters, R. R. J. Chromatogr. Sci. 1984, 22, 353.

25. Huet, M. Eur. J. Biochem. 1975, 59, 627.

26. Loontiens, F. G.; Clegg, R. M.; Jovin, T. M. Biochemistry 1977, 16, 159.

27. Cantor, C. R.; Schimmel, P. R. "Biophysical Chemistry, Part III"; Freeman: San Francisco, 1980; p. 862.

28. Oda, Y.; Kasai, K.; Ishii, S. J. Biochem. 1981, 89, 285.

SECTION III.

EQUILIBRIUM AND RATE CONSTANTS OF IMMOBILIZED CONCANAVALIN A DETERMINED BY HIGH-PERFORMANCE AFFINITY CHROMATOGRAPHY

SUMMARY

Equilibrium constants for the binding of p-nitrophenyl α-D-mannopyranoside, 4-methylumbelliferyl α-D-mannopyranoside, and methyl α-D-mannopyranoside to immobilized concanavalin A were determined by high-performance affinity chromatography. Values obtained by zonal and frontal analysis on columns of variable concanavalin A coverage were in close agreement and were approximately 2-fold greater than literature values from solution studies. The immobilized concanavalin A appeared to have only a slight heterogeneity. Sugars containing aromatic groups were found to be non-specifically adsorbed, but the retention was small under the conditions used for equilibrium and rate constant measurements. Dissociation rate constants for two of the sugars were determined by isocratic elution. Apparent changes in the rate constants with capacity factor were found to be due to errors in calculating the diffusional contributions to band-broadening as a function of retention. The more accurate low retention time data gave rate constants that were approximately one-half of literature values.

INTRODUCTION

One application of high-performance affinity chromatography (HPAC) is the determination of kinetic and thermodynamic parameters of ligand-macromolecule complexes. The theory for the determination of equilibrium constants is well-known (1-4). For the case of "reversed-role" affinity chromatography, in which a macromolecule (L) is immobilized and a solute (E) is isocratically eluted using a competing inhibitor (I) in the mobile phase, the reactions of interest are:

$$E + L \underset{k_{-3}}{\overset{k_3}{\rightleftharpoons}} EL$$

$$I + L \underset{k_{-2}}{\overset{k_2}{\rightleftharpoons}} IL$$

$$K_3 = \frac{\{EL\}}{[E]\{L\}} = \frac{k_3}{k_{-3}} \qquad (1)$$

$$K_2 = \frac{\{IL\}}{[I]\{L\}} = \frac{k_2}{k_{-2}} \qquad (2)$$

where K_2 and K_3 are the binding constants, k_2 and k_3 are the association rate constants, and k_{-2} and k_{-3} are the dissociation rate constants (4-7). The {} represents a surface concentration. K_2 and K_3 can be determined from the

slope and intercept of a plot of $1/k'$ versus $[I]$:

$$\frac{1}{k'} = \frac{V_m}{K_3 m_L} + \frac{V_m K_2 [I]}{K_3 m_L} \qquad (3)$$

where k' is the capacity factor, V_m is the column void volume, and m_L is the number of moles of active ligand in the column (6,7).

The theory for the determination of kinetic parameters is also well-known (4-5,8-10), but few experimental studies have been performed. Although several studies of band-broadening by kinetic processes have been published (11-14), only Muller and Carr (6) have made a thorough examination of the problem. They obtained rate constants which were much lower than expected from solution studies and which varied with k', in contradiction of theory (6). In this paper, the same biochemical system, consisting of immobilized concanavalin A (Con A) with various sugars used as the analyte or inhibitor, will be reexamined, but with changes in the support material, immobilization method, and calculation methods.

To determine dissociation rate constants, other contributions to band-broadening in the column must be negligible, or be separately determined, and subtracted off. The total plate height, H_t, is believed to obey the van Deemter equation (4,5,8,9,15,16):

$$H_t = H_m + H_{sm} + H_k \tag{4}$$

where

$$H_{sm} = \frac{2uV_p(1 + V_m k'/V_p)^2}{k_{-1}V_m(1 + k')^2} \tag{5}$$

and

$$H_k = \frac{2uk'}{k_{-3}(1 + k')^2} \tag{6}$$

In Equation 4, it is assumed that H_m, the eddy diffusion and mobile phase mass transfer term, is independent of k' and flow rate, and that longitudinal diffusion is negligible (15,16). V_p is the pore volume of the column, u is the linear velocity of the mobile phase, H_{sm} is the contribution to the plate height due to slow diffusion in the stagnant mobile phase of the pores, and H_k is the contribution due to slow adsorption-desorption kinetics. The diffusional rate constants k_1 and k_{-1} are related to the support properties (4) through the following equation:

$$\frac{k_1}{k_{-1}} = \frac{V_p}{V_e} \tag{7}$$

where V_e is the exclusion volume of the column. Also,

$$k_{-1} = \frac{60\gamma D_m}{d_p^2} \tag{8}$$

where γ is a tortuosity factor, D_m is the diffusion coefficient of the solute, and d_p is the particle diameter (8,17,18). There is currently some controversy over the flow rate and k' dependence of H_m and H_{sm} (15,16,19). Surface diffusion has been postulated to be important in some cases (19).

Rate parameters can also be calculated directly from peak variances (4,5,8-10). The appropriate equations, in units of time squared, are obtained by multiplying Equations 4-6 by $t_m^2(1 + k')^2/CL$, where t_m is the void time and CL is the column length.

EXPERIMENTAL

Reagents

Concanavalin A (types IV and V), p-nitrophenyl α-D-mannopyranoside (PNPM), 4-methylumbelliferyl α-D-mannopyranoside (MUM), methyl α-D-mannopyranoside (MDM, grade III), p-nitrophenyl α-D-galactopyranoside (PNPG), and 4-methylumbelliferyl α-D-galactopyranoside (MUGA) were obtained from Sigma (St. Louis, MO). The Con A was purified as described previously (7). Hypersil WP-300, 5 μm, and LiChrospher SI 500, 10 μm, were from Alltech (Deerfield, IL). Carboxylate microspheres, 0.1 μm, were from Polysciences (Warrington, PA).

Apparatus

In addition to the HPLC equipment previously described (7), a differential refractometer (Model R401, Waters, Milford, MA) was used for break-through curves with MDM.

Procedure

Diol-bonded LiChrospher SI 500 and Hypersil 300 were prepared according to a published procedure (20). Con A was

coupled to LiChrospher SI 500 diol using the 1,1'-carbonyldiimidazole method (7). Low- and high-coverage Hypersil 300 columns were prepared by the Schiff base method using 4 ml of 3.7 mg/ml Con A or 25 ml of 9.8 mg/ml Con A per 0.8 g support (18,21). The pH 5 acetate buffer, described below, was used for the immobilization. The immobilized Con A on the LiChrospher support was assayed by the Lowry method (22).

The chromatographic columns were thermostated at 25.0 °C. The mobile phase was 0.5 M sodium acetate, 1 mM $CaCl_2$ and $MnCl_2$, pH 5.0. The inhibitor was MDM dissolved in this buffer. Sugars injected into the columns were also prepared in the appropriate MDM-containing buffer. Injection volumes of 6 µM sugar were 20 µL for the LiChrospher affinity column and 10 µL for all other columns. The detection wavelength was 305 nm for PNPM and PNPG, 316 nm for MUM and MUGA, and 280 nm for carboxylate microspheres, uracil, and water. Flowrates were measured volumetrically. Statistical moments were determined from the width-at-half-height and peak-center-at-half-height using a Gaussian approximation (see also Equation 15).

Column void time (t_m) was determined by injection of water. Using the non-Con A-binding sugars PNPG and MUGA (23), a non-specific retention time (t_{ns}) was measured. The exclusion volume (V_e) was obtained by injection of the

carboxylate microspheres diluted to a concentration of 0.25 % onto diol-bonded silica columns in a deionized water mobile phase to prevent agglomeration. The volume V_e was assumed to be the same for the corresponding affinity column.

Extra-column void time and variance were measured without a column and subtracted from the raw retention times and peak variances. A weak non-specific retention of the sugars ($k' \sim 0.2$) was subtracted when appropriate in the calculations. This correction had only a minor effect on the results.

In addition to zonal analysis, equilibrium constant data was obtained from some of the columns by frontal analysis. Flowrates for the break-through studies were between 0.05 and 1 ml/min and were chosen to minimize error in estimating the break-through points. The break-through points were found by integration (24). Uracil break-through curves were used to correct for the column void volume. The number of moles of active ligand in the column was also found using the break-through curves.

Table I lists the columns used in this study and some of the important measured parameters.

Table I. Column parameters

Column	Support	CL[a] (mm)	F[b] (ml/min)	V_m (ml)	V_e (ml)	m_L (nmol)	{L}[c] (nmol/m^2)
Diol	LiChrospher SI 500	49.6	--	0.58	0.25	--	--
Diol	Hypersil 300	50.0	--	0.42	0.23	--	--
Low-coverage Con A	Hypersil 300	50.0	1.00	0.42	0.23	16	0.7
Medium-coverage Con A	LiChrospher SI 500	100.0	0.92	0.94	0.38	290	12
High-coverage Con A	Hypersil 300	49.7	1.01	0.41	0.23	650	29

[a]All columns were 4.1 mm I.D., except the LiChrospher SI 500 diol column, which was 4.6 mm I.D..

[b]Flowrate.

[c]Surface coverage of binding sites based on experimental packing densities and manufacturers' estimates of surface area.

RESULTS AND DISCUSSION

Verification of Linear Elution Conditions

A critical parameter in the experimental design is the sample size. Under linear elution conditions, the data should be independent of sample size. If this is not the case, then the theoretical relationships given earlier will not apply. Since affinity columns contain relatively few adsorption sites, overloading is a common problem. In this work, the low-coverage Hypersil 300 column was the most easily overloaded. Linear elution conditions were established by injecting various concentrations of MUM and measuring the capacity factor and peak asymmetry (Figure 1). Large changes in these parameters were seen at high concentration, but the concentration used in our work (6 μM) was within the linear elution region and corresponded to filling 3 % of the available sites in the worst case.

Determination of Equilibrium Constants by Zonal Analysis

Equilibrium constants for the solutes MUM and PNPM and the inhibitor MDM were determined from plots of Equation 3 using the V_m and m_L data from Table I. The plots (Figure 2) exhibited excellent linearity. The results (Table II) were

Figure 1. Effect of sample concentration on the capacity factor (◆) and peak asymmetry (●). Ten microliter samples of MUM were injected onto the low-coverage Hypersil 300 column

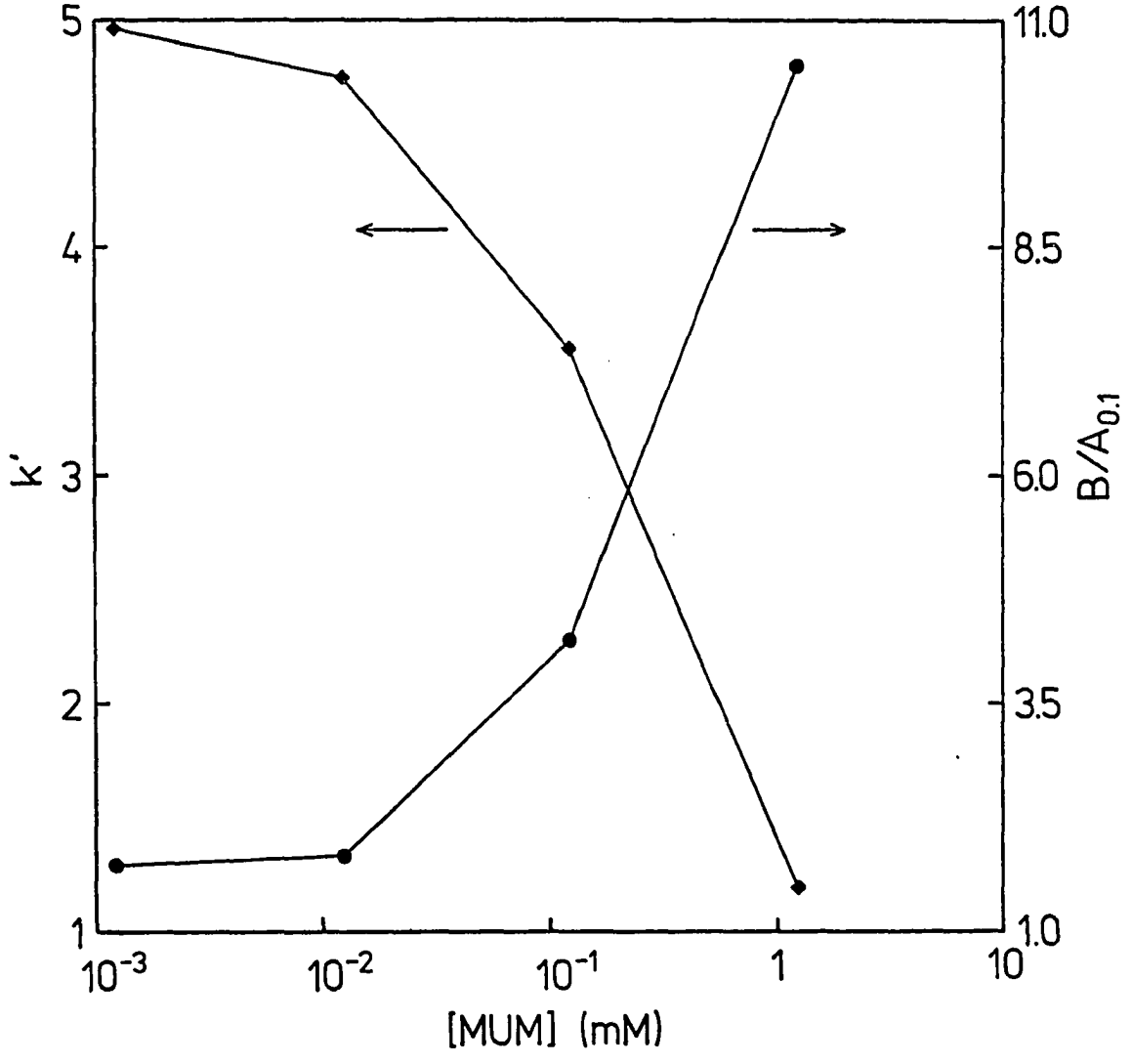
5
4
3
2
1
k'
11.0
8.5
6.0
3.5
1.0
B/A0.1
10-3
10-2
10-1
1
10
[MUM] (mM)

Figure 2. Plots used to determine equilibrium constants for MUM on the high- (+), medium- (◆), and low-coverage (▲) columns and PNPM on the high- (X), medium- (●), and low-coverage columns (■)

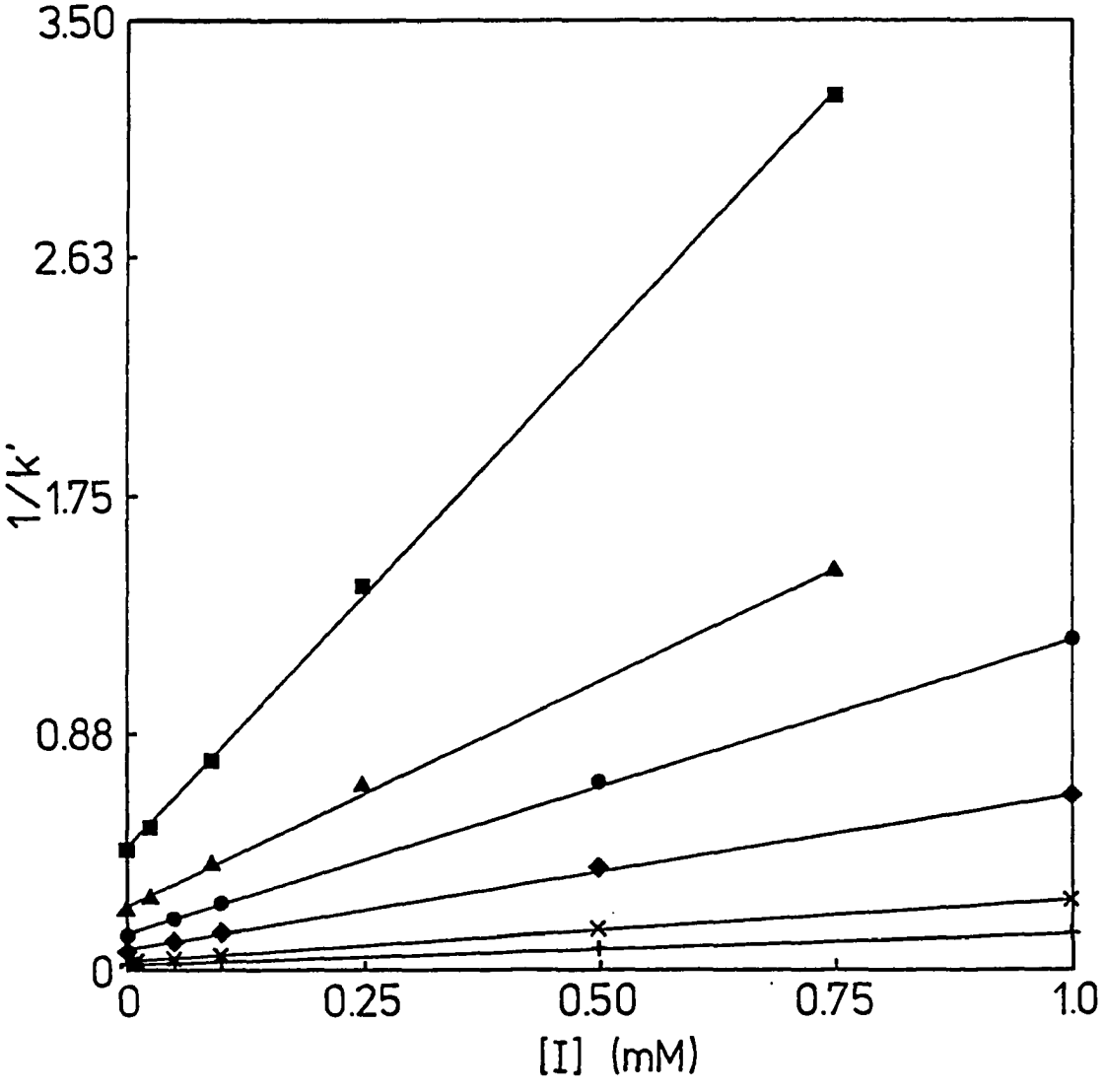
3.50
2.63
1.75
0.88
0
1/k'
0
0.25
0.50
0.75
1.0
[I] (mM)

Table II. Equilibrium constant data

Source	Analysis	K_3,(MUM) (M^{-1})	K_3,(PNPM) (M^{-1})	K_2,(MDM)[a] (M^{-1})
Low-coverage Hypersil 300	Zonal	117000[b]	59000[b]	7400,8400
Medium-coverage LiChrospher SI 500	Zonal	45000	25000	8100,8500
High-coverage Hypersil 300	Zonal	45000	22000	8400,8100
Solution data (25)	---	33000	8700	3300
Muller and Carr (6)	Both	---	16000	7600
Medium-coverage LiChrospher SI 500	Frontal	---	26000	---
High-coverage Hypersil 300	Frontal	---	---	8400

[a]First value from MUM data, second from PNPM data.

[b]Possible error in m_L determination on low-coverage column - see text.

higher than literature values from solution measurements by factors of 1.4 to 2.7-fold, but in good agreement with the results of Muller and Carr (6). The differences from solution values may be due to the fact that on the column K_3 and K_2 are defined in terms of surface concentrations (Equations 1 and 2), which may not be equivalent to the solution concentrations obtained by dissolving the same number of moles in a volume V_p. Equilibrium constants have been measured for many other affinity chromatographic systems and have yielded values typically within a factor of two higher or lower than literature values (1-3,13,14). Thus, such differences may be due to errors in the solution data.

Determination of Equilibrium Constants and Number of Sites by Frontal Analysis

Although the data in Figure 2 were of excellent linearity, at higher inhibitor concentrations some negative deviation from the expected line was observed. This indicated some heterogeneity of the immobilized Con A and was also observed by Muller and Carr (6). The extent of the heterogeneity appeared to be minor. For example, under conditions where only 0.2 % of the Con A sites were free, the measured k' deviated by just 30 % from the value expected using the higher k' data.

In addition to this slight heterogeneity of the specific sites, there appeared to be a population of non-specific sites, since MUGA and PNPG were slightly retained (k' = 0.22 and 0.10, respectively) on the affinity columns, while MUM and PNPM were slightly retained (k' = 0.27 and 0.07, respectively) on the diol columns. This weak retention was subtracted when Figure 2 was made and, thus, should not have affected the zonal data. The effect on frontal data was more severe, however.

Break-through curves were obtained for various concentrations of PNPM on the LiChrospher SI 500 column (Figure 3a) and MDM on the high-coverage Hypersil 300 column (Figure 3b). Using Equation 1, the following equation was derived:

$$m_{EL} = K_3[E]m_L/(1 + K_3[E]) \qquad (9)$$

where m_{EL} is the number of moles of sugar bound, m_L is the total number of free and occupied sites, and $[E]$ is the concentration of sugar applied. This equation defines the well-known Langmuir isotherm.

The PNPM experimental data in Figure 3a did not level off at high concentrations of sugar, as had been expected in the binding constants in Table II. This same behavior can be seen in the data of Muller and Carr (6), but they did not use

Figure 3. Binding isotherms from break-through curves for PNPM on the LiChrospher SI 500 column (a) and for MDM on the high-coverage Hypersil 300 (b) columns. In each case, the upper curve is the total fit to the experimental data, the straight line is the non-specific binding, and the remaining curve is the specific binding

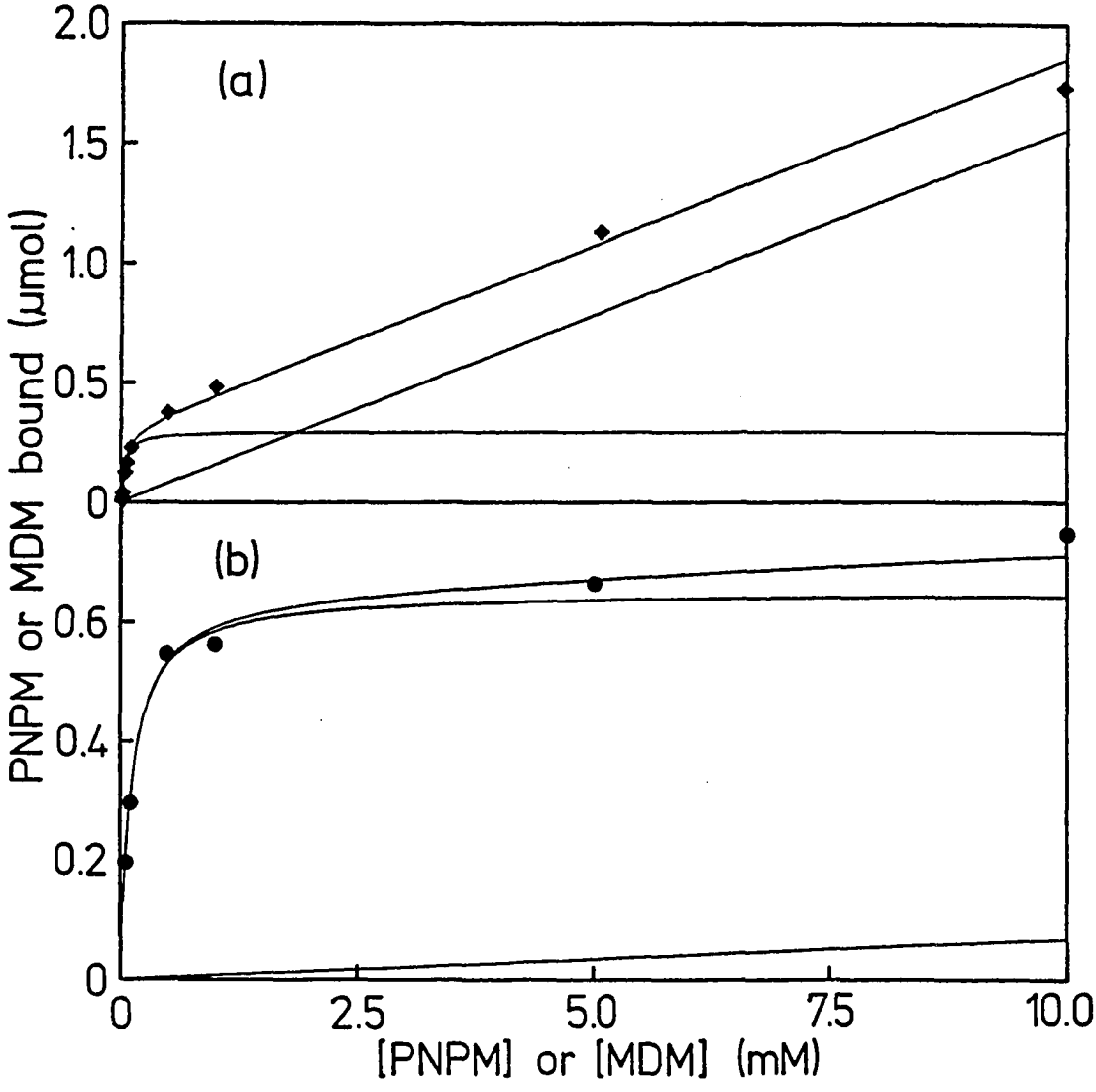
2.0
1.5
1.0
0.5
0
(a)
(b)
0.6
0.4
0.2
0
PNPM or MDM bound (µmol)
0
2.5
5.0
7.5
10.0
[PNPM] or [MDM] (mM)

sufficiently high sugar concentrations to make this trend obvious.

If there is a second group of non-specific sites, of amount m_{ns}, and binding constant, K_{ns}, then the amount bound will be:

$$m_{EL} + m_{Ens} = \frac{K_3[E]m_L}{1 + K_3[E]} + \frac{K_{ns}[E]m_{ns}}{1 + K_{ns}[E]} \qquad (10)$$

If it is further assumed that these are weak sites, so that $K_{ns}[E] << 1$ over the range of $[E]$ studied, then:

$$m_{EL} + m_{Ens} = \frac{K_3[E]m_L}{1 + K_3[E]} + K_{ns}[E]m_{ns} \qquad (11)$$

This equation predicts the linear increase in the amount bound at high concentrations of sugar, as was seen in Figure 3a.

Fitting our data to Equation 11 yielded the number of moles of active sites (Table I, high- and medium-coverage columns) and the frontal analysis equilibrium constants in Table II. The latter were in excellent agreement with the zonal data and, thus, supported the conclusion that there was a population of weak sites on either the support, or hydrophobic residues on the Con A itself, which affected the retention primarily at high sugar concentrations. The value

of $K_{ns}m_{ns}$ for PNPM determined from the fit of Figure 3a was 1.6×10^{-4} L, which was 50-fold smaller than the value of K_3m_L, 7.3×10^{-3} L. On the high-coverage Hypersil 300 column, $K_{ns}m_{ns}$ for the sugar MDM was only 6.8×10^{-6} L (Figure 3b), which suggested that PNPM was retained non-specifically via the hydrophobic phenyl group. MDM was, thus, more suitable for determining m_L.

The LiChrospher SI 500 protein content can be used to calculate a maximum value for m_L of 290 nmol (based on 1 mole of sites per 27000 g Con A, i.e., the molecular weight of a monomer (26)). This can be compared to the isotherm value in Table I (290 nmol) and indicated complete retention of activity of carbonyldiimidazole-immobilized Con A. Muller and Carr (6) observed a 50 % retention of activity using the glutaraldehyde coupling method.

For the low-coverage Hypersil 300 column, m_L was determined by a single break-through curve using 2.0×10^{-3} M MDM. The small break-through volume could not be measured accurately, so the errors in the K_3 values in Table II were probably due to inaccuracies in m_L. Note that this error would not affect the K_2 values.

The above discussion does not rule out the possibility of a subpopulation of very strong sites, although the data of Figure 2 does not indicate the presence of a significant number of stronger sites. Muller and Carr (6) hypothesized

the presence of such sites after plotting their frontal analysis data as a Scatchard plot. Similar plots of our isotherm data were less clear. While the weak sites discussed above were clearly seen, the presence of strong sites was less apparent, because few data points were taken in the low concentration region. In the LiChrospher SI 500 data, there was some indication of a small proportion (~10 %) of stronger sites ($K_3 \sim 2 \times 10^5\ M^{-1}$), but the data were not conclusive.

Determination of Rate Constants

In order to calculate rate parameters, we must assume that the processes involved are fairly homogeneous. With regard to the previous discussion of heterogeneity, two assumptions will be made. First, we will assume that within the range of k' data in Figure 2, the Con A is of a homogenous nature. Data from the non-linear low k' regions of these plots will not be used to calculate rate constants. Secondly, we will assume that the weak, non-specific retention of sugars is kinetically fast and does not contribute to the kinetic band-broadening.

Figure 4 shows theoretical plots of the plate height terms and variances from Equations 4-6 (with $H_m = 0$), and the experimental data. The kinetic plate height, H_k, always has a maximum at k' = 1. Combined with the H_{sm} term, a maximum in

Figure 4. Theoretical and experimental plots of plate height and variance versus k'. From top to bottom in (a) and (c) are the total, diffusional, and kinetic contributions to the plate height and variance calculated from Equations 5 and 6, respectively. In (b) are the experimental data for MUM on the high-coverage Hypersil 300 (+), medium-coverage LiChrosper SI 500 (◆), and low-coverage Hypersil 300 (▲) columns. In (d) are data for MUM on the high-coverage Hypersil 300 column

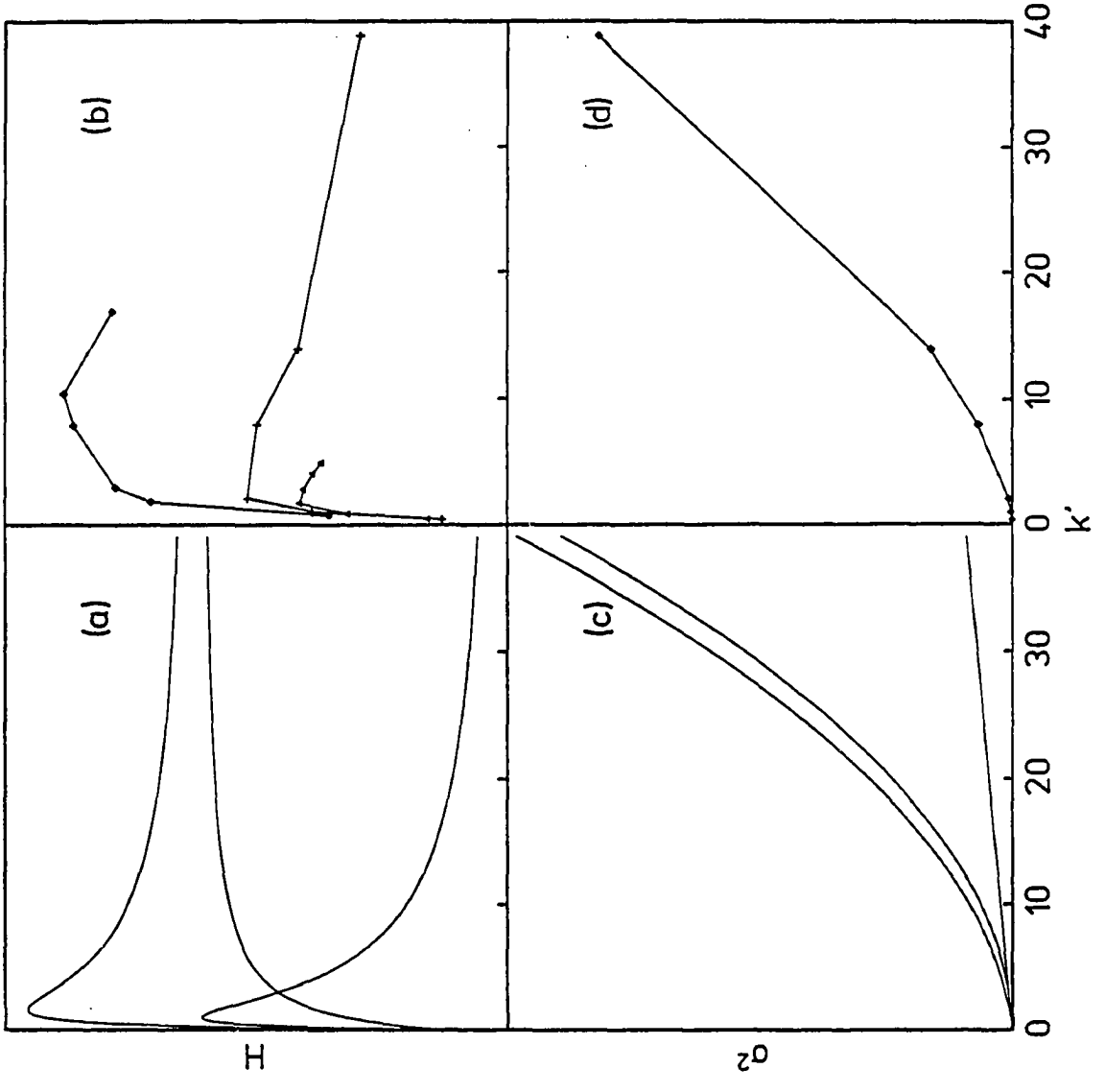
(a)
(b)
(c)
(d)
H
σ2
0
10
20
30
40
k'

the H_t plot is expected in the range of k' = 1-2. This was seen for the two Hypersil 300 columns, but was less apparent for the LiChrospher SI 500 column, suggesting that kinetic band-broadening was less important than diffusional band-broadening on that column. Variance plots are shown in Figure 4c and 4d. The kinetic contribution increases linearly, while the diffusional contribution increases via a squared term. From the experimental data, Figure 4d, it was difficult to visually assess the relative importance of diffusional and kinetic band-broadening. Clearly, from Figures 4a and 4c, it is easier to measure adsorption-desorption kinetic parameters at low k', where the diffusional contribution is smaller.

Muller and Carr (6) calculated k_{-3} in two ways. First, they simply subtracted the plate height for a non-binding sugar from the total plate height for a retained sugar. This was clearly incorrect, since H_{sm} increases greatly with k'. In a second method, they used literature data to estimate various plate height contributions. Both approaches yielded similar results - the non-kinetic contributions were small compared to the total plate height, thus, H_k was assumed to dominate. In support of this, they showed that the band-broadening on a 50 μm support was only 5-fold greater than on a 10 μm support, rather than the expected 25-fold change if H_{sm} were dominant.

We similarly saw a 2-fold reduction in total plate height

as the particle diameter decreased from 10 μm to 5 μm (Figure 4b), rather than the expected 4-fold change if H_{sm} dominated. In addition, total plate heights on the LiChrospher SI 500 support (~ 1000 μm) were similar to those observed by Muller and Carr on the same support. Thus, their raw data was similar to ours, but we have looked at the data somewhat differently. We believe that diffusional contributions were much larger than indicated by Muller and Carr's work.

Independent Estimation of H_{sm} and H_m

If Equation 4 is an accurate representation of the band-broadening in a column, then a non-retained solute will have contributions from only H_m and H_{sm}. By measuring H_t versus u for PNPM and MUM on a diol column (or, alternatively, PNPG and MUGA on an affinity column), one should be able to obtain k_{-1} from the slope and H_m from the intercept. This is shown in Figure 5 for the case of MUM on a LiChrospher SI 500 diol column. Such plots were generally quite linear, thus, indicating good agreement with the van Deemter equation. Table III summarizes the results. Similar results were obtained for MUGA and PNPG on the high-coverage Hypersil 300 column. As one would expect, k_{-1} was larger for the smaller support, but by less than the theoretical factor of four.

To take into account inter-column variation, H_m was also

Figure 5. Total plate height for MUM on the LiChrospher SI 500 diol column as a function of linear velocity

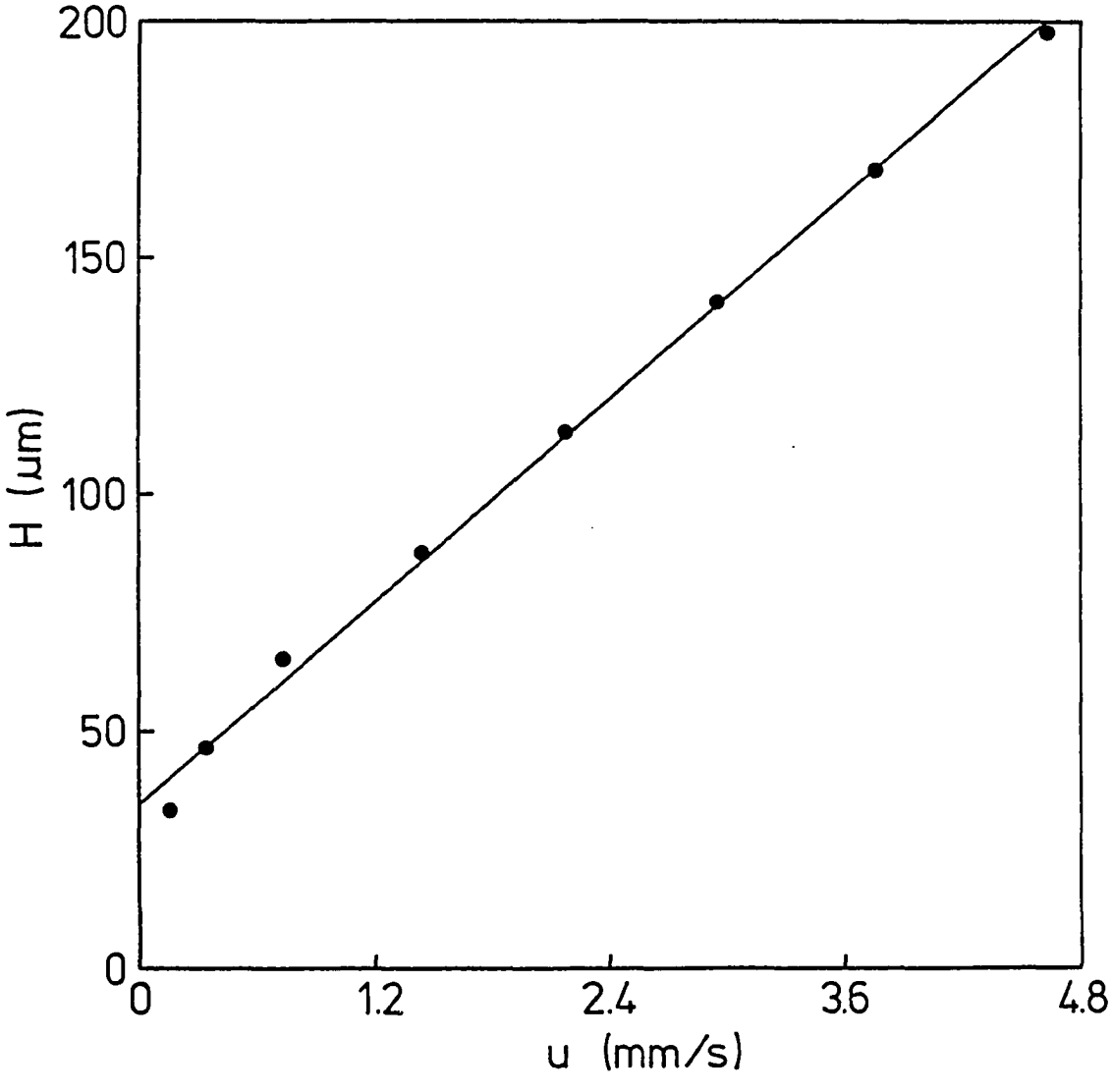
200
150
100
50
0
H (μm)
0
1.2
2.4
3.6
4.8
u (mm/s)

Table III. Diffusional parameters

Column	Sugar	H_m(μm)	k_{-1}(sec^{-1})
LiChrospher SI 500 diol	MUM	34	43
	PNPM	33	78
Hypersil 300 diol	MUM	28	116
	PNPM	30	123
Low-coverage Hypersil 300	MUGA	19	--
	PNPG	23	--
Medium-coverage LiChrospher SI 500	MUGA	85	--
	PNPG	108	--
High-coverage Hypersil 300	MUGA	25	--
	PNPG	39	--

determined for each affinity column using the non-retained sugars and assuming that k_{-1} was the same as the similar sugar on the diol column. As shown in Table III, H_m was, in most cases, of similar magnitude.

Using the values of H_m, k_{-1}, u, V_m, and V_p, $H_{sm} + H_m$ was calculated as a function of k' and subtracted from the measured plate height of each data point. The remaining plate height was assumed to be due to H_k and k_{-3} was calculated for each point using Equation 6. Figure 6 shows the calculated values of k_{-3} as a function of MDM concentration. Not only were different values of k_{-3} obtained on each column, but k_{-3} for the same solute differed from column to column. Muller and Carr also observed that k_{-3} increased as the inhibitor concentration increased (6). They postulated a linear dependence of k_{-3} on [I] from PNPM data on a single column, but our Figure 6 indicates that the dependence is probably not linear. Our values of k_{-3} for PNPM on the LiChrospher SI 500 column were quite similar to their values using the same support.

To account for the change in k_{-3} as a function of [I], Muller and Carr (6) postulated that the inhibitor altered the kinetics of the Con A-PNPM complex by forming a ternary complex intermediate. This is contrary to what one would expect, i.e., that the inhibitor simply fills some of the Con A sites, but has no effect on the remaining unoccupied or

Figure 6. Plots of the calculated dissociation rate constants versus inhibitor concentration. Symbols are the same as in Figure 2

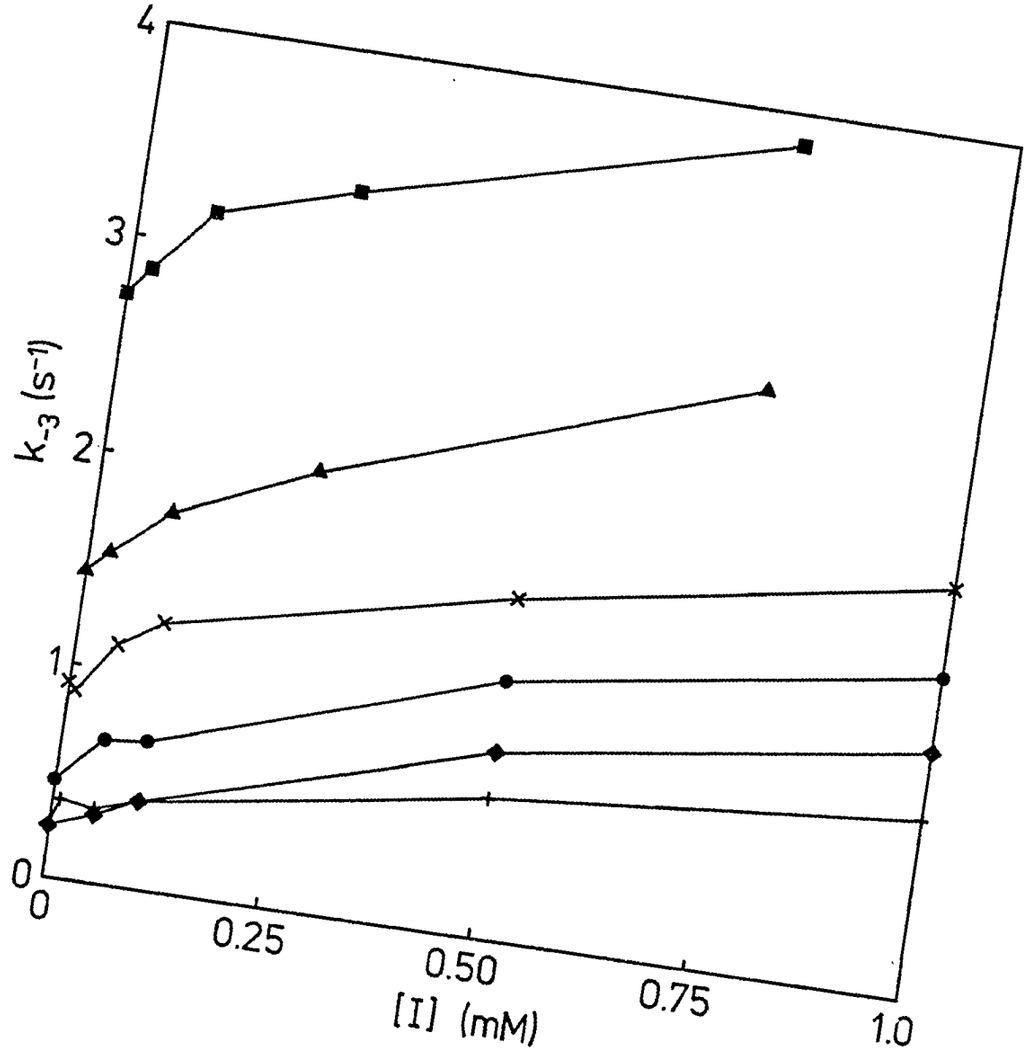
4
3
2
1
0
k_{-3} (s^{-1})
0
0.25
0.50
0.75
1.0
[I] (mM)

PNPM-occupied sites.

If Muller and Carr's hypothesis was true, then k_{-3} should be the same for all of the columns for a given inhibitor concentration and solute. Figure 6 clearly shows this not to be true.

We propose an alternative explanation. We believe that the methods to correct for the diffusional contributions used by ourselves and Muller and Carr were in error, because of an inaccurate calculation of these terms as a function of k'. In this case, one might expect the apparent k_{-3} to be a function of k', rather than [I]. Figure 7, a plot of k_{-3} versus 1/k', indicates that this might be the case. (Note - 1/k' was plotted to make the figure more comparable to Figure 6. The same trends were observed if k_{-3} was plotted versus k'.) The high- and low-coverage Hypersil column data for a given solute, which are shown connected by a dotted line, appeared to be part of a continuous data set, in agreement with our hypothesis. The k_{-3} values seemed to plateau at low k', at values which were close to the literature data from solution (Table IV). This suggested that the error in the diffusional corrections was worse as k' increased, which would be expected, since these diffusional parameters were measured at k' = 0.

On the other hand, the LiChrospher SI 500 data points were not on these curves and did not even show differences

Figure 7. Plots of the calculated dissociation rate constants versus 1/k'. Symbols are the same as in Figure 2

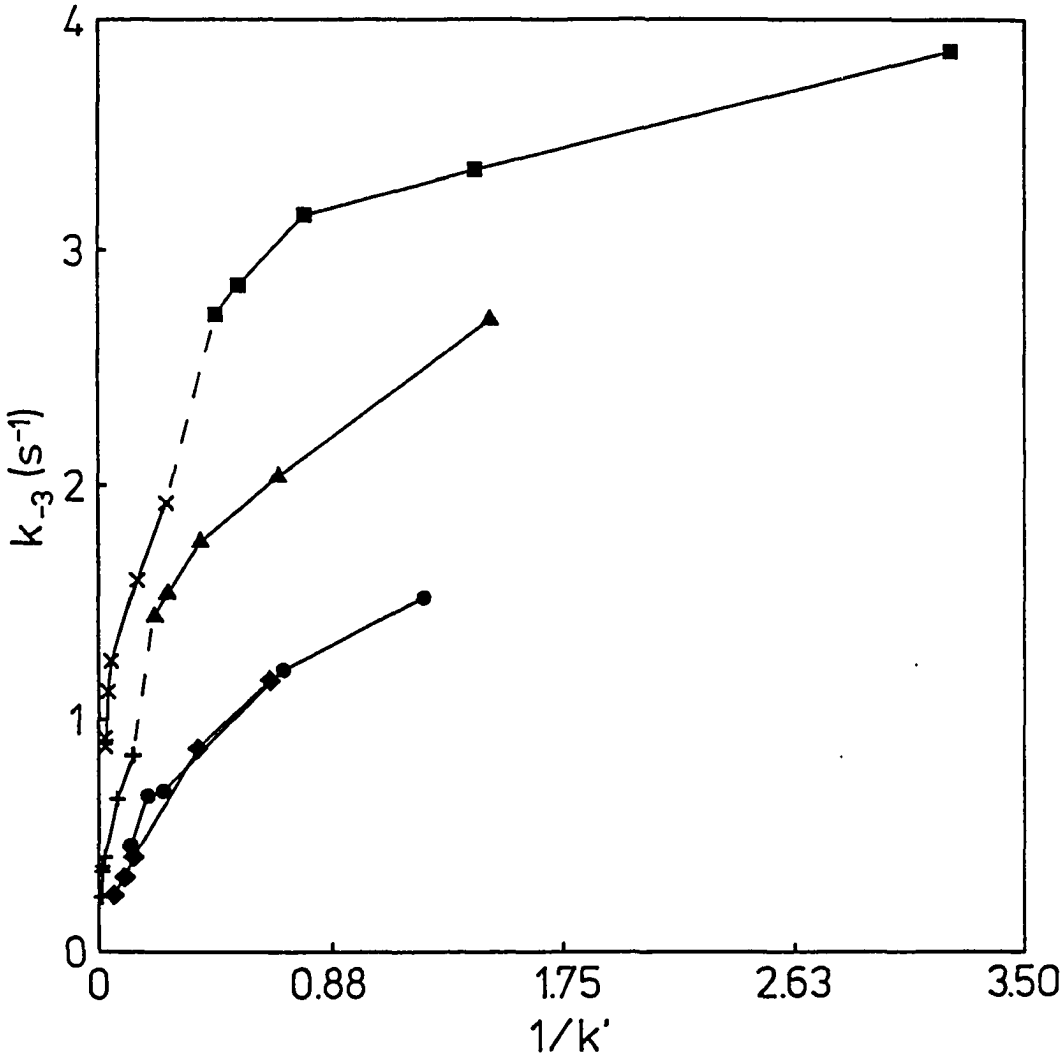
4
3
2
1
0
k_{-3} (s^{-1})
0
0.88
1.75
2.63
3.50
1/k'

Table IV. Rate constant values obtained by various methods from the low-coverage Hypersil 300 column

Method	MUM		PNPM	
	$k_3(sec^{-1})$	$k_3{}^a(M^{-1}sec^{-1})$	$k_{-3}(sec^{-1})$	$k_3{}^a(M^{-1}sec^{-1})$
Literature (25)	3.4	11.3×10^4	6.2	5.4×10^4
Visual extrapolation of Figure 7	3	14×10^4	4	9.6×10^4
Plate height with H_m and k_{-1} fixed at expt. values	1.9	8.6×10^4	3.1	7.4×10^4
Plate height with H_m and k_{-1} variable	2.1	9.5×10^4	3.5	8.4×10^4
Variances with H_m and k_{-1} fixed at expt. values	1.5	6.8×10^4	2.9	7.0×10^4
Variances with H_m and k_{-1} variable	1.7	7.7×10^4	3.3	7.9×10^4

[a]Assuming K_3 = 45000 for MUM and 24000 M^{-1} for PNPM, from the HPAC data in Table II.

between MUM and PNPM (Figure 7). Since the diffusional properties of the two supports were different, this suggested that the corrections for the LiChrospher SI 500 support were so grossly in error that differences in kinetic properties of the two solutes were no longer apparent. This might be expected, since Figure 4b showed very little apparent kinetic contribution for this support.

Total Curve-Fitting Approach

The problem described above is shown more clearly in Figure 8a. The contributions of H_m and H_{sm} calculated from the data in Table III obviously did not come anywhere close to accounting for the band-broadening at high k', where the kinetic contribution must always be small. Thus, calculating k_{-3} from the high k' data invariably led to low values of k_{-3}.

An alternative method was to fit an entire data set to Equation 4. Such fits typically gave unrealistic (negative) values for H_m. We also did the best fit to the kinetic data after constraining H_m and k_{-1} to the values given in Table III. This is shown in Figure 8a, and the fit is obviously not good. In Figure 8b, H_m and k_{-1} were allowed to vary, but with the constraints that H_m had to be positive and that the sum of H_m and H_{sm} at k' = 0 equaled the measured value for the non-retained sugar MUGA or PNPG. This yielded somewhat better

Figure 8. Plots of plate height versus k' for the PNPM data on the high-coverage Hypersil 300 columns (◆). In (a) the calculated H_m and H_{sm} from Table III are shown along with the best fit of H_k to the remaining plate height. In (b) the value of H_{sm} was allowed to increase to better account for the band-broadening at high k'

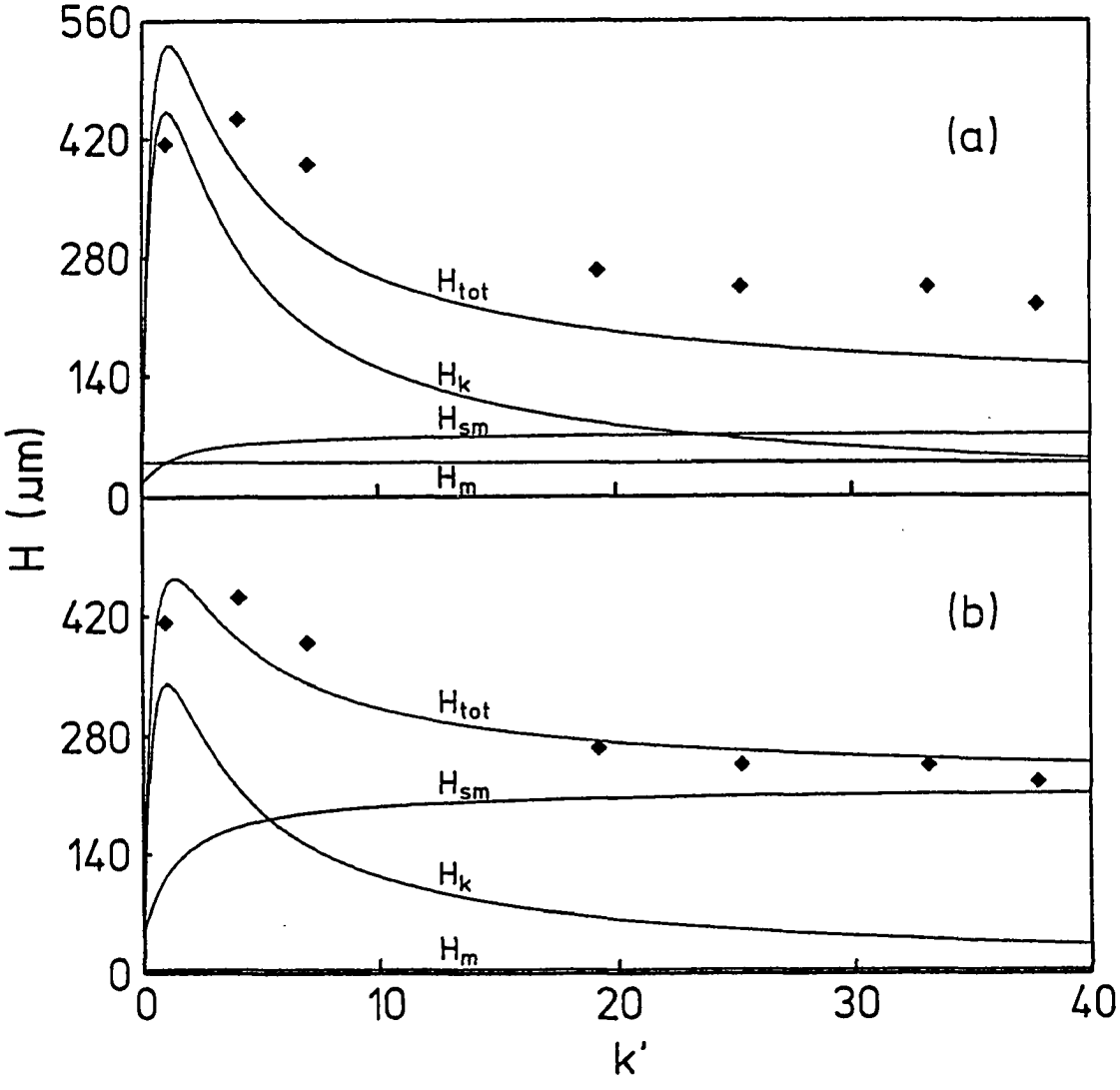
560
420
280
140
0
H (μm)
(a)
H_{tot}
H_k
H_{sm}
H_m
420
280
140
0
(b)
H_{tot}
H_{sm}
H_k
H_m
0
10
20
30
40
k'

results. Similar fits using variances were also tried. Table IV summarizes some of the results for the low-coverage columns, which we believe yielded the most accurate data. The values of k_{-3} were somewhat smaller than literature values but were in the region expected given the somewhat larger equilibrium constants previously determined. Thus, association rate constant values were similar to those measured in solution.

Although these results were reasonable, in general, the curve-fitting results were unsatisfactory in that H_t declined more slowly after peaking out than the equations predicted. Golay-type equations (15,16) did not give any better results. The inescapable conclusion is that the chromatographic theory used here did not adequately describe the band-broadening over a wide range of k'. Further work is needed to examine this problem.

Peak Shape Data

In addition to the discrepancies between experimental and theoretical H_t versus u plots, we have examined discrepancies in the peak shapes, as another way of comparing experimental data with the model used to derive Equations 5 and 6. This study also provided useful information on how to measure the statistical moments of the peaks.

Computer simulations of the stagnant mobile phase and adsorption-desorption kinetic terms were performed at various plate numbers and capacity factors using first-order rate equations.

The moment coefficient of skewness, G_1, is one measure of peak shape (17). It is calculated from the second and third moments of a peak (27). For reversed-role affinity chromatography, G_1 can be written as (27):

$$G_1 = 3\sqrt{\frac{uV_m}{2CLV_p}} \cdot \frac{\frac{(1+V_m k'/V_p)^3}{k_{-1}^2} + \frac{2V_m k'(1+V_m k'/V_p)/V_p}{k_{-1}k_{-3}} + \frac{V_m k'/V_p}{k_{-3}^2}}{\left(\frac{(1+V_m k'/V_p)^2}{k_{-1}} + \frac{V_m k'/V_p}{k_{-3}}\right)^{3/2}} \quad (12)$$

If diffusion is very rapid, this reduces to:

$$G_1 = 3\sqrt{u/2CLk'k_{-3}} \quad (13)$$

which shows that the peaks become more symmetric as k' or k_{-3} increase. If desorption is very rapid, the equation reduces to:

$$G_1 = 3\sqrt{uV_m/2V_pCLk_{-1}} \quad (14)$$

which is the same as given previously (17) and which indicates that the peak shape is independent of retention.

Various values of k_{-1}, k_{-3}, L, V_p, and V_e were used to simulate peaks with k' from zero to 5, plate numbers from 2 to 100, and V_m/V_p from 2 to 11. The peak skewness ($B/A_{0.1}$), a peak shape parameter that is experimentally measured more accurately than the higher statistical moments (28), but which is difficult to predict theoretically, was determined for each peak. Figure 9 shows that there is predicted to be a direct relationship between $B/A_{0.1}$ and G_1 even under widely varying conditions. Plots of $B/A_{0.1}$ or G_1 versus plate number do not yield a 1:1 relationship, although there is a general improvement in symmetry as N increases.

Our experimental data showed almost no change in $B/A_{0.1}$ as k' changed. This is an indication that diffusional band-broadening dominated over most of the range of k', as we have postulated earlier.

Plate numbers were also calculated from the width-at-half-height ($W_{0.5}$) and the peak-center-at-half-height ($V_{0.5}$):

$$N_{0.5} = 5.545(V_{0.5}/W_{0.5})^2 \qquad (15)$$

It was found that $N_{0.5}$ was an excellent measure of the true plate number, since the simulated peaks were generally close

Figure 9. Plot of the peak asymmetry from a computer simulation versus the moment coefficient of skewness calculated from Equation 12 under a variety of conditions and assuming that only H_{sm} and H_k caused band-broadening. The scatter at high skewness was due to inaccuracies in the computer program

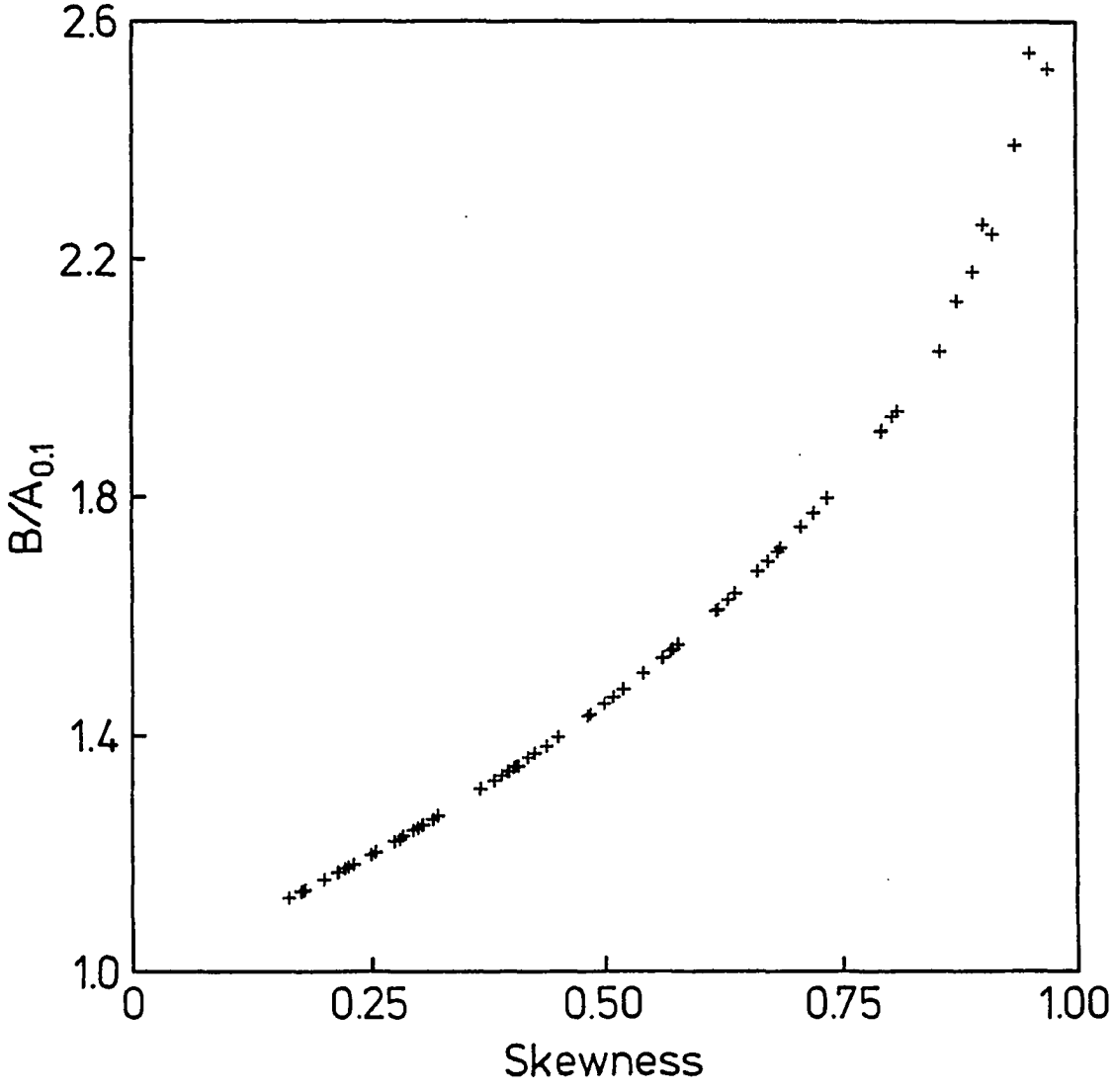
2.6
2.2
1.8
1.4
1.0
B/A0.1
0
0.25
0.50
0.75
1.00
Skewness

to Gaussian. Even under the extremes examined, $N_{0.5}$ was within ±5 % of the true plate number in the range $N \geq 10$. The only exceptions were the unusual cases of "split-peaks" (18).

Figure 10 compares the experimental $B/A_{0.1}$ values for the Con A columns with the simulated values at various plate numbers. It can be seen that the experimental peaks were more tailed than predicted and, thus, there was some discrepancy between the model and real data. One source of such discrepancies could be heterogeneities, such as a range of particle sizes.

Table V shows the results of a simulation experiment in which diffusional heterogeneity was studied under conditions where adsorption-desorption kinetics were negligible. The column of k_{-1} values indicates the percentage of particles with the given rate constant. Note that a 10-fold change in k_{-1} corresponds to an approximately 3-fold change in particle diameter. Commercial supports are somewhere between the values given in the last two rows of the table. It is apparent that such heterogeneity could account for much of the peak asymmetry experimentally observed. It is also seen that there was a moderate decrease in the accuracy of $N_{0.5}$ as the peaks became less symmetric, with $N_{0.5}$ tending to overestimate the plate number. However, the errors were small compared to experimental errors often encountered in determining the

Figure 10. Scatter diagrams showing peak asymmetries as a function of plate number from the affinity column data (◘) and the computer simulations (◇)

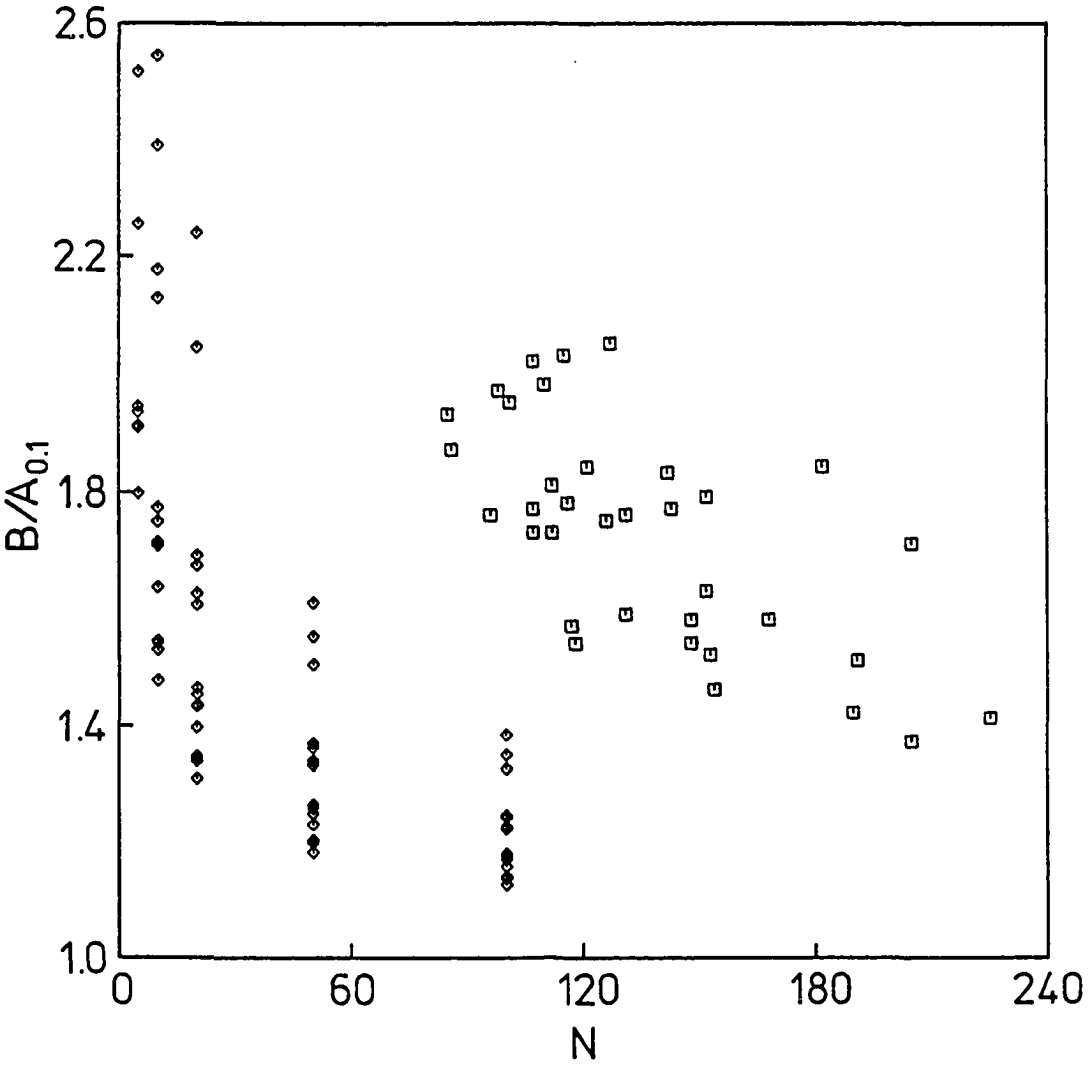
2.6
2.2
1.8
1.4
1.0
B/A0.1
0
60
120
180
240
N

Table V. Effect of diffusional heterogeneity at k' = 1

k_{-1}	N_m[a]	$N_{0.5}/N_m$	$B/A_{0.1}$
0.2 (100%)	177	0.99	1.11
0.02 (20%), 0.2 (80%)	63	1.13	1.62
0.2 (80%), 2.0 (20%)	216	0.98	1.12
0.02 (10%), 0.2 (80%), 2.0 (10%)	98	1.18	1.52
0.1 (10%), 0.2 (80%), 0.4 (10%)	169	0.99	1.13

[a] N_m is the true statistical moments plate number.

"true" plate number by the summation method (29), and so $N_{0.5}$ was used in all the experimental data presented previously.

The diffusional heterogeneity should not affect the accuracy of the kinetic determinations, because it was found that the apparent k_{-1} value calculated from the peak profiles obeyed Equation 5 exactly, even when the peak shape changed. The same conclusion has been obtained theoretically (29). However, it may be that other sources of heterogeneity not considered here might be less well-behaved and could cause the non-ideal H_t versus k' behavior.

CONCLUSIONS

While retention data appear to be adequately described by theory, kinetic data were inadequately described as a function of k'. Since diffusional band-broadening was significant even when small sugars were chromatographed on 5 μm supports, it is apparent that even smaller or non-porous particles are needed to accurately measure dissociation rate constants in the range of 5 sec^{-1}. Further work is also needed to study the causes of non-ideal peak shapes and H_t versus k' plots.

ACKNOWLEDGEMENTS

This work was supported by the National Science Foundation under Grant CHE-8305057 and by the Petroleum Research Fund of the American Chemical Society.

REFERENCES CITED

1. Dunn, B. M.; Chaiken, I. M. Proc. Nat. Acad. Sci. USA 1974, 71, 2382.

2. Dunn, B. M. Applied Biochem. Biotechnol. 1984, 9, 261.

3. Turkova, J. "Affinity Chromatography"; Elsevier: Amsterdam, 1978; p. 35.

4. Hethcote, H. W.; DeLisi, C. J. Chromatogr. 1982, 248, 183.

5. Hethcote, H. W.; DeLisi, C. In "Affinity Chromatography and Biological Recognition"; Chaiken, I. M.; Wilchek, M.; Parikh, I., Eds.; Academic Press: Orlando, FL, 1983; p. 119.

6. Muller, A. J.; Carr, P. W. J. Chromatogr. 1984, 284, 33.

7. Anderson, D. J.; Walters, R. R. J. Chromatogr. 1985, 331, 1.

8. Giddings, J. C. "Dynamics of Chromatography"; Marcel Dekker: New York, 1965; pp. 38, 138, 244.

9. Horvath, C.; Lin, H. -J. J. Chromatogr. 1978, 149, 43.

10. Denizot, F. C.; Delaage, M. A. Proc. Nat. Acad. Sci. USA 1975, 72, 4840.

11. Kasche, V.; Buchholz, K.; Galunsky, B. J. Chromatogr. 1981, 216, 169.

12. Walters, R. R. J. Chromatogr. 1982, 249, 19.

13. Nilsson, K.; Larsson, P. -O. Anal. Biochem. 1983, 134, 60.

14. Chaiken, I. M. Anal. Biochem. 1979, 97, 1.

15. Katz, E. D.; Scott, R. P. W. J. Chromatogr. 1983, 270, 29.

16. Katz, E.; Ogan, K. L.; Scott, R. P. W. J. Chromatogr. 1983, 270, 51.

17. Hethcote, H. W.; DeLisi, C. J. Chromatogr. 1982, 240, 269.

18. Hage, D. S.; Walters, R. R.; Hethcote, H. W. Anal. Chem. 1986, 58, 274.

19. Stout, R. W.; DeStefano, J. J.; Snyder, L. R. J. Chromatogr. 1983, 282, 263.

20. Walters, R. R. In "Affinity Chromatography: A Practical Approach"; Dean, P. D. G.; Johnson, W. S.; Middle, F. A., Eds.; IRL Press: Oxford, 1985; p. 25.

21. Larsson, P. -O.; Glad, M.; Hansson, L.; Mansson, M. -O.; Ohlson, S.; Mosbach, K. Adv. Chromatogr. 1983, 21, 41.

22. Lowry, O. H.; Rosebrough, N. J.; Farr, A. L.; Randall, R. J. J. Biol. Chem. 1951, 193, 265.

23. Goldstein, I. J.; Hollerman, C. E.; Smith, E. E. Biochemistry 1965, 4, 876.

24. Lund, U. J. Liq. Chromatogr. 1981, 4, 1933.

25. Clegg, R. M.; Loontiens, F. G.; Van Landschoot, A.; Jovin, T. M. Biochemistry 1981, 20, 4687.

26. Kalb, A. J.; Lustig, A. Biochem. J. 1968, 109, 669.

27. Hethcote, H. W., Dept. of Mathematics, University of Iowa, Iowa City, IA; personal communication.

28. Anderson, D. J.; Walters, R. R. J. Chromatogr. Sci. 1984, 22, 353.

29. DeLisi, C.; Hethcote, H. W.; Brettler, J. W. J. Chromatogr. 1982, 240, 283.

SECTION IV.

HIGH-PERFORMANCE AFFINITY CHROMATOGRAPHY OF DIVALENT CONCANAVALIN A ON MATRICES OF VARIABLE LIGAND DENSITY

SUMMARY

Divalent concanavalin A was chromatographed under isocratic conditions on matrices of variable ligand density, containing immobilized p-aminophenyl α-D-mannopyranoside or D-glucosamine. Methyl α-D-mannopyranoside was used as a competing inhibitor in the mobile phase. As the ligand density increased, retention was observed to change from a primarily monovalent interaction to a primarily divalent interaction. Several retention models were used to examine the data and to evaluate the extent of cooperative binding. Especially when possible heterogeneity in the distribution of ligand molecules was taken into account, it was found that several retention models fit the data reasonably well.

INTRODUCTION

While retention modeling of monovalent solute-ligand interactions in affinity chromatography is straightforward and has been extensively studied (1-6), only a few affinity chromatographic studies have been performed modeling retention of solutes interacting divalently with immobilized ligands (7-10). Several models of retention for divalent solutes in affinity chromatography have been proposed. One model widely used in affinity chromatography is the "independent, equivalent-site" model, in which the two adsorption steps have identical equilibrium constants and in which the binding of one site is unaffected by the binding of the other site (11-15). A second model used in ion-exchange (16,17), reversed-phase (18), hydrophobic-interaction (19-22), and affinity (23,24) chromatography is the "high-cooperativity" model, in which adsorption always occurs via two (or more) ligand molecules. Recently, a "general" divalent model has been proposed, in which the adsorption process occurs in two steps, but with no assumption as to the extent of cooperativity or independence of the two binding steps (9,10).

Although each of these models has been employed in affinity chromatographic studies, only one previous study has compared more than one model (10). In the present work, high-performance affinity chromatographic studies of a divalent

solute on matrices of variable ligand density were performed to critically examine how well each model fit the data.

THEORY

The three major models for adsorption of divalent solute, E, onto a matrix containing immobilized ligands, L, are shown in Figure 1. The equilibrium constant, K_3, is the monovalent binding constant and K_4 is the binding constant of the second step. While K_3 is expressed in units of M^{-1}, K_4 is most correctly expressed in units of dm^2/mol, since surface concentrations are involved (9). A monovalent inhibitor, I, is usually present in the mobile phase to control retention of E. The equilibrium constant for the binding of I to E is K_2 (9). An expression for the capacity factor (k') as a function of experimental variables has recently been derived for the general model (9):

$$k' = \frac{K_3\{L\}A}{V_m} \cdot \frac{2(1+K_2[I])+K_4\{L\}}{(1+K_2[I])^2} \qquad (1)$$

where {L} is the average ligand density (mol/dm^2), A is the surface area of the matrix, and V_m is the column void volume. In this model, the adsorption process is thought of as a monovalent binding step followed by possible binding of the second site on the solute to a second ligand molecule. Depending on the magnitude of K_4, the overall binding can range from purely monovalent (K_4=0) to primarily divalent

Figure 1. Schematic diagram of three retention models: general model (a), independent, equivalent-site model (b), and high-cooperativity model (c). In the latter model, the quantity K_3K_4 represents a single equilibrium constant

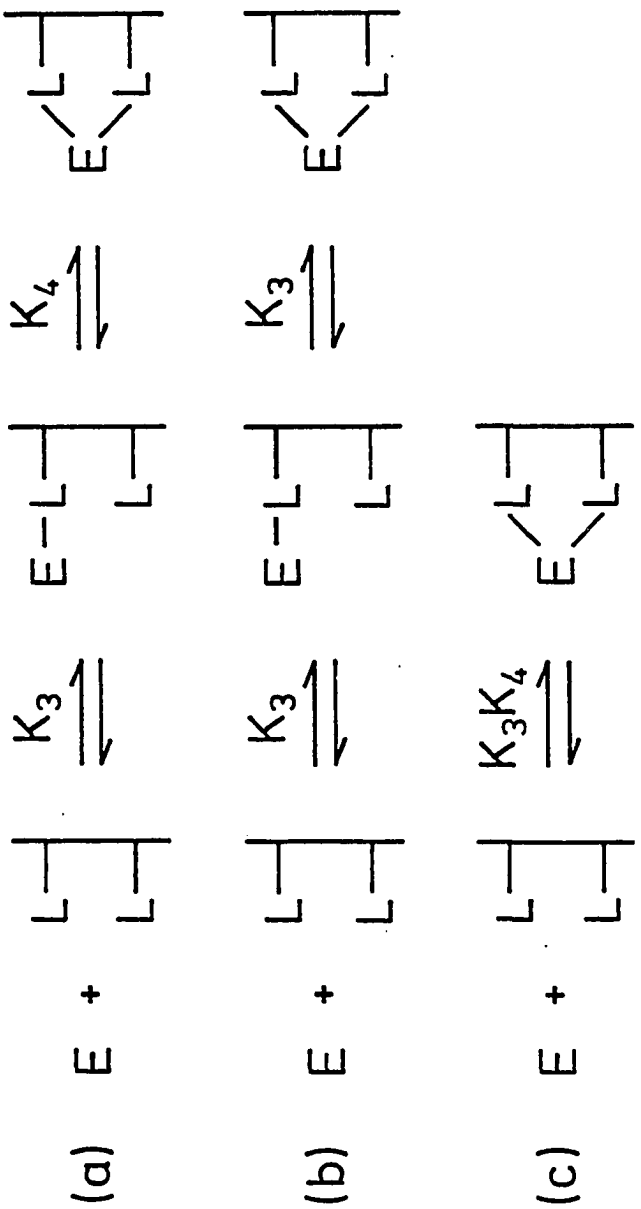
(a)
(b)
(c)
E
+
L L
K_3
E L L
K_4
K_3
K_3K_4

($K_4V_p/A >> K_3$, where V_p=column pore volume).

Expressions for the other models can be obtained easily, since they are limiting cases of the general model. Although free monovalent ligands in solution may bind to a divalent solute non-cooperatively (i.e., binding of a second ligand molecule is not affected by binding of the first molecule), if the ligands are attached to a surface, the second binding step may be more strongly favored because of the close proximity of the solute to the second ligand molecule. Therefore, there may be cooperative binding of immobilized ligands to a multivalent solute, even if the sites on the solute are all independent and equivalent. In the extreme case, which we will call the high-cooperativity model, all adsorption occurs divalently (i.e., only EL_2, but no EL or ELI present):

$$k' = \frac{K_3K_4\{L\}^2A}{V_m(1+K_2[I])^2} \qquad (2)$$

The quantity of K_3K_4 in Equation 2 really represents a single equilibrium constant, but for consistency we will express it as the product of the individual binding steps.

Some confusion can occur because the ligand always binds monovalently to the solute, while the solute can bind divalently to two ligands. In addition, when discussing cooperativity, one must think of the ligands binding

cooperatively to the solute; but in chromatographic terms one thinks of the solute adsorbing on the ligands.

For the independent, equivalent-site model the expression is:

$$k' = \frac{K_3\{L\}A}{V_m} \cdot \frac{2(1+K_2[I])+K_3\{L\}A/V_p}{(1+K_2[I])^2} \qquad (3)$$

The independent, equivalent-site model is basically a more limited form of the general model, in which the second ligand binding step has the same binding constant as the first step, i.e., $K_3=K_4V_p/A$. (Note - the factor V_p/A is necessary to account for the different units of K_4 versus K_3.)

A possible fourth model is one in which only divalent binding takes place, but in which $K_3=K_4V_p/A$. The equation is similar to Equation 2, but with K_4 replaced by K_3A/V_p. This will be called the divalent, equivalent-site model.

From Equation 1, it is also seen that for purely monovalent binding:

$$k' = \frac{2K_3\{L\}A}{V_m(1+K_2[I])} \qquad (4)$$

The factor of two accounts for the two sites per solute molecule.

Table I summarizes the conditions under which the

Table I. Description of limiting cases of the general model

Condition	Explanation
$K_4=0$	monovalent binding of solute (second site empty or contains inhibitor), Equation 4
$0<K_4V_p/A<K_3$	mixed monovalent and divalent (with negative cooperativity) binding
$K_4V_p/A=K_3$	divalent, independent, equivalent binding of sites, with monovalent binding allowed, Equation 3
$K_3<K_4V_p/A$	mixed monovalent and divalent (with positive cooperativity) binding
no EL or ELI	high-cooperativity model, no monovalent adsorption of solute, Equation 2
no EL or ELI, $K_4V_p/A=K_3$	divalent, equivalent-site model, in which no monovalent adsorption takes place

limiting cases of the general model apply.

A factor not taken into account in previous treatments is the possible heterogeneous distribution of ligand molecules. It is quite likely, especially at intermediate ligand densities, that some ligand molecules will be far enough from neighboring ligands that divalent adsorption will not be possible. In that case, purely monovalent interactions will occur in addition to the divalent interactions. To take this into account, one can assume that there is a fraction of the ligand molecules, f_L, occupying a fraction of the surface area, f_{SA}, with which the solute can interact divalently or monovalently, while with the remaining fraction of the ligand molecules ($1-f_L$), the solute can only interact monovalently. One can then derive heterogeneous versions of the above models. The heterogeneous, general model is described by:

$$k' = \frac{K_3\{L\}A}{V_m} \cdot \frac{2(1+K_2[I])+f_L^2 K_4\{L\}/f_{SA}}{(1+K_2[I])^2} \qquad (5)$$

Monovalent interactions in the general model (Equation 1) are due only to the position of the equilibrium between monovalently and divalently adsorbed forms of the solute. In the heterogeneous, general model, a fraction of the ligands is sterically unable to bind the solute divalently, while the remaining fraction can bind the solute monovalently and

divalently, as in the general model.

The heterogeneous, high-cooperativity model expression is:

$$k' = \frac{K_3\{L\}A}{V_m} \cdot \frac{2(1-f_L)(1+K_2[I])+f_L^2K_4\{L\}/f_{SA}}{(1+K_2[I])^2} \qquad (6)$$

In this model, only monovalent adsorption occurs in regions of low ligand density and only divalent adsorption occurs in regions of high ligand density.

The equation for the heterogeneous, independent, equivalent-site model is:

$$k' = \frac{K_3\{L\}A}{V_m} \cdot \frac{2(1+K_2[I])+f_L^2K_3\{L\}A/V_pf_{SA}}{(1+K_2[I])^2} \qquad (7)$$

This is the same as the heterogeneous, general model, except $K_3=K_4V_p/A$.

EXPERIMENTAL

Reagents

Concanavalin A (Con A, types IV and V), bovine serum albumin (BSA), D(+)-glucosamine hydrochloride, p-aminophenyl α-D-mannopyranoside (PAPM), and methyl α-D-mannopyranoside (MDM, grade III) were obtained from Sigma (St. Louis, MO). The Con A was purified as described previously (9). The 1,1'-carbonyldiimidazole (CDI) was obtained from Aldrich (Milwaukee, WI). Hypersil WP-300, 5 μm, and LiChrospher SI 500, 10 μm, were from Alltech (Deerfield, IL).

Procedure

The high- and medium-coverage PAPM columns and the glucosamine columns were prepared as described earlier (9). Note that the medium-coverage column in this work was referred to as low-coverage PAPM in the previous study. The low-coverage PAPM column (this work) was prepared by a CDI activation method (25), with changes in a previously published procedure (9), as described in the rest of this paragraph. Diol-bonded Hypersil 300 was prepared according to a published procedure (26). An amount of 1.9 g diol-bonded Hypersil 300 was activated by the addition of 4.8 mg CDI. The amount of

CDI added corresponded to 10 % of the total diol content of the silica. The amounts used in the immobilization reaction were 0.6 g activated silica, 100 mg PAPM, and 5 ml 0.1 M sodium phosphate buffer (pH 7). PAPM and glucosamine silicas were assayed as described previously (9).

Chromatographic apparatus and conditions were described previously (9). The mobile phase consisted of MDM-containing acetate buffers (pH 5.0), prepared as described previously (9). At this pH, Con A existed as a dimer (27), containing two identical sugar binding sites (28). Chromatography was performed with the column thermostated at 25.0 °C. Con A samples (10μL), 4 mg/ml, were injected. The samples were prepared in the appropriate MDM-containing buffer. Sample concentrations were found to be within linear elution conditions, as determined by concentration studies of Con A on the low-coverage column (29). Column parameters are summarized in Table II. The column void volume was determined by injection of water. The first moment of each peak was determined as the peak-center-at-half-height. Capacity factors were calculated from first moments for Con A and water, and corrected for extra column time and slight non-specific retention of Con A on diol columns ($k' \sim 0.1$ for LiChrospher SI 500 and negligible for Hypersil 300). A linear least squares analysis was used for fitting the experimental

Table II. Column parameters

Column	Matrix	Dimensions[a] ID (mm)	Dimensions[a] CL (mm)	V_p[b] (ml)	V_m (ml)	A[c] (m^2)	{L}[d] (μmol/m^2)	Avg. distance between ligands (Å)
Low-coverage PAPM	5 μm Hypersil 300	4.1	50.0	0.18	0.41	22	0.018	96
Med.-coverage PAPM	10 μm LiChrospher SI 500	4.6	50.0	0.38	0.67	15	0.28	24
High-coverage PAPM	10 μm LiChrospher SI 500	4.6	45.0	0.34	0.58	13	0.98	13
Glucosamine	10 μm LiChrospher SI 500	4.1	50.3	0.29	0.50	12	0.73	15

[a]ID and CL stand for internal diameter and column length, respectively.

[b]Determined by multiplying V_m by an experimentally determined ratio of V_p/V_m for LiChrospher SI 500 and Hypersil 300 diol columns (27).

[c]Based on column volume, experimentally determined packing density, and manufacturers' estimates of surface area.

[d]Based on ligand assays and manufacturers' estimates of surface area.

data to the monovalent model. A non-linear least squares analysis (30) was used for all other fits.

RESULTS AND DISCUSSION

Valency of Con A Interaction with Each Column

Three PAPM matrices of different ligand densities, as well as a glucosamine matrix of high ligand density, were synthesized. All columns had the potential for divalent adsorption of Con A, except for the low-coverage PAPM column, as determined from estimates of the average ligand spacing on the matrix. The average distance between ligands was calculated for each column, assuming an even distribution of immobilized ligand on the silica surface, and is given in Table II. Only the low-coverage PAPM column had an average distance between ligands greater than 80 Å, which is the distance between sugar binding sites on the Con A dimer (31).

A preliminary assessment of the valency of Con A interaction with each affinity matrix was made by examination of $1/k'$ versus $[I]$ plots, which are given in Figure 2. According to Equation 4, a straight line would be expected for purely monovalent adsorption. This was observed only for the low-coverage PAPM column, as anticipated from the estimates of the average ligand spacing on the silica surface. The other data sets showed curvature in the $1/k'$ versus $[I]$ plots, indicating multivalent interaction of the Con A with the matrix. The multivalent nature of this data is clearly

Figure 2. Plots of 1/k' versus the concentration of methyl α-D-mannopyranoside for the immobilized glucosamine column (●) and the immobilized PAPM columns of low (▲), medium (■), and high (◆) ligand densities. The inhibitor concentrations for the glucosamine and low-coverage PAPM columns were actually 1/500 of those shown

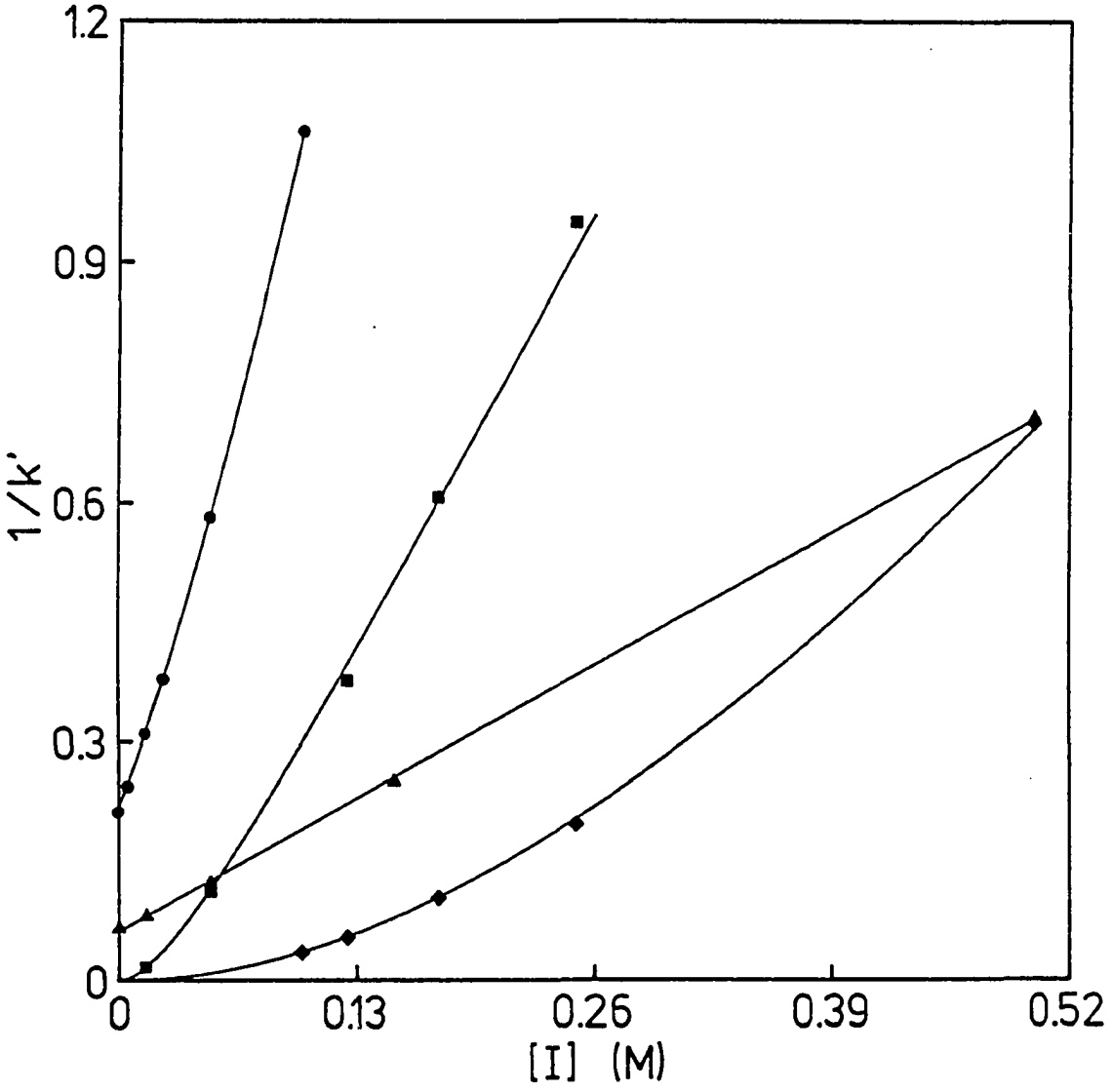
1.2
0.9
0.6
0.3
0
1/k'
0
0.13
0.26
0.39
0.52
[I] (M)

illustrated by some simple calculations for the higher-coverage PAPM columns, using the monovalent values of K_2 and K_3 (obtained from the monovalent fit of the low-coverage PAPM data) given in Table III. For the medium- coverage PAPM column, the monovalent k' should be 0.20 at $[I]$ = 0.05 M; the experimental value was 9.0. For the high-coverage column, k' should be 0.14 at $[I]$ = 0.25 M; the experimental value was 5.1.

Precision of the Fit for Various Models for Each Column

Data for each column were fit to Equations 1-4, to determine which model most precisely fit the experimental data. In order to quantitatively compare the fitting precision for each of the various models, a percent error of fit was calculated, as specified and tabulated in Table III. No assumption regarding values for the equilibrium constants (K_2, K_3, and K_4) was made in fitting the low-coverage PAPM and glucosamine data sets. However, it was necessary to assume a value for K_2 for the medium- and high-coverage PAPM columns. This is because the experimental conditions were such that $K_2[I] >> 1$, which resulted in the incorporation of the K_2 term within the other equilibrium constants (see Equations 1-4). Based on previous work (29), a value for $K_2 = 8.3 \times 10^3\ M^{-1}$ was used.

Table III. Equilibrium constant data

	Low-coverage PAPM	Medium-coverage PAPM[a]	High-coverage PAPM[a]	Glucosamine
Monovalent fit (Eq. 4)				
K_2 (M^{-1})	1.0×10^4	----	----	2.3×10^4
K_3 (M^{-1})	8.5×10^3	3.9×10^5	3.8×10^5	1.6×10^2
% error of fit[b]	4.5	88.2	97.8	8.0
Independent sites (Eq. 3)				
K_2 (M^{-1})	3.8×10^3	----	----	1.1×10^4
K_3 (M^{-1})	2.2×10^3	1.2×10^5	1.1×10^5	69
% error of fit	4.7	14.4	19.9	3.0

High-cooperativity (Eq. 2)				
K_2 (M^{-1})	2.3×10^3	----	----	6.2×10^3
$K_3K_4V_p/A$ (M^{-2})	6.6×10^6	2.2×10^{10}	2.4×10^{10}	9.0×10^3
% error of fit	12.8	57.8	10.3	1.9
General (Eq. 1)				
K_2 (M^{-1})	5.6×10^3	----	----	7.6×10^3
K_3 (M^{-1})	4.3×10^3	1.6×10^5	3.9×10^4	24
K_4V_p/A (M^{-1})	7.8×10^2	7.0×10^4	5.2×10^5	310
% error of fit	0.6	3.4	1.5	0.3

[a]Using a value of 8.3×10^3 M^{-1} for K_2.

[b]Calculated from the experimental k' values (k'_{exp}) and the k' values from the fit (k'_{fit}), by the equation: $100[\Sigma\{(k'_{exp}-k'_{fit})/k'_{exp}\}^2/(n-1)]^{1/2}$, where n is the number of experimental points.

Comparison of the percent error of the fits for each model in Table III, as well as examination of the plots for each model given in Figure 3, shows that the data sets for all four columns were most precisely fit by the general model (Equation 1). This finding was expected, however, because the high-cooperativity (Equation 2), the independent, equivalent-site (Equation 3), and the monovalent (Equation 4) models are limiting cases of the general model and, therefore, can never exceed the general model in fitting precision. What needs to be determined, however, is whether retention could also be accurately depicted by any of the simpler models. This is particularly of interest for multivalent solutes, for which the independent, equivalent-site model has been extensively used to model affinity chromatographic retention (11-15).

Determination of the adequacy of these limiting-case models requires examination of the percent error of the fits (Table III), which in a simplistic way can be viewed as the average percent deviation of the experimental points from the fitted plot. An overview of all the columns showed the range of percent error for the general model to be lowest, varying from 0.3 to 3.4 %. In contrast, the errors for the other models were several-fold larger.

Whether the limiting-case models gave fits with adequate precision (less than 5 % error in the fit) depended on the column used. Good fits were obtained for the glucosamine data

Figure 3. Fits of the retention data to the independent, equivalent-site model (a), the high-cooperativity model (b), and the general model (c). The symbols are the same as in Figure 2. The capacity factors and inhibitor concentrations for the glucosamine column were actually 1/10 and 1/2000 of those shown, respectively, and 1/2 and 1/500, respectively, for the low-coverage PAPM column

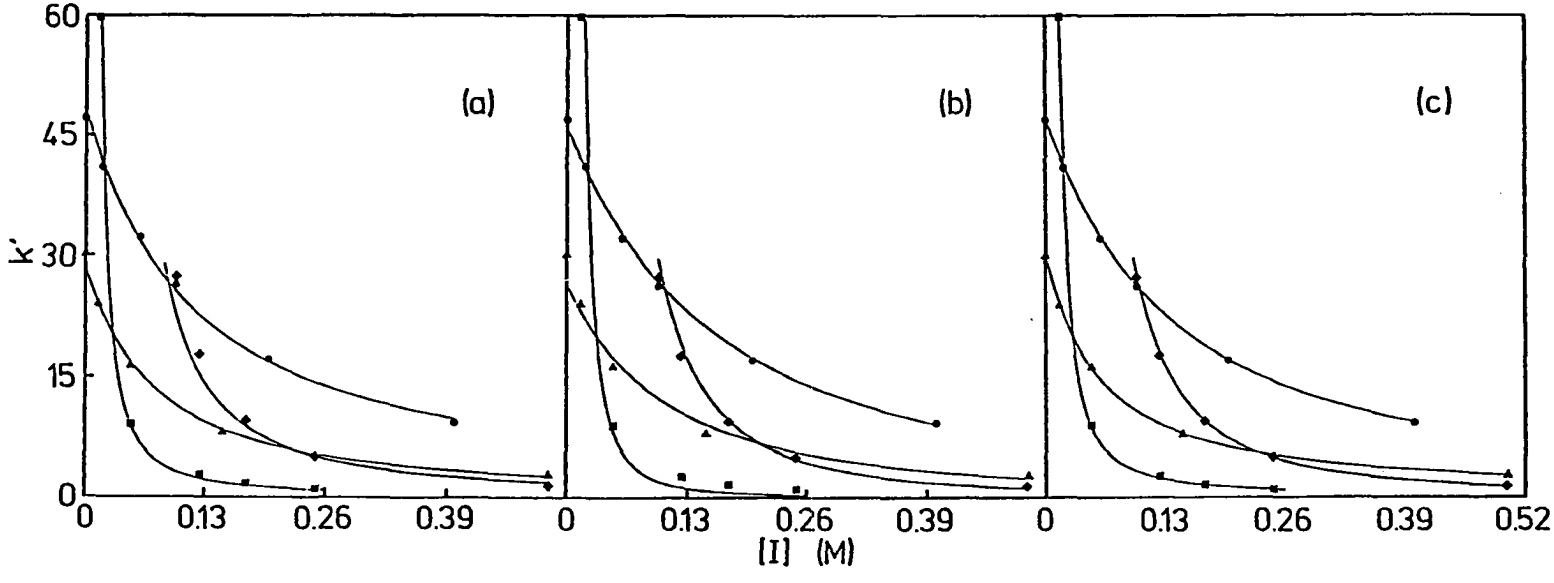
60
45
30
15
0
k'
(a)
(b)
(c)
0
0.13
0.26
0.39
0.52
[I] (M)

set for the high-cooperativity (1.9 % error) and independent, equivalent-site (3.0 % error) models. The fit of the glucosamine data to the monovalent model was moderately good. The 8 % error for this fit, however, was nearly double the error for the same fit of the low-coverage PAPM data set, reflecting a greater degree of divalent interaction for the glucosamine column.

The greatest deviation for the limiting-case models was noted for the higher-coverage PAPM columns. The total failure of the monovalent model to predict retention for these columns is seen by the very high percent errors (90-100 %) for these fits. High percent errors were also noted for the independent, equivalent-site (14-20 % error) and high-cooperativity (10-58 % error) models. The seriousness of this deviation was best exemplified by the medium-coverage PAPM data, in which both the independent, equivalent-site and high-cooperativity models significantly overestimated k' for the lower MDM concentration (71.5 and 90.8, respectively, compared to an experimental value of 59.9). Thus, with fitting errors of 10 % and greater for the limiting-case models, the appropriateness of these models for fitting the data from the two higher-coverage PAPM columns was determined to be inadequate.

Comparison of the model fits for the low-coverage PAPM data set indicated that there was a small amount of divalent

adsorption of Con A occurring on this column. The good linear fit of Equation 4 (0.9999 correlation coefficient) to the data, as well as the results of the ligand assays, which showed that the density of immobilized ligand molecules was low enough to exclude divalent interaction of Con A, supported the contention that the majority of Con A adsorption on this column was monovalent. The fitting error for the monovalent model, however, was 4.5 %. Fitting the general model improved the percent error of the fit to 0.6 %, by finding a small value for the $K_4\{L\}$ term. This finding suggests that, in addition to the monovalent adsorption, there was also a small fraction of higher density immobilized ligand molecules with which Con A could divalently interact. This mixed valency of interaction due to a heterogeneous distribution of immobilized ligand molecules is modeled by Equation 5, which is of the same form as the general model, and will be discussed in more detail later.

Comparison of the percentage error of the fits (Table III) for the two multivalent limiting-case models (Equations 2 and 3) shows that the independent, equivalent-site model gave the most precise fit for the lower ligand density columns (low- and medium-coverage PAPM columns), while the high-cooperativity model gave the most precise fits for the higher ligand density columns (glucosamine and high-coverage PAPM columns). This trend suggests an increase in

cooperativity with an increase in surface density of affinity ligands.

The data presented so far support the conclusion that choosing one of the limiting-case models for the determination of equilibrium constants may be too restrictive. While each of the models gave good fits in some cases, only the general model gave good fits in all of the cases. Although some of the goodness of fit was related to the number of fitted parameters, the data suggest that equilibrium constants determined using the independent, equivalent-site model, or any of the other limiting-case models, may be in error.

Calculated Equilibrium Constants

Equilibrium constant values were calculated from the fits by using independently determined values for {L}, A, V_p, and V_m (Table II) and are given in Table III. The equilibrium constant, K_4, which is written in terms of surface concentrations, was converted to a solution equilibrium constant by multiplying by the factor V_p/A. The solution equilibrium constant, K_4V_p/A, assumes that all affinity ligand molecules were evenly distributed within the volume V_p. The experimental values of K_2 for the binding of MDM to Con A in the mobile phase can be compared to $K_2=8.3 \times 10^3$ M^{-1} for the adsorption of MDM on immobilized Con A (29). Experimental K_3

values for PAPM can be compared to K_3=2.4 x 10^4 M^{-1}, for p-nitrophenyl α-D-mannopyranoside (PNPM) chromatographed on immobilized Con A (29), and K_3=8.7 x 10^3 M^{-1}, for PNPM and Con A in free solution (32). Experimental K_3 values for glucosamine can be roughly compared to the solution binding constant for N-acetyl-D-glucosamine of 1.4 x 10^2 M^{-1} determined at 5 °C (33).

Equilibrium constants calculated for the glucosamine column varied according to the model used; however, K_2 and K_3 values were all reasonable in comparison with the values given above, with the exception of the K_2 value estimated from the monovalent fit, which was a factor of three too high. The general model yielded a value of K_2 (7.6 x 10^3 M^{-1}) that was closest to the expected value.

The discussion following will concentrate on the equilibrium constant results determined for the PAPM columns, as several discrepancies were noted in comparing the results for the different ligand coverage columns. All of the values for K_2 and K_3 obtained from the low-coverage PAPM data were within a factor of five of the expected values. The monovalent and general models yielded estimates of K_2 closest to the expected value. The general model provided the best fit to the data and indicated weak divalent adsorption (K_4V_p/A ~ 1/5 of K_3). The use of the general model for this data set seemed reasonable, particularly when examined in the context

of possible heterogeneity (see below).

The value for K_3 obtained for the low-coverage PAPM column can be compared to the K_3 values obtained for the higher-coverage PAPM columns. One would expect the value of K_3 to remain constant as the ligand density changed. However, none of the models showed this expected constancy in the K_3 term (Table III). Although a similar value for K_3 was calculated for both the medium- and high-coverage PAPM columns using the independent, equivalent-site model, the value was at least one order of magnitude greater than the value calculated for the low-coverage PAPM column. This increase in K_3 undermines the independence presumption of the model, which states that the binding strength of one site is unaffected by the binding of the other site. The general model also showed an increase in the value of K_3 from the low- to the higher-coverage PAPM columns. In addition, the value for K_3 varied widely for the three columns, showing no particular trend with surface concentration of immobilized ligand. At present, these inconsistencies cannot be explained, although several suggestions are offered later in this paper.

While in theory, K_3 values should be constant for different immobilized ligand concentrations, it is not known how K_4 should vary with immobilized ligand concentrations, much less what the value for K_4 should be. The extent of cooperativity will be reflected in the value of K_4V_p/A

relative to K_3. K_4 will necessarily be zero, due to steric considerations, below a certain ligand density. One might imagine that K_4 would increase to a constant value above this critical density of ligand molecules. On the other hand, K_4 might continue to increase with ligand density, as more ligand molecules become accessible to the second solute binding site.

No matter which model was chosen, the data suggested a significant degree of cooperative binding of the ligands to Con A. From the independent, equivalent-site fit, this was suggested by the higher values of K_3 determined for the higher-coverage columns compared to the low-coverage column. From the high-cooperativity model, this was suggested by the values of $K_3K_4V_p/A$ for the higher-coverage columns, which were larger than the value of K_3^2 from the monovalent data. For the same reason, this suggests that the divalent, equivalent-site model was a poor model. Finally, from the general model, the value of K_4 was observed to increase with ligand density, as one would expect if K_4 itself was a function of ligand density. Note that the value of K_4V_p/A was smaller than K_3 for the low-coverage column, but larger than K_3 for the high-coverage column. This also suggested that the divalent adsorption process became more favorable as the ligand density increased.

Explanations for Discrepancies Found for the Equilibrium Constants

Several factors could explain the discrepancies found in the K_3 results. Accurate determinations of the equilibrium constants K_3 and K_4 depended on the ability to determine {L}, V_m, V_p, and A with minimum error. For the present study, determination of {L} presented the greatest difficulty, since the desired immobilized ligand concentration (which will be referred to as the functional ligand concentration) was that which was active and accessible to the Con A molecule. To determine the functional ligand concentration requires a break-through analysis. This was not feasible for the present system for several reasons. First, the concentration of Con A required to saturate most of the ligand molecules on the column was too high for practical considerations. Second, saturation of the higher ligand density columns would not be a true determination of the amount of accessible ligand molecules, as an unknown number of immobilized ligand molecules would be covered, but not bound to, the Con A molecules. The best estimate for the functional ligand concentration was the determination of the total ligand concentration by chemical analysis, which was the procedure used in this work. Differences in the percent of the total ligand content that were functional for the three PAPM columns

could explain the variability in K_3. This may be particularly true in comparing the low-coverage PAPM column to the higher-coverage PAPM columns, in which different silica matrices were used.

Retention by other mechanisms, such as hydrophobic interactions, could also present a problem. This is of particular concern for the Con A system, which, in addition to its sugar binding sites, has two hydrophobic binding sites for each dimer molecule (31). This effect would be multiplicative in the same way that the retention of Con A was multiplicative through the K_3K_4 term, as seen in Equation 1, but might show a different dependence with the concentration of the hydrophilic inhibitor MDM. This could explain the increase of K_3 found for the higher-coverage PAPM columns (in which simultaneous mixed retention mechanisms could occur) over the low-coverage PAPM column (in which simultaneous mixed retention mechanisms were precluded from occurring by the low density of the immobilized ligand molecules).

An additional cause for high K_3 values could be the presence of tetravalent Con A. Although the pH of the mobile phase was chosen such that Con A was present predominantly as the dimer, the presence of small amounts of tetravalent Con A could increase retention and alter the shape of the k' versus [I] plots. This would affect the values of the equilibrium constants calculated.

Heterogeneity

One of the most likely models would seem to be one in which an uneven distribution of ligands results in a mixture of monovalent and of divalent interactions. This would be especially likely on low- to medium-coverage columns. The general, high-cooperativity, and independent, equivalent-site models incorporating this effect of heterogeneity of interaction are given as Equations 5-7, respectively. These equations are seen to be identical in form to the general model given in Equation 1, which fit the data excellently (Figure 3c). Thus, one can reinterpret the fits to the general model (Table III) in terms of the various heterogeneous models.

Since there are two new parameters (f_L and f_{SA}) in the heterogeneous equations whose values would be difficult to determine experimentally, and since all three heterogeneous models are of the same form as the general model (a quadratic equation), one cannot rule out any of the models based on fits to the chromatographic data. However, in some instances some of the equilibrium constants can still be determined. Examination of Equations 5 and 7 indicate that it should still be possible to determine K_2 and K_3 in the heterogeneous versions of the general and independent, equivalent-site model, while K_2 can still be determined in the case of the

heterogeneous, high-cooperativity model.

Examination of the heterogeneous equations also indicates that heterogeneity could not be the cause of the unexpected increase in K_3 values noted for the higher-coverage PAPM columns.

For all of the heterogeneous models, one could interpret changes in the value K_4V_p/A from the data in Table III to be due either to changes in the strength of divalent interaction (K_4) or due to changes in the extent of divalent interaction (f_L and f_{SA}). This latter interpretation is particularly attractive for the low-coverage PAPM column, since it could explain why some divalent interactions appeared to take place, even though the average ligand density was lower than what was necessary. This could also explain why K_4 appeared to increase with ligand density (i.e., $f_L^2K_4/f_{SA}$ was actually being determined).

CONCLUSIONS

The equilibrium constants determined for the competing sugar from the low-coverage PAPM and glucosamine studies were in good agreement with literature values. However, K_3 values for the medium- and high-coverage PAPM columns were larger than expected from the monovalent data. This discrepancy was not accounted for by any of the models.

Hogg and Winzor (10) have reported closer fits of affinity chromatographic data using an independent, equivalent-site model, as compared to the high-cooperativity model. This was not found to be true for all of the data in the present work. Only the general and heterogeneous models gave reasonably good fits to the data over a wide range of ligand density.

Values calculated for the equilibrium constants varied with the retention model used to fit the data. Thus, without additional experimental information to elucidate the exact mechanism of retention, it was not possible to obtain reliable equilibrium constants for divalent solutes.

ACKNOWLEDGEMENTS

Synthesis of, and chromatography on, the low-coverage PAPM column was done by Jacqueline S. Anhalt. Synthesis of the glucosamine column was done by Mary Landgrebe. This work was supported by the National Science Foundation under Grant CHE-8305057.

REFERENCES CITED

1. Andrews, P.; Kitchen, B.; Winzor, D. Biochem. J. 1973, 135, 897.

2. Dunn, B. M.; Chaiken, I. M. Proc. Nat. Acad. Sci. USA 1974, 71, 2382.

3. Turkova, J. "Affinity Chromatography"; Elsevier: Amsterdam, 1978; p. 35.

4. Chaiken, I. M. Anal. Biochem. 1979, 97, 1.

5. Nilsson, K.; Larsson, P. -O. Anal. Biochem. 1983, 134, 60.

6. Dunn, B. M. Applied Biochem. Biotechnol. 1984, 9, 261.

7. Eilat, D.; Chaiken, I. M. Biochemistry 1979, 18, 790.

8. Inman, J. K. In "Affinity Chromatography and Biological Recognition"; Chaiken, I. M.; Wilchek, M.; Parikh, I., Eds.; Academic Press: New York, 1983; p. 153.

9. Anderson, D. J.; Walters, R. R. J. Chromatogr. 1985, 331, 1.

10. Hogg, P. J.; Winzor, D. J. Arch. Biochem. Biophys. 1985, 240, 70.

11. Chaiken, I. M.; Eilat, D.; McCormick, W. M. Biochemistry 1979, 18, 794.

12. Nichol, L. W.; Ward, L. D.; Winzor, D. J. Biochemistry 1981, 20, 4856.

13. Winzor, D. J.; Ward, L. D.; Nichol, L. W. J. Theor. Biol. 1982, 98, 171.

14. Hogg, P. J.; Winzor, D. J. Arch. Biochem. Biophys. 1984, 234, 55.

15. Winzor, D. J.; Yon, R. J. Biochem. J. 1984, 217, 867.

16. Kopaciewicz, W.; Rounds, M. A.; Fausnaugh, J.; Regnier, F. E. J. Chromatogr. 1983, 266, 3.

17. Rounds, M. A.; Regnier, F. E. J. Chromatogr. 1984, 283, 37.

18. Geng, X.; Regnier, F. E. J. Chromatogr. 1984, 296, 15.

19. Jennissen, H. P.; Heilmeyer Jr., L. M. G. Biochemistry 1975, 14, 754.

20. Jennissen, H. P. Biochemistry 1976, 15, 5683.

21. Jennissen, H. P. J. Chromatogr. 1978, 159, 71.

22. Jennissen, H. P. J. Chromatogr. 1981, 215, 73.

23. Kyprianou, P.; Yon, R. J. Biochem. J. 1982, 207, 549.

24. Yon, R. J.; Kyprianou, P. In "Affinity Chromatography and Biological Recognition"; Chaiken, I. M.; Wilchek, M.; Parikh, I., Eds.; Academic Press: New York, 1983; p. 143.

25. Bethell, G. S.; Ayers, J. S.; Hearn, M. T. W.; Hancock, W. S. J. Chromatogr. 1981, 219, 353.

26. Walters, R. R. In "Affinity Chromatography: A Practical Approach"; Dean, P. D. G.; Johnson, W. S.; Middle, F. A., Eds.; IRL Press: Oxford, 1985; p. 25.

27. Huet, M. Eur. J. Biochem. 1975, 59, 627.

28. Loontiens, F. G.; Clegg, R. M.; Jovin, T. M. Biochemistry 1977, 16, 159.

29. Anderson, D. J.; Walters, R. R. J. Chromatogr. 1986, 376, 69.

30. Christian, S. D.; Tucker, E. E. Am. Lab. 1982, 14(9), 31.

31. Hardman, K. D.; Ainsworth, C. F. Biochemistry 1976, 15, 1120.

32. Lewis, S. D.; Shafer, J. A.; Goldstein, I. J. Biochem. Biophys. 1976, 172, 689.

33. Oda, Y.; Kasai, K.; Ishii, S. J. Biochem. 1981, 89, 285.

SUMMARY AND DISCUSSION

Reasons for Using HPAC Over Existing Techniques

In this work, high-performance affinity chromatography was assessed as a technique for the measurement of equilibrium and rate constants. Conclusions from this work are summarized below. Prior to discussing the results, however, it is important to understand the limitations of the conventional techniques used for the determination of equilibrium and rate constants. As discussed below, the development of affinity chromatography as an alternate methodology will provide additional capabilities not available in these conventional techniques.

The most widely used technique for the measurement of equilibrium constants is equilibrium dialysis (44). The techniques of ultracentrifugation and ultrafiltration have also been used for the determination of equilibrium constants (44). These latter techniques are variations of the equilibrium dialysis method and, thus, face many of the same limitations. Other less-used techniques have been summarized (44).

In the equilibrium dialysis technique, equilibrium constants are determined for small molecules (L) binding to macromolecules (E). A solution of E (of known volume and

concentration) is placed in a dialysis bag, which is then placed in a solution containing L. Molecules of L diffuse through the dialysis membrane to bind to E. Eventually, equilibrium is attained, at which point the concentration of free L inside and outside the dialysis bag is equal. The concentration of all forms of L inside ([L] + [EL]) and outside ([L]) the dialysis bag is measured, from which the equilibrium constant can be determined.

There are three limitations for equilibrium dialysis, which restrict its applicability to certain biochemical systems: (1) the requirement for a substantial size difference between E and L; (2) the requirement for the detection of L in the presence of E; and (3) the limitation in the range of binding strengths that can be determined.

Affinity chromatography is not limited in this way. Probably the biggest advantage of affinity chromatography over the other equilibrium constant determination techniques is its capability of determining binding constants which are extremely weak or extremely strong. Association constants as low as 100 M^{-1} and as high as 10^9 M^{-1} can be determined by conventional affinity chromatography (3). This range can be expanded by HPAC, because of the high precision and high efficiency of this technique. The high precision of HPAC expands the lower range of equilibrium constant determination, through a more accurate determination of very short retention

times. The technique's high efficiency improves the detection limit, which allows for the detection of stronger interacting compounds.

Affinity chromatography can also conveniently determine equilibrium constants for compounds which are difficult to detect. It was shown in the present work that equilibrium constants for a UV-transparent competitive inhibitor (MDM) can be readily and precisely determined by measuring the change in the retention of a UV-absorbing solute (PNPM or MUM) with the change in inhibitor concentration.

Another potential advantage of affinity chromatography over existing methodology is the determination of equilibrium constants for macromolecular pairs. This is not possible for the equilibrium dialysis and similar techniques, which require a substantial size difference between the interacting pair.

In addition to the advantages of HPAC in equilibrium analysis, important improvements in kinetic analysis might be possible. Rate constants are conventionally measured in two ways, depending upon the magnitude of the rate constant (45). For relatively slow kinetic processes, the reactants are rapidly mixed and the rate of product increase (or reactant decrease) is measured. This is the basis for the steady-state and stopped-flow techniques. The stopped-flow technique measures reactions occurring in the one millisecond to ten second time range (46). For reactions occurring at faster

rates, "perturbation methods" are used. These techniques are based on monitoring the rate of the return of an equilibrated system to equilibrium following a disrupting impulse. The most popular of these techniques is the temperature-jump method. The practical lower limit for reaction times that can be determined by these techniques is 10^{-6} seconds (46).

Both the mixing and perturbation techniques monitor the rate of product change (or reactant change) in determining rate constants. This requirement limits the biochemical systems that can be studied to systems having only one reactant or product which give a detector response. This is a severe limitation, especially for studying the kinetics of binding interactions between macromolecules.

HPAC can be used as an alternate technique for studying the kinetics of binding interactions, which have dissociation rate constants of 10 sec^{-1} or less. This overlaps the time range of the stopped-flow techniques. HPAC, however, is not limited by the restraint mentioned above for the stopped-flow technique. This is because the basis for the kinetic measurements is completely different for HPAC. HPAC is a dynamic technique, in which the flow of reactant E past immobilized reactant L causes a spreading of E, due to the kinetics of interaction (in addition to other effects). The separation of reactant E from L is accomplished through the mobile phase transport of E out of the column, with the

integrity of the band being maintained. Thus, interference between reactant components, with regard to detection, is eliminated as a problem.

HPAC has much potential application for determination of equilibrium and rate constants. The power in the technique not only lies in the additional capabilities it has over existing equilibrium and kinetic techniques, but in the fact that both rate and equilibrium constants can be determined simultaneously.

In this work, HPAC was assessed for its capability to determine equilibrium and rate constants for monovalent solutes, and to determine equilibrium constants for divalent solutes.

Assessment of the Determination of Equilibrium Constants for Monovalent Solutes

For monovalent solutes in the reversed-role mode (with immobilized Con A and free sugar solute), association constant values determined by zonal and frontal methods were in excellent agreement with one another. For PNPM, the average values for the zonal and frontal analysis were 24000 M^{-1} and 26000 M^{-1}, respectively. For MDM, the average value was 8300 M^{-1} for the zonal studies and 8400 M^{-1} for the frontal studies. It should be noted that non-specific adsorption had

a considerable effect on the Langmuir plot for PNPM and, thus, the frontal equation used for calculating the equilibrium constant for PNPM (and MDM) was modified to account for this (Equation 11, Section III). Only zonal studies were done for the determination of the association constant for the binding of MUM to a Con A site, and a value of 45000 M^{-1} was found.

HPAC was found to be a very precise technique. From the relative standard deviations of the slope (1 %) and intercept (5 %) of the 1/k' versus [I] plots, of the fit of the Langmuir isotherm equation in the determination of m_L (3 %), and of the experimental value of V_m (0.5 %), the precision for K_2 and K_3 values from zonal analysis was ~ 5 %.

One way to assess the accuracy of HPAC in the measurement of equilibrium constants is from a determination of the validity of the retention model used. The monovalent retention model (Equation 3, Section III) was found to fit the monovalent solute data sets very well. The expected linearity in the data sets was seen over a wide range of inhibitor concentrations (Figure 2, Section III). Negative deviations in the 1/k' versus [I] plots were noted at higher inhibitor concentrations (not shown in Figure 2). However, these deviations were small considering the number of free ligand sites (30 % deviation with only 0.2 % of the sites free) and were likely due to a slight heterogeneity of the immobilized Con A.

In addition to the excellent fit of the theory to the data, the validity of the theory was considerably strengthened by the close agreement of equilibrium constant values for the two chromatographic methods (zonal and frontal), as shown above. This agreement of equilibrium constant values is significant, because zonal and frontal studies test different aspects of the same retention model. In the zonal analysis [I] is changed with [E] constant, while in the frontal analysis [I] is constant ([I] = 0 in this work) and [E] is varied.

Finally, HPAC values can be compared with values obtained by other techniques. The magnitude of the HPAC values were between one to three times higher than the magnitude of the literature values obtained from solution studies (Table II, Section III). This difference may reflect an uncertainty in the literature values, or it may be indicative of a systematic error in the HPAC technique. Potential sources of error in the HPAC technique will be discussed below.

There are several factors which will affect the accuracy of the results obtained from zonal studies. One factor is the concentration of the solute injected. The theory employed assumes linear isotherm conditions and, thus, low concentrations of solute need to be used. If this condition is not met, retention times will be decreased from what thermodynamics predict.

A good illustration of how the concentration of injected

solute affects the equilibrium constant result is seen by comparing the results of this work with the results of Muller and Carr (7). Muller and Carr used a column that was similar in active Con A surface coverage to the medium-coverage column described in Section III. Muller and Carr injected 1 mM PNPM samples and were clearly working in the non-linear isotherm region, as indicated by their own concentration studies. PNPM concentrations for the present work were more than two orders of magnitude less (6 μM), with linear isotherm conditions being verified by concentration studies. The effect on the results of the sample overload in Muller and Carr's work was a lower association constant for the immobilized macromolecule, free ligand pair, in comparison with the present work. Muller and Carr obtained an association constant (K_3) of 1.6×10^4 M^{-1} for the PNPM-immobilized Con A site interaction, compared to 2.5×10^4 M^{-1} for the present work. Interestingly, non-linear conditions apparently had no effect on the inhibitor, immobilized macromolecule site association constant (K_2). Both studies obtained values of 8300 M^{-1} (after refitting Muller and Carr's data to Equation 3 in Section III).

Another source of error in the zonal studies is the determination of the moles of immobilized sites on the column (m_L). The quantity m_L can be determined either from break-through studies or from chemical assays. Break-through

determination is the best method, from the point of view that it determines the number of active sites. There are, however, a number of problems associated with this method.

One problem is that the frontal studies cannot measure accurate break-through points for the low-coverage columns. This leads to considerable error in the K_3 values, as was seen for the low-coverage column results listed in Table II, Section III.

A second problem is that even a slight amount of non-specific adsorption ($k' = 0.1$) can cause a considerable overestimation of m_L if not corrected for. This is strikingly illustrated in Figure 3a, Section III. At a concentration of 10 mM PNPM, 85 % of the solute adsorbed was due to non-specific adsorption (presumably through hydrophobic interaction). In order to circumvent this problem, one can use solutes which exhibit minimal non-specific retention. For immobilized Con A, MDM was shown to be a much better choice for m_L determination, as a near-ideal Langmuir isotherm was obtained (Figure 3b, Section III). Alternatively, one can modify the Langmuir equation to account for non-specific adsorption. When this was done, reasonable fits and reasonable K_3 values were obtained. Thus, accurate m_L values can presumably be determined, even with non-specific adsorption.

A third problem for the frontal determination of m_L

concerns the use of macromolecular solutes. Two problems arise. First, the concentrations of the macromolecule needed for the saturation of the immobilized ligand sites on the column might be impractically high. For example, for a PAPM column, a solution ~ 60 mg/ml Con A monomer is needed in order to occupy 90 % of the immobilized ligand sites. This is beyond the solubility of the Con A in the buffer solutions used in this work. For matrices having a high immobilized ligand concentration, another problem exists for the frontal studies using macromolecular solutes. In this case, the macromolecule might cover (but not bind to) ligand sites besides those to which it is bound, and low results for m_L will be obtained.

The use of chemical assays provides an alternate route for determining m_L. Although this technique determines the concentration of the total ligand sites (the desired quantity, however, is that which is active and accessible), it is the only reasonable methodology for the several difficult cases mentioned above. In order to determine m_L from chemical assay results, one must also know the column volume and packing density. For the immobilized Con A of this work, the Lowry protein assay and the frontal technique gave identical results. This indicates that 100 % of the Con A sites were active and accessible.

Continuing with the discussion of the sources of error

for the HPAC technique, non-specific adsorption can also interfere. This effect would lead to the greatest error at high inhibitor concentrations, when retention is the least. In the present studies, the non-specific retention of the monovalent solutes was readily estimated and subtracted off. Comparable galactoside sugars, which do not biospecifically interact with Con A (42), were injected, in order to estimate the amount of non-specific retention. Injection of the solute onto blank columns (columns containing matrices without the immobilized species) is an alternate way of estimating non-specific retention, being useful for cases in which a comparable non-interacting compound cannot be found. The disadvantage of using a blank column, however, is that the non-specific interaction of the solute with the immobilized species is not assessed.

The final consideration, and probably the most important, is the effect of the immobilization on the thermodynamics (and kinetics) of the interaction. It is quite possible that the immobilization alters the physicochemical properties of the species that is immobilized. For example, immobilization of a macromolecule might change the shape or accessibility of the binding site. For immobilization of small ligand molecules, the strength of the interaction can be changed by steric limitations or a concomitant interaction of the macromolecule solute with the matrix. For these reasons, so-called spacer

arms have been used to separate the small ligand from the matrix (47). The diol phase, in addition to the non-sugar part of the ligand molecule, served as a spacer arm linkage for the small ligand molecules (glucosamine and PAPM) used in the present study.

The effect of immobilization on the equilibrium constants must be studied on a case by case basis. For the present work, the effect of immobilization of Con A on the association constants can be seen by comparing the association constant for MDM, immobilized Con A (K_2) given in Table II, Section III, and the association constant for MDM, free Con A (K_2 values from the general equation) given in Table III, Section IV. An average value of 8300 ± 200 M^{-1} was obtained for MDM, immobilized Con A, while values for MDM, free Con A were 5600 M^{-1} and 7600 M^{-1}, for the low-coverage PAPM and glucosamine column, respectively. Thus, immobilization did not appear to greatly affect the value for the equilibrium constant, although slightly higher values were obtained for the immobilized Con A.

Another facet of the immobilization effects is the heterogeneity in the binding sites that may result from the immobilization step. This will result in a leveling off of the 1/k' versus [I] plots at high [I]. Examination of Figure 2, Section III shows no leveling off of the plots over a wide range of [I]. However, at concentrations of MDM higher than

given in Figure 2, negative deviations in the plots were evident. This indicated a slight heterogeneity in the Con A binding sites. The effect of this heterogeneity was to underestimate the value for K_3, because the 1/k' intercept was higher than it should be. Comparison of the K_3 values calculated from the retention times of the runs with no inhibitor present in the mobile phase with those calculated from the intercept of 1/k' versus [I] plots bears this fact out. K_3 values calculated by the graphical method were consistently lower than K_3 values calculated from the retention of the peak at [I] = 0, by an average of 8 %.

The most appropriate use of HPAC in the determination of equilibrium constants might be the normal-role mode of operation. Chromatography in the normal mode allows both the macromolecule and the competing inhibitor to interact free in solution. In this case, only K_3 is affected by immobilization and not K_2. Thus, from the chromatography of the macromolecule injected into mobile phases containing various concentrations of the compound of interest, one can obtain free solution equilibrium constants (K_2). Limitations, however, exist for the normal-role mode use of HPAC in determining equilibrium constants for multivalent solutes. As seen in Section IV, the theory for multivalent interaction of the solute with immobilized ligands has not been verified. This will be discussed later.

Assessment of the Determination of Rate Constants for Monovalent Solutes

The present work gives the most in depth study to date, in the examination of the capability of HPAC in the determination of rate constants. Studies involving three columns of different coverage of Con A, two different solutes (PNPM and MUM), and at least five different inhibitor concentrations (MDM) were performed. The broad extent of this work allowed for adequate examination of the band-broadening models employed. From this assessment of theory, conclusions could be made with respect to the accuracy of the rate constants determined. All the data for the kinetic determinations were obtained from the reversed-role studies, in which Con A was immobilized onto the silica matrix.

Before kinetic rate constants could be determined from plate height data, H_m and H_{sm} contributions were estimated and subtracted off from H_t. The use of van Deemter plots to estimate H_m and H_{sm} appeared reasonable from the H_t versus u plots for the diol columns (an example is given in Figure 5, Section III). van Deemter plots were done for each solute on the two different diol columns (SI 500 and Hypersil 300). These plots were linear, as predicted by the van Deemter relationship, with H_m being determined from the intercept and

k_{-1} from the slope (Equation 19, General Introduction). For this work, k_{-1} was assumed to be the same for the diol and the Con A column (of the same silica base), for a particular solute. The H_{sm} value could be determined at any k' by using Equation 16 (General Introduction). The H_m was determined for each solute-column combination by measuring H_t for a comparable non-retained galactoside sugar and subtracting off the value of H_{sm} for the galactoside sugar. Having thus isolated the H_k component of H_t, dissociation rate constants (k_{-3}) could be calculated using Equation 17 (General Introduction).

At least five different runs were performed for each solute chromatographed on a column, each at a different mobile phase inhibitor concentration. The values for k_{-3} versus [I] for each column are graphed in Figure 6, Section III. By comparison of the k_{-3} values for PNPM and MUM for a particular column, it is seen that the values for MUM were less than PNPM at any given [I]. This order was expected from the known values for the dissociation rate constants for these sugars (3.4 sec^{-1} and 6.2 sec^{-1} for MUM and PNPM, respectively (30)).

What was unexpected, however, was that k_{-3} varied with [I], as k_{-3} increased with increased [I]. Muller and Carr (7) also observed this trend. They explained this behavior by assuming an S_N2 type mechanism, in which the inhibitor molecule promotes dissociation of the solute molecule via an

intermediate ternary complex. This hypothesis has important implications for chromatographic analysis. If this were true, plate heights for a solute chromatographed on a low-coverage column would be higher than the same solute chromatographed on a high-coverage column (under conditions in which the k' for the solute on the high-coverage column was adjusted to the k' of the solute on the low-coverage column, through the addition of inhibitor). Thus, systems of high immobilized ligand coverage at high mobile phase strengths would be favored over low ligand coverage columns operating at low mobile phase strengths.

The hypothesis of Muller and Carr, however, was based on limited experimental data, i.e., only one column was used. Our data from columns of variable Con A density did not support this hypothesis. If k_{-3} were a function of $[I]$, then one would expect Figure 6 (Section III) to consist of two plots, one plot for each sugar solute, regardless of the column coverage. In actuality, a different plot was obtained for each sugar-column combination, refuting the hypothesis of Muller and Carr. In addition to this work, Lewis, et al. (48) and Farina and Wilkins (49) showed no enhancement of the dissociation rate of PNPM and Con A in solution, in the presence of competitor. However, in contrast to this, Podder, et al. (50) found the dissociation rate constants of RC_1 (a protein) and Con A to increase with increased inhibitor

concentration.

The variation of k_{-3} was believed to result from an inaccurate estimation of H_k, due to an inability to correctly predict H_{sm} and H_m as a function of k'. If this were the case, one might expect the apparent k_{-3} to be a function of k', rather than [I]. Figure 7, Section III supports this hypothesis, as the data for the two Hypersil columns appeared to be part of a continuous data set. The k_{-3} values seemed to plateau at low k', at values which were close to the results from solution studies in the literature. This suggested that the error in the diffusional corrections was worse as k' increased. This would be expected, since these diffusional parameters were measured at k' = 0.

Figure 8, Section III clearly illustrates the problem; theory did not adequately describe the band-broadening with respect to retention. Figure 8a shows the best fits of Equation 4 (Section III) to the data, constraining H_m and k_{-1} to the experimental values. It was seen that H_k dropped off too quickly at high k' to account for the plate heights experimentally determined at high k'. A fit allowing variability in the H_m and H_{sm} terms, as well as the H_k term, is shown in Figure 8b. This fit was better. However, the H_t fit was still noticed to drop off too quickly in comparison to the experimental points.

Thus, a serious deficiency in chromatographic

band-broadening theory was evident from the present study, calling into question the accuracy of rate constant values determined by HPAC. From our studies, rate constants determined by HPAC for a particular sugar varied by a factor of 10, depending on k'. This variability points to the need for a better understanding of chromatographic band-broadening processes, before rate constants can be determined by HPAC with confidence.

Several assumptions implicit in the band-broadening model used in this work (Equations 4, 5, and 6, Section III) need to be critically examined. The basis for this model is described below. The solute molecule is depicted to be in one of three states: in the mobile phase, in the stagnant mobile phase, or adsorbed on an immobilized site. Only when the solute is in the mobile phase does it move lengthwise within the column. The stagnant mobile phase has two boundary regions, one at the mobile phase interface and the other at the stationary phase interface. These different boundaries are at opposite sides of the stagnant mobile phase region. Transfer of the solute between the phases only occurs with neighboring phases, e.g., transfer from the mobile phase to the stationary phase does not occur without transfer into the stagnant mobile phase first. The rate of transfer is stipulated by the rate constants (k_1 and k_{-1} for the transfer between the mobile phase and the stagnant mobile phase, and k_3 and k_{-3} for the

transfer between the stagnant mobile phase and the stationary phase). Band-broadening results from a difference of time spent in each of these phases for different solute molecules.

There are several assumptions in this model that may not be valid. One assumption is that all solute molecules have equal access to the boundary region(s) of that phase. That is, a solute molecule that has just entered the stagnant mobile phase has immediate access to the stationary phase interface, as well as the mobile phase interface through which it entered. With this assumption, the probability of transfer through the boundary is the same for any molecule in the phase, as given by the rate constant for the transfer. This is probably not the case, particularly within the stagnant mobile phase. A molecule that has just entered the stagnant mobile phase, through either boundary, must be transported by diffusion to the other boundary. It, thus, has a greater probability to re-enter the boundary layer through which it recently passed. In a related point, the model does not account for any solute concentration gradient that is probably present within the stagnant mobile phase.

A second assumption under question is the independence of the H_k and H_{sm} term. In reality, adsorption of the solute on the stationary phase might change the expression for H_{sm}. This was demonstrated through a theoretical treatment by Giddings, for the case of a uniform film surrounding a

stationary phase (9, p. 162).

A further assumption of the model employed is that H_m does not change with retention. This is open to question, as was discussed in the General Introduction.

Withstanding these theoretical problems, the most accurate kinetic measurements are made at low k' (k' = 1), where the contributions of H_k are supposedly largest relative to H_m and H_{sm}. Dissociation rate constants obtained from the fits to the low-coverage column data were, therefore, taken to be the most accurate. Values of 2 sec^{-1} for MUM and 3 sec^{-1} for PNPM were determined (Table IV, Section III). These values are between 2/3 to 1/2 of solution values. This is opposed to previous studies, which obtained values a factor of 10 to 100 lower than the solution values. The lower values obtained by the previous studies were probably due to the use of matrices having a larger particle diameter (10 μm compared to 5 μm), improper data analysis (failure to correct for H_m and H_{sm}), and/or measurements made at high k'.

Assessment of Equilibrium Constant Determination for Divalent Solutes

Three retention models for divalent solutes were presented in Section IV; the general, high-cooperativity, and independent, equivalent-site models. The high-cooperativity

and independent, equivalent-site models are limiting cases of the general model. Surprisingly, very little work has been undertaken to determine which model most accurately represents the chromatographic process of multivalent solutes. Most workers favor the independent, equivalent-site model. The purpose of this part of the work was to determine which model most closely fit the data points. Equilibrium constants determined from the model which fit the data the best would presumably be more reliable than those determined from the other models.

Studies were performed involving divalent Con A, chromatographed on three columns of variable PAPM coverage and one glucosamine column. As seen in Figure 3 and Table III of Section IV, excellent fits for the general model were obtained for all columns. Fits for the other models were poor to moderate in comparison. This suggests that the general model was the most appropriate model to use in the determination of equilibrium constants.

Inconsistencies, however, were noted in comparing the general model results for the different coverage columns. The main discrepancy is that the value of K_3 was not constant with variable ligand coverage. K_3 values for the higher-coverage PAPM columns were at least ten times higher than the K_3 value determined for the low-coverage PAPM column. Non-specific retention, the presence of tetravalent Con A, and/or errors in

the estimation of the functional ligand density were conjectured to explain this discrepancy.

A discussion on the effect of ligand density heterogeneity was also presented in Section IV. Equations incorporating this heterogeneity were derived for each of the three models. It was found that all the equations had the same quadratic form as the general model. Thus, the appropriateness of a particular model could not be assessed from the precision of the fit, without knowledge of the extent of the ligand density heterogeneity. However, important information concerning the reliability of the equilibrium constant determinations can be ascertained from these equations. In most cases, comparison of the general equations (Equation 1, Section IV) with the heterogeneous equations (Equations 5, 6, and 7, Section IV) shows only the K_4 term to be different. The one exception is the heterogeneous, high-cooperativity model (Equation 6, Section IV), in which both the K_3 and K_4 terms are different from the general model (multiplication of Equation 6 by $(1-f_L)/(1-f_L)$ makes this evident). This means that no matter what the heterogeneity in the ligand density, fitting the data to the general model gives reliable values for K_3, in most cases, and for K_2, in all cases.

It appears, then, that the most reliable equilibrium constant determined by HPAC for divalent solutes is K_2. In

addition to being unaffected by ligand density heterogeneity, determination of K_2 does not require knowledge of the functional ligand concentration, as does the determination of K_3 and K_4. This reliability was confirmed in the present studies, as the value of K_2 (for the Con A binding site, MDM inhibitor) was similar for the low-coverage PAPM and glucosamine columns (5.6×10^3 M^{-1} and 7.6×10^3 M^{-1}, respectively).

There are limitations in determining K_2, however. Inhibitor concentrations must be chosen in the approximate range of $10 > K_2[I] > 0.1$. Outside this range, the K_2 constant is incorporated into the other equilibrium constants in the retention equations. Thus, for a given solute, inhibitor pair, the affinity and surface coverage of the immobilized ligand must be properly chosen, such that appropriate inhibitor concentrations can be used (so that $K_2[I]$ is in the desired range).

Another limitation is non-specific adsorption. Non-specific adsorption of the macromolecule on the matrix does not interfere with the determination of K_2, as long as the inhibitor does not compete for the non-specific sites on the macromolecule. This is the case for the present work, in which the hydrophilic inhibitor, MDM, does not affect the non-specific, hydrophobic retention of Con A. It is best, however, to minimize non-specific adsorption effects. This

can be accomplished in the present studies by immobilizing a less hydrophobic ligand, such as glucosamine. With such matrices, K_2 values for the more hydrophobic inhibitors can be determined.

A different approach for obtaining equilibrium constants by HPAC for divalent solutes would be to preclude divalent interaction of the solute with the matrix. This can be accomplished by sufficiently spreading the immobilized ligand sites on the matrix. The equation derived for this case is the same as the equation for a monovalent solute, differing only by a multiplication factor of two (Equation 4, Section IV).

In principle, this strategy appears reasonable. In practice, however, difficulties arise because of the regions of high ligand density that are present on the low ligand density matrices. This fact has been documented by Lochmuller et al. from a study of the luminescence of pyrene-bonded silica (51).

In the low-coverage PAPM studies, the average distance between ligands was larger than that of the distance between the Con A binding sites on the dimer. The fit to the monovalent model (Equation 4, Section IV) was very good (0.9999 correlation coefficient). One cannot assume, however, that only monovalent interactions were occurring. A fit to the heterogeneous, general equation (Equation 5, Section IV)

was ten times better. The magnitude of the K_4 term (780 M^{-1}; Table III, Section IV) indicated a small amount of divalent adsorption of Con A, presumably due to regions of high ligand density. The effect of this slight amount of heterogeneity was seen to be significant; K_2 and K_3 values determined from the monovalent fit were two times the values determined from the heterogeneous, general model.

Other Conclusions

In addition to the assessment of equilibrium and rate constant determination of HPAC, other studies were performed. A critical aspect of this work was the accurate determination of the first and second moments of the peak. In some runs, peaks eluted over a long period of time. In these cases, it was difficult to ascertain when the signal had returned to the baseline, resulting in considerable uncertainty in the moments calculated by the summation approach.

The effect of baseline errors on the moments, determined by several methods, was examined in Section I. The empirical relationships of Foley and Dorsey (52) involving peak width, asymmetry, and retention time were found to be the least sensitive to baseline errors. The relationships based on half-height parameters were found to be more accurate than the relationships based on tenth-height parameters, with respect

to baseline uncertainty. Further support for using half-height parameters comes from the fact that impurities within a peak affect the tenth-height measurements more than the half-height measurements. Opposing these arguments is the fact that the half-height measurements are less precise (especially for sharp peaks) than the tenth-height parameters.

The empirical equations of Foley and Dorsey were modified, in order to expand the range of applicability beyond $B/A_{0.1}$ of 2.8. Using simulated peaks with $B/A_{0.1}$ values of 1.0 to 5.2, equations for the first and second moments were determined. It is likely that these equations are fairly accurate beyond $B/A_{0.1}$ of 5.2, since the form of the modified M_1 and M_2 equations is exponential and not quadratic.

In Section II, the high-cooperativity retention model was employed to obtain Z values, the number of binding sites on the solute which interact with the column, for affinity chromatographic analysis. Such studies have been done in ion-exchange and reversed-phase chromatography, but not affinity chromatography.

The Z values were obtained from the slope of log k' versus log $1/[I]$ plots. In most cases, non-integer Z values and curved plots were obtained. This was due to the inadequacy of the high-cooperativity model in modeling retention. These results may explain the curvature of the log

k' plots and non-integer values of Z frequently observed in ion-exchange studies.

SUGGESTIONS FOR FUTURE WORK

Simplification in experimental strategy is needed to properly test chromatographic theory. Experiments to date have encompassed too many sources of band-broadening to be of value. Experiments which determine the band-broadening for each source separately are the appropriate starting points for testing theory. From this point, the complex phenomena involving a combination of band-broadening sources can be studied.

The goal of the present work was to separately determine H_k, by minimizing the contributions of H_m and H_{sm}. This goal was not fully realized. Further work is needed to minimize the relative contributions of H_m and H_{sm}. This can be accomplished through two routes: (1) reduce further the H_m and H_{sm} contributions, by changing to even higher efficiency matrices; and/or (2) increase the H_k component, by choosing a biochemical system with slower dissociation kinetics. Once this is done, one can do experiments to verify the kinetic plate height equation (Equation 17, General Introduction) with respect to k'.

Further reductions in H_m and H_{sm} can be made by using matrices smaller than the 5 μm silica used in the present work. Spherical silica, 3 μm in size, is commercially available. Recently, non-porous silica matrices of 0.7 μm and

1.5 μm have been developed, as described in a symposium review (53). These matrices have a high surface area (comparable to 5 and 10 μm silica with 1000 Å pores) and a narrow size distribution (10 %) (53) and, thus, should prove to be excellent for theoretical studies. Substantial reduction in the non-kinetic plate height terms can be accomplished with these matrices, because of the approximate five-fold decrease in the particle size. In addition, the non-porous nature of these matrices effectively eliminates the H_{sm} contribution to the total plate height. The small particle diameter necessitates shorter columns and/or slower flowrates, because of the pressure considerations.

In addition to (or conjunction with) the changes in the matrix suggested above, a biochemical system with slower dissociation constants can be used. An excellent system to study is the glucocorticoid hormone, receptor system. Dissociation rate constants at 0 °C for nine glucocorticoids dissociating from its receptor have been determined, and range from 2.8×10^{-3} sec^{-1} to 8.2×10^{-6} sec^{-1} (54). This is three to six orders of magnitude less than the Con A, sugar system studied in the present work.

The design of the experiments is to inject one glucocorticoid on a column of immobilized receptor, into a mobile phase containing different concentrations of another glucocorticoid. Doing these experiments requires a different

detection system; one that has greater sensitivity and one that can differentiate between the "inhibitor" and "solute" steroids. Electrochemical detection is a possible choice. Even though there is little precedence for using electrochemical detection of steroids in liquid chromatography, an extensive study detailing the polarographic behavior of glucocorticoids has been published (55), which shows that it could be quite useful for the proposed study. A suitable glucocorticoid pair to study are hydrocortisone and prednisolone, which have reduction half-wave potentials at pH of 5 of approximately -1.3 and -1.1 V versus an Ag/AgCl reference electrode, respectively (55). This separation of half-wave potentials should provide ample electrochemical resolution, so that prednisolone (solute) can be detected without the detection of hydrocortisone (inhibitor). The low potential required for the reduction necessitates the use of a mercury working electrode.

In addition to these experiments examining kinetic band-broadening, experiments need to be done to resolve the discrepancies in the retention data of divalent solutes on different ligand coverage columns. Hydrophobic interaction of the Con A with ligands on the matrix has been suggested to be the cause of the variation of K_3 with ligand surface coverage. Chromatographic experiments using Con A dimer solute on matrices with a less hydrophobic immobilized ligand than PAPM,

such as glucosamine or mannosamine, can be done to see if K_3 is constant with varying immobilized ligand coverage.

LITERATURE CITED

1. Andrews, P.; Kitchen, B. J.; Winzor, D. J. Biochem. J. 1973, 135, 897.

2. Dunn, B. M.; Chaiken, I. M. Proc. Nat. Acad. Sci. USA 1974, 71, 2382.

3. Chaiken, I. M. Anal. Biochem. 1979, 97, 1.

4. Dunn, B. M. Applied Biochem. Biotechnol. 1984, 9, 261.

5. Kasche, V.; Buchholz, K.; Galunsky, B. J. Chromatogr. 1981, 216, 169.

6. Nilsson, K.; Larsson, P. -O. Anal. Biochem. 1983, 134, 60.

7. Muller, A. J.; Carr, P. W. J. Chromatogr. 1984, 284, 33.

8. Snyder, L. R.; Kirkland, J. J. "Introduction to Modern Liquid Chromatography"; John Wiley and Sons: New York, 1979.

9. Giddings, J. C. "Dynamics of Chromatography"; Marcel Dekker: New York, 1965.

10. van Deemter, J. J.; Zuiderweg, F. J.; Klinkenberg, A. Chem. Eng. Sci. 1956, 5, 271.

11. Kennedy, G. J.; Knox, J. H. J. Chromatogr. Sci. 1972, 10, 549.

12. Horvath, C.; Lin, H. -J. J. Chromatogr. 1976, 126, 401.

13. Horvath, C.; Lin, H. -J. J. Chromatogr. 1978, 149, 43.

14. Katz, E. D.; Scott, R. P. W. J. Chromatogr. 1983, 270, 29.

15. Katz, E. D.; Ogan, K. L.; Scott, R. P. W. J. Chromatogr. 1983, 270, 51.

16. Stout, R. W.; DeStefano, J. J.; Snyder, L. R. J. Chromatogr. 1983, 282, 263.

17. Karger, B. L.; Snyder, L. R.; Horvath, C. "An Introduction to Separation Science"; John Wiley and Sons: New York, 1973.

18. Hethcote, H. W.; DeLisi, C. J. Chromatogr. 1982, 248, 183.

19. Hethcote, H. W.; DeLisi, C. In "Affinity Chromatography and Biological Recognition"; Chaiken, I. M.; Wilchek, M.; Parikh, I., Eds.; Academic Press: Orlando, FL, 1983; p. 119.

20. Horvath, C.; Melander, W. R. In "Chromatography; Fundamentals and Applications of Chromatographic and Electrophoretic Methods; Part A"; Heftmann, E., Ed.; Elsevier Scientific Publishing Company: Amsterdam, 1983; Chapter 3.

21. Sternberg, J. C. In "Advances in Chromatography"; Giddings, J. C.; Keller, R. A., Eds.; Marcel Dekker: New York, 1966; Vol. 2, p. 205.

22. Atwood, J. G.; Golay, M. J. E. J. Chromatogr. 1981, 218, 97.

23. Giddings, J. C. Anal. Chem. 1963, 35, 1338.

24. Huber, J. F. K. J. Chromatogr. Sci. 1969, 7, 85.

25. Done, J. N.; Kennedy, G. J.; Knox, J. H. In "Gas Chromatography 1972"; Perry, S. G.; Adlard, E. R., Eds.; Applied Science Publishers: Barking, England, 1973; p. 145.

26. Knox, J. H. J. Chromatogr. Sci. 1977, 15, 352.

27. Grubner, O. Advan. Chromatogr. 1968, 6, 173.

28. Giddings, J. C. J. Chem. Ed. 1958, 35, 588.

29. Denizot, F. C.; Delaage, M. A. Proc. Nat. Acad. Sci. USA 1975, 72, 4840.

30. Clegg, R. M.; Loontiens, F. G.; Van Landschoot, A.; Jovin, T. M. Biochemistry 1981, 20, 4687.

31. Dixon, H. B. F. Nature 1981, 290, 192.

32. "Concanavalin A"; Chowdhury, T. K.; Weiss, A. K., Eds.; Plenum Press: New York, 1975.

33. Hardman, K. D.; Goldstein, I. J. In "Immunochemistry of Proteins"; Atassi, M. Z., Ed.; Plenum Press: New York, 1977; Vol. 2, Chapter 8.

34. Sand, T. T. Ph D. Dissertation, University of Minnesota, Minneapolis, MN, 1982.

35. Huet, M. Eur. J. Biochem. 1975, 59, 627.

36. Huet, C.; Lonchampt, M.; Huet, M.; Bernadac, A. Biochim. Biophys. Acta 1974, 365, 28.

37. McKenzie, G. H.; Sawyer, W. H. J. Biol. Chem. 1973, 248, 549.

38. Liener, I. J. In "Concanavalin A as a Tool"; Bittiger, H.; Schnebli, H. P., Eds.; John Wiley and Sons: New York, 1976; p. 17.

39. Hardman, K. D.; Wood, M. K.; Schiffer, M.; Edmundson, A. B.; Ainsworth, C. F. Proc. Nat. Acad. Sci. USA 1971, 68, 1393.

40. Kalb, A. J.; Lustig, A. Biochem. J. 1968, 109, 669.

41. Hardman, K. D.; Ainsworth, C. F. Biochemistry 1976, 15, 1120.

42. Goldstein, I. J.; Hollerman, C. E.; Smith, E. E. Biochemistry 1965, 4, 876.

43. Sumner, J. B.; Howell, S. F. J. Biol. Chem. 1936, 115, 583.

44. Steinhardt, J.; Reynolds, J. A. "Multiple Equilibria in Proteins"; Academic Press: New York, 1969; Chapter 3.

45. Dunford, H. B. In "Fast Methods in Physical Biochemistry and Cell Biology"; Sha'afi, R. I.; Fernandez, S. M., Eds.; Elsevier Science Publishers: Amsterdam, 1983; Chapter 2.

46. Espenson, J. H. "Chemical Kinetics and Reaction Mechanisms"; McGraw-Hill Book Company: New York, 1981; Chapter 10.

47. Scouten, W. H. "Affinity Chromatography"; John Wiley and Sons: New York, 1981; p. 38.

48. Lewis, S. D.; Shafer, J. A.; Goldstein, I. J. Arch. Biochem. Biophys. 1976, 172, 689.

49. Farina, R. D.; Wilkins, R. G. Biochim. Biophys. Acta 1980, 631, 428.

50. Podder, S. K.; Surolia, A.; Bachhawat, B. K. Eur. J. Biochem. 1974, 44, 151.

51. Lochmuller, C. H.; Colborn, A. S.; Hunnicutt, M. L.; Harris, J. M. Anal. Chem. 1983, 55, 1344.

52. Foley, J. P.; Dorsey, J. G. Anal. Chem. 1983, 55, 730.

53. Berry, V.; Shansky, R. E. LC 1985, 3, 364.

54. Jones, T. R.; Bell, P. A. Biochem. J. 1982, 204, 721.

55. De Boer, H. S.; Den Hartigh, J.; Ploegmakers, H. H. J. L.; Van Oort, W. J. Anal. Chim. Acta 1978, 102, 141.

ACKNOWLEDGEMENTS

Foremost on my mind as I write these acknowledgements are God and my parents. To say I could not have done it without God seems too trite to convey the sincerity with which I mean it. God was the source of my strength through the discouraging times. That is, however, only one aspect in which God has helped me. The full picture is that the person that I am is a result of the changes that God has made in me, and continues to make in me. Everything that I do, and the diligence with which I do it, I try to do to the glory of God (Colossians 3:17).

I am so grateful to my parents for their love, encouragement, and support. Only now do I fully realize how terrific my parents are, and I love them very much. In a special way I remember my father, and dedicate this dissertation in his memory. He always took great concern for my education. In many ways, Dad was my best friend; I really miss him.

I want to express thanks to my major professor, Dr. Rodney Walters, for his guidance and help in my graduate studies. Being Dr. Walters' first graduate student was quite challenging, but was well worthwhile. Dr. Walters has been a great help towards improving my work skills, especially in those areas in which I was weak. I feel that working for Dr.

Walters has made me more well-rounded professionally, and thus, I have been prepared well for meeting the challenges in future positions. Thanks much.

I would also like to acknowledge the many people who helped in the preparation of this dissertation. I am grateful to Jackie Anhalt for her experimental contributions. Thanks go to the following people for helping proof the dissertation: Sam and Melissa Crowley, Bob Moore, Jackie Anhalt, King Chan, Steve Gilles, and Jim Carpenter. In addition, I especially want to recognize Melissa Crowley for her typing help into the wee hours of the morning, to rescue me from one of my "lines of death". The typing help of Connie Hodnefield was also much appreciated.

To the members of the Walters' research group: Bob Moore, Sam Crowley, John Graham, Dave Hage, Danlin Wu, Larry Larew, Jackie Anhalt, King Chan, Mary Landgrebe, and Steve Gilles, a more cohesive group in Gilman there is not. Thank you for being my friends. The support of other friends is also greatly appreciated: Jim Carpenter, Bill Sheard, Ron Haas, Wayne Jones, Scott Stoner, Bill Tong, and Zamir Uddin. I would also like to thank my aunt, Andrea Stadlin, who provided the spark for my interest in nutrition and clinical chemistry.

Encore thank yous to Sam and Melissa Crowley, and Dave and Jill Hage are a must, as they have taken me into their

homes for the last six months. They have made me feel like a part of their family and I will always be grateful.

Finally, I would like to thank Johnny Orr for some mighty exciting basketball, that made the long, cold Iowa winters bearable.